NASA Technical Memorandum 104101

LASER TRANSIT ANEMOMETER AND PITOT PROBE COMPARATIVE MEASUREMENTS IN A SHARP CONE BOUNDARY LAYER AT MACH 4

W. W. Hunter, Jr., S. L. Ocheltree, and C. E Russ, Jr.

JULY 1991

National Aeronautics and Space Administration

Langley Research Center
Hampton, Virginia 23665-5225

INTRODUCTION

This report describes test results obtained using a laser transit anemometer (LTA) instrument to obtain nonintrusive measurements of velocity profiles in the boundary layer of a sharp cone model in the Air Force Arnold Engineering Development Center (AEDC) Supersonic Tunnel (A). This test was the first of two conducted at AEDC using the NASA Langley Research Center (LaRC) LTA instrument. These cooperative experiments were part of a formal interlaboratory Memorandum of Agreement between the NASA LaRC, the NASA Lewis Research Center (LeRC), and the AEDC to investigate the LTA technique and to develop an advanced LTA instrument for aerodynamic research facility nonintrusive measurements.

The overall goal of this test was to explore the LTA instrument system performance in a supersonic wind tunnel flow seeded with atomized oil droplets by obtaining LTA velocity measurements in the supersonic boundary layer of a 7 degree half angle sharp cone model. The test objectives were to obtain velocity profiles in both the laminar and turbulent regions of the cone model boundary layer using the LTA instrument and a pitot survey probe in regions where the boundary layer velocity profiles were well characterized by theory. The results of these LTA boundary layer velocity surveys are compared with pitot probe surveys and theoretical predictions.

SYMBOLS

b	background value
d	measurement location above model surface (mm)
d_c	corrected measurement location above model surface (mm)
d_e	measurement location where measured velocity equals V_e (mm)
h	peak store number
i	integer
m	exponent value of velocity
n_i	number of events occurring with transit time t_i

Q	dynamic pressure (N/m^2)
P_t	total pressure (N/m^2)
P	static pressure (N/m^2)
R	range of valid transit events
Re	Reynolds number (/m)
SS	spot separation (um)
T	static temperature (^oK)
T_t	total temperature (^oK)
$\overline{V}$	local mean velocity (m/sec)
$\overline{V}e$	mean velocity value at edge of boundary layer, 99% of free stream value (m/sec)
V_i	velocity of ith measured event (m/sec)
$\overline{V}v$	LTA mean velocity computed in velocity space (m/sec)
$\overline{V}_\tau$	LTA mean velocity computed in Tau space (m/sec)
t_i	transit time of the ith event (sec)
$\overline{\tau}$	mean transit time (sec)
$\Delta\tau$	counting time interval (sec)

APPARATUS

Test Facilities

The supersonic Tunnel A of AEDC's von Karman Gas Dynamics Facility is a continuous flow closed circuit wind tunnel which is described in reference 1. For the tests described in this report the tunnel was operated at one of the following test conditions to create either laminar or turbulent flow in the boundary layer of the model.

Mach	P_t, N/m^2	T_t, ^oK	V, m/sec	Q, N/m^2	T, ^oK	P, N/m^2	Re,/m x 10^6
4.0	4.8×10^4	311	690	3.6×10^3	74	3.2×10^2	2.0
4.0	2.3×10^5	322	702	1.7×10^4	77	1.5×10^3	8.9

The model used in these tests was a 7-degree half-angle cone with nominal length of 1 meter and a base diameter of 0.25 meters. It was constructed of 304 stainless steel. The model was located 5.0 centimeters below tunnel centerline and had a pitch angle of 0 degree. Pitot measurements included in this report were made using a probe with a cylindrical tip, 0.18 millimeter inside diameter and 0.30 millimeter outside diameter. The probe was mounted on a boundary layer survey mechanism. The probe and probe support longitudinal axis was inclined 7 degrees to the model axis so that it was aligned parallel to the local flow direction.

Laser Transit Anemometer

The LTA system was a Spectron Development Laboratories, Inc., Model 104. Reference 2 contains a detailed description of the design and operation of this instrument. Basically, the LTA measures the transit time of particles that pass through the focal volume of each of two focused laser beams that form a plane parallel to the flow direction. The optical package sketched in figure 1 forms "two spots" in space and detects light scattered from particles upon passage through each spot. Detected signals are correlated in time with an electronic correlator, the Correlex, which has an adjustable time resolution from 10 nanoseconds to 800 milliseconds. The LTA system control, data acquisition, and data processing is performed by a microprocessor based computer system.

The optics package is designed so that the plane formed by the optical axis of the two beams may be rotated about an axis that is equidistant from and parallel to the two beams. This capability permits the determination of the flow angle using a "best angle" search. The procedure is to make velocity magnitude measurements at several spot rotation angles at fixed preselected incremental steps. A plot is then made of the "two spot" angular position against contrast; where contrast is defined as $(h - b/\sqrt{b})$, h, is the value of the peak store in a transit time histogram and b, is a background value. A least squares fit of a parabolic equation through the maximum three adjacent points is performed and the abscissa of the parabolic vertex is taken to be the mean flow angle or best estimate of flow angle. Finally, the system is positioned at this angle and a velocity magnitude measurement is performed. The LTA system has a specified angular resolution capability of 0.1 degrees

that is limited by its electromechanical rotation mechanism. For the current experiment the transceiver lens focal length was 600 millimeters, the spot separation is 860 micrometers and the diameter of each spot was approximately 20 micrometers at the 1/e point.

EXPERIMENTAL PROCEDURES

LTA System Alignment

Prior to each test run, it was necessary to accurately position the LTA sample volume with respect to the reference pitot probes and the centerline of the model. The first step to accomplish this was to align the front surface of a machinist scale parallel with centerline of the model. The satin finish of this scale creates a speckle pattern when illuminated by the laser beam. Next, the scan rig was translated normal to a plane parallel and normal to the tunnel and model centerline until the speckle point size pattern was maximized on a distant wall. This position was taken to be the center of the LTA sample volume in plane parallel and normal to the centerline of the 7-degree cone model and the tunnel. This procedure, based on earlier laboratory tests, has positioning repeatability to better than 0.0254 mm. Next, a vertical scribe line was made on the model 20 millimeters from the base and the two spots were rotated to a vertical position. The relative fore and aft position of the model and the LTA was established by moving the model along the centerline of the tunnel for rough positioning in the stream line direction and precise location was accomplished with the scan rig positioning control to within 0.0254 mm, the readout accuracy of the scan rig. The spots were then rotated to be parallel to the 7-degree cone model surface and moved by the scan rig vertically until they just touched the surface of the model, which again could be accomplished to an accuracy of 0.0254 mm. This position could be readily determined by the reflection of the two spots from the model surface to the test section wall. The spots were then moved to an initial position 7.37 mm above the model for the laminar boundary layer surveys and to an initial position 15.0 mm above the model for the turbulent boundary layer surveys. LTA velocity profile surveys were conducted for each test run with the LTA measurement volume scanned normal to the model axis and transit time data acquired as a function of sample volume location (d) above the model surface.

Seeding System

The flow field was seeded with atomized olive oil droplets. The droplets were generated with a commercial TSI seeder, model 9306. A Laskin nozzle was also used to generate droplets in one test in which data were obtained. The seed particles were injected into the tunnel stilling chamber through a 25.4 millimeter diameter tube. Measurement data rates obtained with the LTA system were approximately 3000 per second with three TSI seeders. This was reduced to about 2000 per second by securing a single TSI seeder. These data rates were obtained in the free stream and typically decreased to about 100 per second as the model surface was approached during boundary layer velocity surveys. There was a single observation, prior to termination of these tests, that revealed a shift in the data distribution from a multimode to a single mode with an increase in operating pressure with the Laskin nozzle seeding system.

DATA ANALYSIS

Measurement (Tau) Space

The fundamental measurement of the LTA system is the transit time of an individual scattering particulate crossing the "two spots." A fundamental assumption in this technique is that each of the particulates sensed by the LTA faithfully represents the local flow field conditions in which they are embedded and that their measured velocity is the same as the local flow velocity in the region between the LTA focal volumes. In order to obtain a good statistical representation of the local flow velocity, an ensemble of transit time measurements for a number of particulates is collected. A statistical evaluation of this ensemble provides a measurement of both the mean and higher order moments of velocity. This ensemble of transit time measurements is graphically displayed as number-of-events versus transit time or tau, i.e., a correlogram. These correlograms are displayed on-line in real time and are the researcher's visual representation of the measurement process and raw data results. The counting time interval of the tau measurements, delta tau, is operator selected and can range from 10 nanoseconds to 800 milliseconds.

The data reduction software provided with the LTA system determined the mean velocity from the estimated mean transit time.

$$\bar{V} = SS/\bar{\tau} \tag{1}$$

$$\bar{\tau} = \Sigma n_i \tau_i / \Sigma n_i. \tag{2}$$

$\bar{V}$ is the mean velocity, SS is the spot separation, $\bar{\tau}$ is mean transit time, τ_i is the indicated time of the ith particle and n_i the number of events occurring with elapse time of τ_i.

$$\tau_i = i\Delta\tau \tag{3}$$

In the above equation, $\Delta\tau$ is the counting time interval and **i** is an integer indicating the number of elapse time intervals.

To further improve the precision of the mean velocity estimate, the LTA system software includes a routine for estimating an average "background" level. The background level, b, contribution is then subtracted uniformly from the data set, i.e.,

$$(n_i - b). \tag{4}$$

Now the estimate of the mean transit time $\bar{\tau}$, is determined by:

$$\bar{\tau} = \Sigma (n_i - b) \tau_i / \Sigma (n_i - b) \tag{5}$$

Velocity Space

As noted previously, data analysis is routinely performed in measurement or tau space coordinates. This section describes the considerations for data analysis in velocity space coordinates, $1/\tau_i$. Beginning with

$$\bar{V}i = SS/\bar{\tau}_i \tag{6}$$

$$= SS/i\Delta\tau$$

a statistical mean estimate is performed where

$$\bar{V}_v = \frac{\Sigma n_i V_i}{\Sigma n_i} \tag{7}$$

$$\bar{V}_v = \frac{\Sigma n_i \ (SS/i\Delta\tau)}{\Sigma n_i} \tag{8}$$

$$\bar{V}_v = \frac{SS}{\Delta\tau} \frac{\Sigma n_i / i}{\Sigma n_i} \tag{9}$$

But, the above expressions are not complete because of the nonlinear relation between V_i and τ_i. To account for this nonlinear relationship, a weighting factor is incorporated in the statistical analyses. The weighting factor Wi choice is based on the following notion. Consider the relative change of V_i with τ_i. Using equation (6)

$$\Delta V_i = - \frac{SS}{i^2\Delta\tau} \ \Delta i \tag{10}$$

For a unit i change (i.e., $\Delta i = 1$)

$$\Delta V_i = \left| \frac{SS}{i^2\Delta\tau} \right| \tag{11}$$

The velocity resolution per increment i is inversely proportional to i^2. The smallest transition time, τ_i, has a larger velocity acceptance bandwidth compared with a long transit time based on the same counting time increment, $\Delta\tau$. This means that for a uniform velocity distribution the lower ith channels will have a higher probability of acquiring counts, n_i, then higher ith channels. Hence, the weighting

factor, W_1, is taken to be inversely proportional to the velocity bandwidth, ΔV_i. Therefore

$$\bar{V} = \frac{\Sigma W_i n_i V_i}{\Sigma W_i n_i} \tag{12}$$

with the result

$$\bar{V} = \frac{SS\ \Sigma i n_i}{\Delta\tau\ \Sigma i^2 n_i} \tag{13}$$

Similar results are obtained for higher moments.

The process is completed when the background, b, is included.

ANALYSIS OF TEST RESULTS

Introduction

Eight test runs were conducted to obtain LTA measurements. Two of these, runs 2 and 17, were conducted at a high Reynolds number condition, 2.7 x 10^6/ft. for turbulent boundary layer measurements. Six runs--3, 13, 21, 22, 23, and 24--were conducted for laminar boundary layer measurements at a Reynolds number of 0.62 x 10^6/ft. Data were obtained for all runs except 23.

Data for all runs were retained in hard copy form which includes a listing of raw correlogram data, position information, and estimated mean velocity value as determined in tau space. Raw correlogram data was also retained on disk for runs 2, 17, and 22. Additional analyses of runs 3, 17, and 22 in velocity space were also conducted.

First, a discussion of results as obtained from Tau space analysis is presented. This is followed by a review of data analyzed in velocity space for runs 3, 17, and 22.

TAU SPACE RESULTS

Laminar Boundary Layer

Initial examination of the LTA laminar boundary layer velocity profile data for runs 3, 13, 21, and 24 was performed on graphs of distance above the model surface plotted versus measured normalized velocity as shown in figure 2. These graphs revealed that all LTA test data sets appeared to have similar characteristics. These characteristics included (1) a closely grouped set of data indicative of low statistical errors, (2) a region of constant slope for the boundary layer region near the model surface followed by a region of rapidly changing slope as the free stream was approached, and (3) a non-zero ordinate intercept, i.e., measured distance (d) from model surface, that randomly varied for each test run data set.

In order to quantify and examine these LTA data set observations in more detail, the data sets were organized into three classes for graphical representation and statistical least squares analysis, viz., (1) a linear plot of recorded (uncorrected) distance (d) versus measured normalized velocity (Fig. 2 cited above), (2) a Log-Log plot of the same data (Fig. 3), and (3) a Log-Log plot of corrected distance (d_c) versus measured normalized velocity (V/Ve) (Fig. 4). The first linear least squares analysis was performed on the class 1 data to examine the uncorrected

distance versus velocity data sets by calculating the best estimate of the slope and ordinate intercept and the standard deviation estimates of both values. This was accomplished by restricting the data used in the statistical least squares computation to the linear portion of each data set. Several trial computations were run by changing the range of accepted data in order to get the best estimate of slope and ordinate intercept using an acceptance criterion of minimization of the slope and intercept standard deviation estimates. These results are given in tables 1 and 2. Next, the data sets in the class 2 (Log-Log) format were examined to determine if the statistical errors were percentage of "reading" or "full scale" errors. Figure 3 shows the data in this format. Finally, a new logarithmic least squares analysis was performed in the class 3 format using the logarithm of corrected distance, i.e., distance minus the estimated ordinate (distance) intercept determined from the class 1 linear least squares analysis. A special examination was made of the slope and ordinate values of these latter logarithmic graphs listed in tables 1 and 2. It can be shown that the slope value is the exponent of the independent variable in the function that represents the first order approximation of the distance versus normalized velocity curves in figure 2. All slope values in the Log-Log data sets are approximately unity, thus indicating that the "of reading" weighted least square fit gives a linear slope estimate as predicted by theory. The corresponding Log plots (Fig. 4) combined with the previous analysis indicated that the errors are "of reading" percentage errors and that use of a corrected distance substantially improves the quality of all reduced data sets. Examination of these results shows that (1) the standard error estimates of slopes of the linear least squares analysis for all data sets is less than 3 percent and indicates a highly linear relationship between distance and velocity for distances from approximately 0 to 2.5 mm from the model surface, station 25, (2) the deviation from linearity in the linear region is small for all LTA data sets and is substantially improved at small distances by using a corrected distance as the ordinate when plotting the data sets, (3) the average of the best estimates of the slope for each of the four LTA data sets was 4.98e-3 mm/m/s with a maximum deviation of 2.1 percent, and (4) there is no evidence of distortion of the data due to particle lag effects.

The same analytical procedure described above was performed on two pitot data sets and three theoretical data sets provided by the AEDC staff and which correspond to tunnel conditions set to match the LTA test conditions as closely as possible. The least squares slopes and intercepts are also listed in tables 1 and 2. The results of this analysis on the two pitot data sets show that probe interference effects are present near the model surface. In

addition, the least square analysis indicates that there is a limited region where the curve is linear and which extends from approximately 1.6 to 3.8 mm. The computed slopes of the two pitot data sets are 6.06e-3 and 6.36e-3 mm/m/s and are greater than the average LTA data slope by 21 percent. Another observation was that the pitot probe data also had an ordinate offset that differed for the two pitot test runs. The results of the three theoretical data set analyses are similarly shown in tables 1 and 2.. These results indicate that (1) the theory predicts a highly linear--0.2 to 0.3 percent standard deviation--relationship between velocity and distance up to 2.5 mm, (2) there is a negligible ordinate offset of 0.01 mm which is probably due to computational inaccuracy, and (3) the average theoretical data slope is 4.92e-3 and agrees with the LTA data average slope of the LTA data sets to within 0.6 percent.

The final data analysis performed was a comparison of the three types of data sets, i.e., theory, LTA, and pitot. This was accomplished by first correcting the pitot data for a 21 percent slope conversion constant error which was discovered during post test data analysis. Once this was done the corrected LTA data sets were plotted along with a pitot data set (run 12) and a tricone theory data set (run 24) on a linear graph in figure 5 and on a log-log graph in figure 6. Examination of figure 6 reveals that LTA data for runs 13, 21, and 24 agree with the corrected pitot and tricone theory to within ±3 percent. The LTA data for run 3 is also linear but has a displacement on the log-log plot indicating a slope constant difference of 1.057. This scaling constant difference could be due to a scanning position error. The corrected pitot data agrees well with theory at boundary layer distances greater than 1.8 mm but sharply increased deviations from theory at smaller distances reveals the effect of probe interference near the model surface.

Turbulent Boundary Layer

Two turbulent boundary layer tests were conducted, runs 2 and 17. Three graphs for each run are presented. Figures 7 and 8 illustrate the data in a Log-Log plot of the velocity ratio, V/V_e vs position ratio d/d_e. Where, V and d are the LTA measured velocity values and the respective positions above the model normalized to an edge velocity value, V_e, taken to be 99 percent of the freestream value, ~680 m/sec, and its respective position value, de. Initial comparison of the two figures indicates that the run 2 data is not as linear as the run 17 data. This is attributed to a positioning error which has been noted in the laminar

boundary layer data sets and is random between runs. When considering a fit to the following expression

$$d/d_e = C(V/V_e)^m \qquad (14)$$

runs 2 and 17 best fit exponent values were m = 4.56 and 7.26 with a standard deviation about the best fit of 7.5 and 1.6 percent, respectively.

Again, preceding as in analyses of the laminar boundary layer data, adjustments in the position were made and the correction selected was based on a minimization of the scatter of the data about the best fit. Figures 9 and 10 show the result of this procedure. Run 2 fit was significantly improved with a position correction of 0.117 mm. Run 17 was not improved but illustrated the effects of a small position change of -0.0335 mm. The results of these position corrections were m = 6.57 and 6.92 with a standard deviation about the best fit of 1.7 and 1.7 percent, respectively.

The third set of graphs, figures 11 and 12, present the final results in a linear plot of V/V_e vs d/d_e (corrected).

The corrected data provides a reasonably good linear fit in the Log-Log plots from which an estimate of the velocity ratio exponent could be made. Both corrected sets of data had 1.7 percent standard deviation about the best fit and the velocity ratio exponents agreed to within better than 10 percent with an average value of approximately 6.7. These measurements again demonstrate the need for a very precise and accurate positional capabilities. The positioning errors ranging from 25 to 120 micrometers have been estimated. Positioning accuracy requirements approaching 1 micrometer are clearly justified in measurement surveys of the turbulent boundary layer where small changes significantly effect the estimated exponential value, m.

VELOCITY SPACE RESULTS

Additional Considerations

First consider the possible outcome of analyzing data in velocity space versus Tau space. One possible outcome is a bias result. In the case of a well behaved distribution in Tau space the difference, $V - V_v$, will result in a negative or positive result. The results of an examination of the difference between equations (1) and (8) for a Gaussian

distribution in Tau space is plotted in figure 13. Figure 13 is a plot of the percent velocity bias, $V - V_v$, versus the mean transit time, τ bar ($\bar{\tau}$). Four curves are shown for difference standard deviations of τ_1, σ_τ, of 2%, 5%, 10%, and 20%. The reason for these large bias differences is that the symmetrical distribution in Tau space are skewed in velocity space because of the nonlinear relationship between Tau and velocity space. In general, analysis of the results of runs 3, 17, and 22 illustrate the positive bias effects of the Tau space analyses.

Laminar Boundary Layer

Two laminar boundary layer cases were examined in velocity space, runs 3 and 22. Run 3 measurements were conducted at model station 35, 12.7 centimeters from the model base, and run 22 measurements were conducted at model station 17.5, 57.2 centimeters from the model base. These two sets of data present two different results.

Comparison of run 3 results below shows that there was not a significant difference between the Tau and velocity space analyses.

	Tau Space	Velocity Space
Slope	196.5 m/sec/mm	198.0 m/sec/mm
Std. Dev. of Slope	2.1%	1.5%

Examination of the respective correlogram for Tau space and velocity space, appendix A, illustrate the possibility for significant differences.

Analysis of run 22 revealed a significant difference between Tau space and velocity space outcomes. An examination of the two sets of individual position results below reveals the Tau space analyses were misleading.

Position (mm)	Tau Space (m/sec)	Velocity Space (m/sec)
1.52	585.4	567.8
1.02	501.4	446.0
0.76	423.9	373.4
0.51	397.9	291.5
0.51	398.0	289.2
0.25	442.8	239.8
0.13	422.5	163.3
0.13	395.4	167.2

The correlograms for run 22, Tau and velocity space, are contained in appendix B.

A set of plots for runs 3 and 22 are included in figures 14-17. These plots are similar to those described in the Tau space. Comparison of final values for these runs is listed below.

	Run 3	Run 22
Slope	198.0 m/sec/mm	269.5 m/sec/mm
Slope Std. Dev.	1.5%	3.7%

The difference in the slope represents the difference in the boundary layer thickness at the two measurement stations, 17.5 and 35.0.

Turbulent Boundary Layer

Run 17 measurements were examined in Tau and velocity space. The major change between previously examined Tau space results and the velocity space results was approximately a 9 percent decrease in the exponent value, equation (14). The new exponential value is 6.32, versus 6.92, with a 1.5 percent standard deviation. The data set of run 17 was the only data set examined which required an ordinate correction of less than 0.01 mm to achieve a reasonably linear logarithmic plot. Plots for run 17 velocity space data is presented in figures 18 and 19 for comparison with previously presented Tau space plots. Correlograms of this turbulent boundary layer data, Tau and velocity space, are presented in appendix C.

CONCLUDING REMARKS

Laser transit anemometer measurements have been successfully performed in the AF/AEDC Supersonic Tunnel A

using the NASA LaRC LTA instrument. High spatial resolution measurements (<0.1 mm) of boundary layer velocity profiles were obtained in both the laminar and turbulent regions of a 7 degree sharp cone model. Extensive post-test LTA data analysis was subsequently performed and has revealed high quality velocity data for both the laminar and turbulent boundary layer velocity profile tests when compared with pitot probe data and theory.

The majority of the post test data analysis was performed using the data reduction software and procedures supplied with the LTA system. This analysis was performed in the transit time domain or Tau space. Several sets of data were also analyzed in the reciprocal transit time domain or velocity space. Because of the nonlinear relationship between Tau space and velocity space the Tau space results will provide a higher mean velocity value than that calculated in velocity space. The degree of this bias error in Tau space analyses depends on the variance of the measurement ensemble and relative position in the transit time based correlogram. Further complications are also produced when the measurement ensembles are not well behaved, i.e., not single peaked with a "small" variance. In spite of this potential for measurement error, the Tau space analyses of the present laminar boundary layer data revealed a highly linear set of data with an average slope of 200.7 ±2.8 m/sec/mm at model station 35. This compared well with theory which, for the cases examined, provided an average slope of 202.2 ±3.8 m/sec/mm. The standard deviation of the slope for the experimental data was 3 percent or less.

It should be noted that it was necessary to apply a position correction to the data to achieve a proper linear fit predicted by the theory. Examination of log-log plots of velocity versus position revealed positioning errors which were random from data set to data set. Although the position corrections were quite small--ranging from 0.01 to 0.6 millimeters--they had a significant effect on final velocity profiles. These position correction values were chosen to minimize the standard deviation of the slope, i.e., scatter of data about the best fit. Similar error minimization procedures were used to reduce the turbulent boundary layer data. Analyses of the data in a log-log plot of V/V_e vs d/d_e displayed an average power law dependence of the normalized position on the normalized velocity of 6.92.

Analyses of several cases in the velocity space for both the laminar and the turbulent boundary layer were also performed. One laminar boundary layer data set, for model station 35, revealed only a slight shift of the velocity gradient through the boundary layer, i.e., a gradient increase from 196.5 to 198.0 m/sec/m. This difference is

statistically indistinguishable since the standard deviation of the slope for both cases was approximately 1.5 percent. A second laminar boundary layer case at the model station 17.5 was examined. In this situation the velocity results in Tau space did not conform to the expected velocity gradient. The velocity space analyses provided a reasonable set of data with a velocity gradient of 276.0 m/sec/mm which exhibited a steeper velocity gradient for the thinner boundary layer at this model station. One turbulent boundary layer velocity data set was also examined. In this case, there was a 9 percent change in the power law dependence, i.e., decrease from 6.92 to 6.32, from the value obtained in Tau space.

Comparison of the pitot survey probe data with both theory and LTA data consistently showed a small, but significant positioning error in the linear region similar to that of the LTA. In addition, it also revealed the effects of probe interference near the model surface. When this latter observation was examined closely it was seen that the boundary layer velocity profile--as measured by the pitot probe--had a very limited region with a constant slope. This linear region is bounded on the low velocity side by interference effects and on the high velocity side by the approach of the constant freestream velocity. These LTA and pitot probe comparative tests dramatically show the value of the LTA instrument in particular, and the potential of nonintrusive measurements, in general, in conducting detailed investigations of boundary layer flow field phenomena.

REFERENCES

1. Test Facilities Handbook (Twelfth Edition) "Von Karmon Gas Dynamics Facility, Vol. 3," Arnold Engineering Development Center, March 1984.

2. "Photon Correlation Techniques in Fluid Mechanics," Proceedings from the 4th International Conference, Joint Institute for Aeronautics and Acoustics, Stanford University, Stanford, California, August 24-27, 1980. Edited by: W. T. Mayo and A. E. Smart, pp. I-1 through II-36.

Table 1

Run No.	Data Type	Total No. of Data Points	No. of Data Points Used in L.S. Analysis	L.S. Analysis Data Range	
				Lower Value (m/s)	Upper Value (m/s)
3	LTA uncorrected linear plot	25	13	103.9	554.4
13	LTA uncorrected linear plot	15	9	76.0	614.0
21	LTA uncorrected linear plot	15	9	77.9	618.1
24	LTA uncorrected linear plot	12	9	57.0	605.1
3	LTA corrected log/log plot	12	9	76.0	465.0
13	LTA corrected log/log plot	15	9	76.0	614.0
21	LTA corrected log/log plot	15	9	77.9	618.1
24	LTA corrected log/log plot	12	9	57.0	605.1
12	Pitot uncorrected linear plot	17	6	254.2	630.6
12	Pitot corrected log/log plot	17	6	254.2	630.6
20	Pitot uncorrected linear plot	17	3	481.4	639.9
20	Pitot corrected log/log plot	17	3	481.4	639.9
12	Theory linear plot	23	15	0.0	543.0
12	Theory log/log plot	23	15	0.0	543.0
20	Theory linear plot	23	14	0.0	524.0
20	Theory log/log plot	23	14	0.0	524.0
24	Theory linear plot	23	14	0.0	519.7
24	Theory log/log plot	23	14	0.0	519.7
	Data Comparison				
12	Theory	23	15	0.0	543.0
13	LTA	15	9	76.0	614.0
12	Pitot	17	6	254.2	630.6
	Data Comparison				
20	Theory	23	15	0.0	528.1
21	LTA	15	9	77.9	618.1
20	Pitot	17	3	481.4	639.9
	Data Comparison				
24	Theory	23	15	0.0	512.0
24	LTA	12	9	77.9	605.1

Table 2

Run No.	Data Type	********** Slope ******** Value	Units	Standard Deviation (%)	******** Intercept ******** Value	Units	Standard Deviation (%)
3	LTA uncorrected linear plot	5.038E-03	(mm)/(m/s)	1.7	-0.28	mm	8.9
13	LTA uncorrected linear plot	4.970E-03	(mm)/(m/s)	2.4	0.05	mm	76.7
21	LTA uncorrected linear plot	5.013E-03	(mm)/(m/s)	1.7	-0.12	mm	24.7
24	LTA uncorrected linear plot	4.950E-03	(mm)/(m/s)	1.6	-0.03	mm	78.9
3	LTA corrected log/log plot	1.027E+00		2.5	-2.36	Log(mm)	2.5
13	LTA corrected log/log plot	1.003E+00		2.0	-2.31	Log(mm)	2.0
21	LTA corrected log/log plot	9.990E-01		1.4	-2.30	Log(mm)	1.5
24	LTA corrected log/log plot	9.812E-01		1.0	-2.26	Log(mm)	1.0
12	Pitot uncorrected linear plot	6.060E-03	(mm)/(m/s)	1.5	-0.30	mm	14.0
12	Pitot corrected log/log plot	1.051E+00		1.7	-2.23	Log(mm)	2.0
20	Pitot uncorrected linear plot	6.360E-03	(mm)/(m/s)	6.7	-0.08	mm	308.5
20	Pitot corrected log/log plot	9.920E-01		6.6	-2.17	Log(mm)	8.3
12	Theory linear plot	5.050E-03	(mm)/(m/s)	0.3	0.01	mm	41.3
12	Theory log/log plot	9.991E-01		0.2	-2.29	Log(mm)	0.2
20	Theory linear plot	4.920E-03	(mm)/(m/s)	0.2	0.01	mm	37.5
20	Theory log/log plot	9.966E-01		0.1	-2.30	Log(mm)	0.2
24	Theory linear plot	4.800E-03	(mm)/(m/s)	0.2	0.01	mm	33.6
24	Theory log/log plot	9.997E-01		0.2	-2.32	Log(mm)	0.2
	Data Comparison						
12	Theory	1.980E+02	(m/s)/(mm)	0.3	0.00	mm	
13	LTA	2.012E+02	(m/s)/(mm)	2.4	0.00	mm	
12	Pitot	1.650E+02	(m/s)/(mm)	1.5	0.00	mm	
	Data Comparison						
20	Theory	2.033E+02	(m/s)/(mm)	0.2	0.00	mm	
21	LTA	1.994E+02	(m/s)/(mm)	1.7	0.00	mm	
20	Pitot	1.572E+02	(m/s)/(mm)	6.7	0.00	mm	
	Data Comparison						
24	Theory	2.053E+02	(m/s)/(mm)	0.2	0.00	mm	
24	LTA	2.020E+02	(m/s)/(mm)	1.6	0.00	mm	

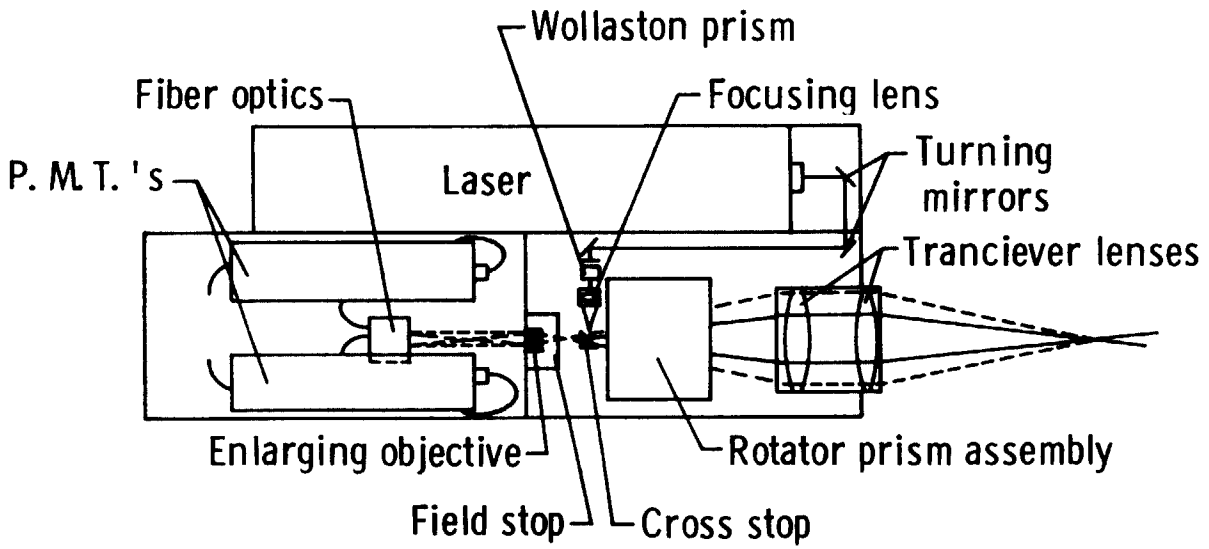

Figure 1. - LTA Laser/Optical Package

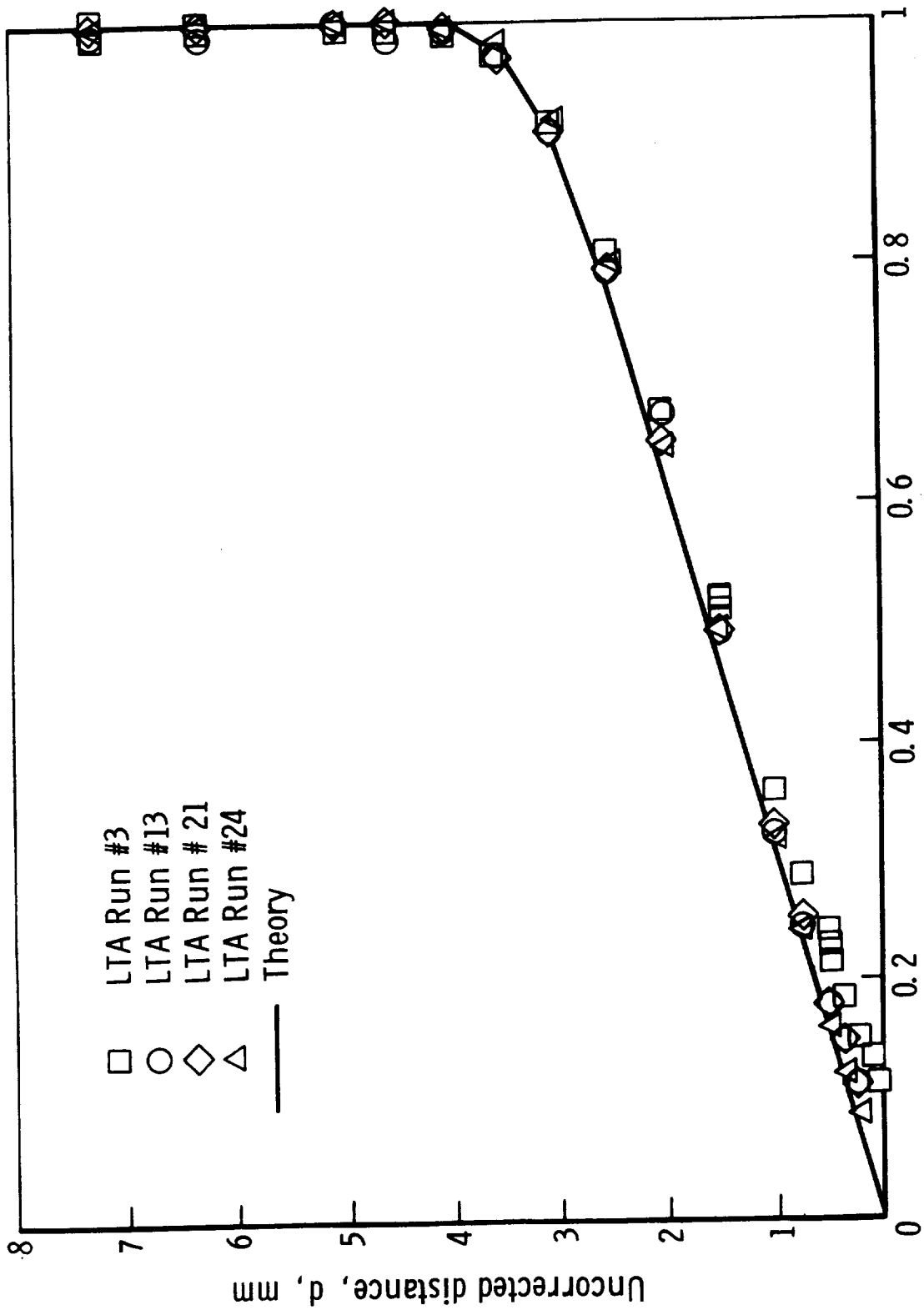

Figure 2. - Linear graph of LTA measurement and tricone theory data for velocity profiles in the laminar boundary layer using uncorrected LTA distance measurements.

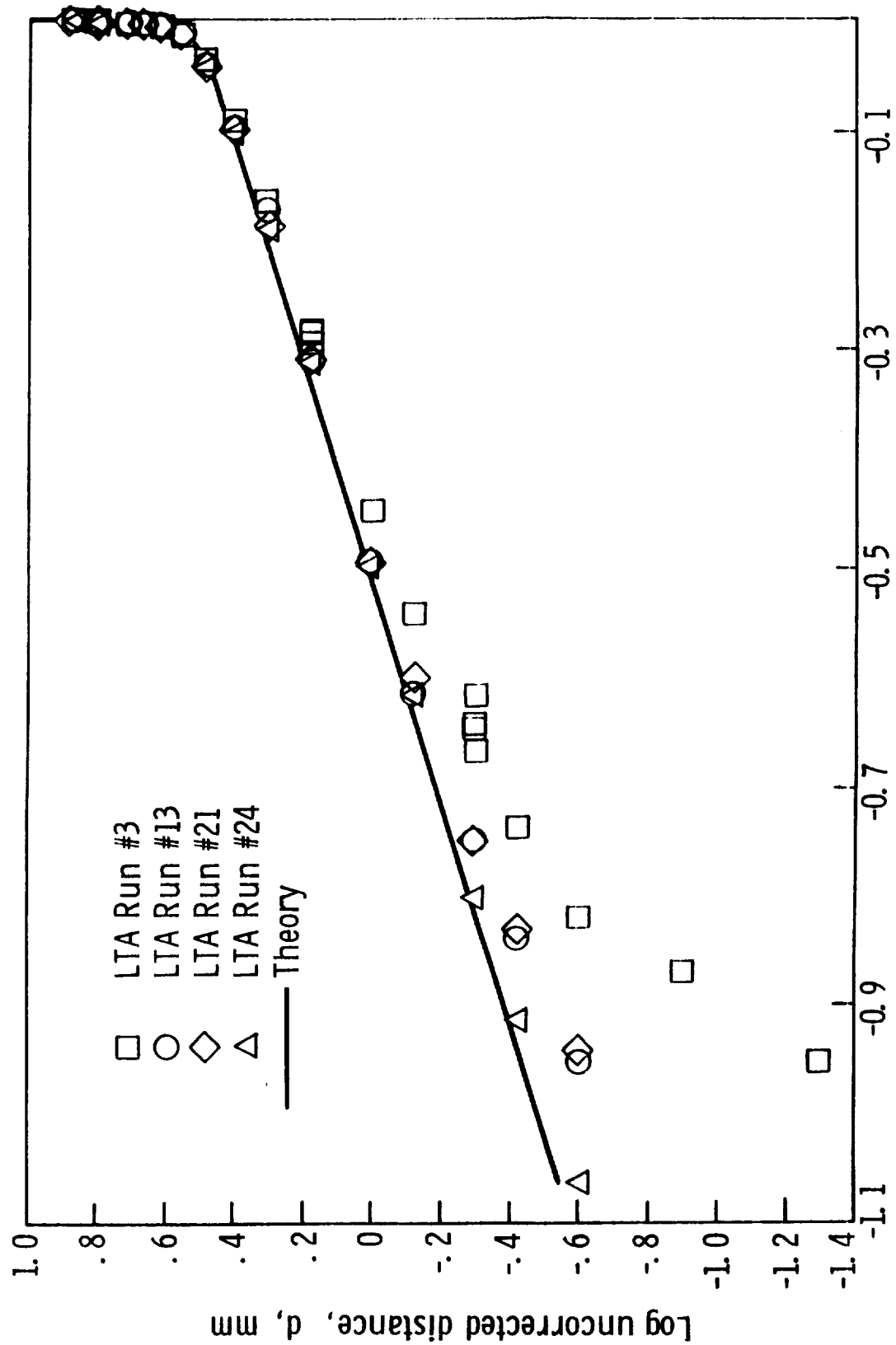

Figure 3. - Log-Log graph of LTA measurement and tricone theory data for velocity profiles in the laminar boundary layer using uncorrected LTA distance measurements.

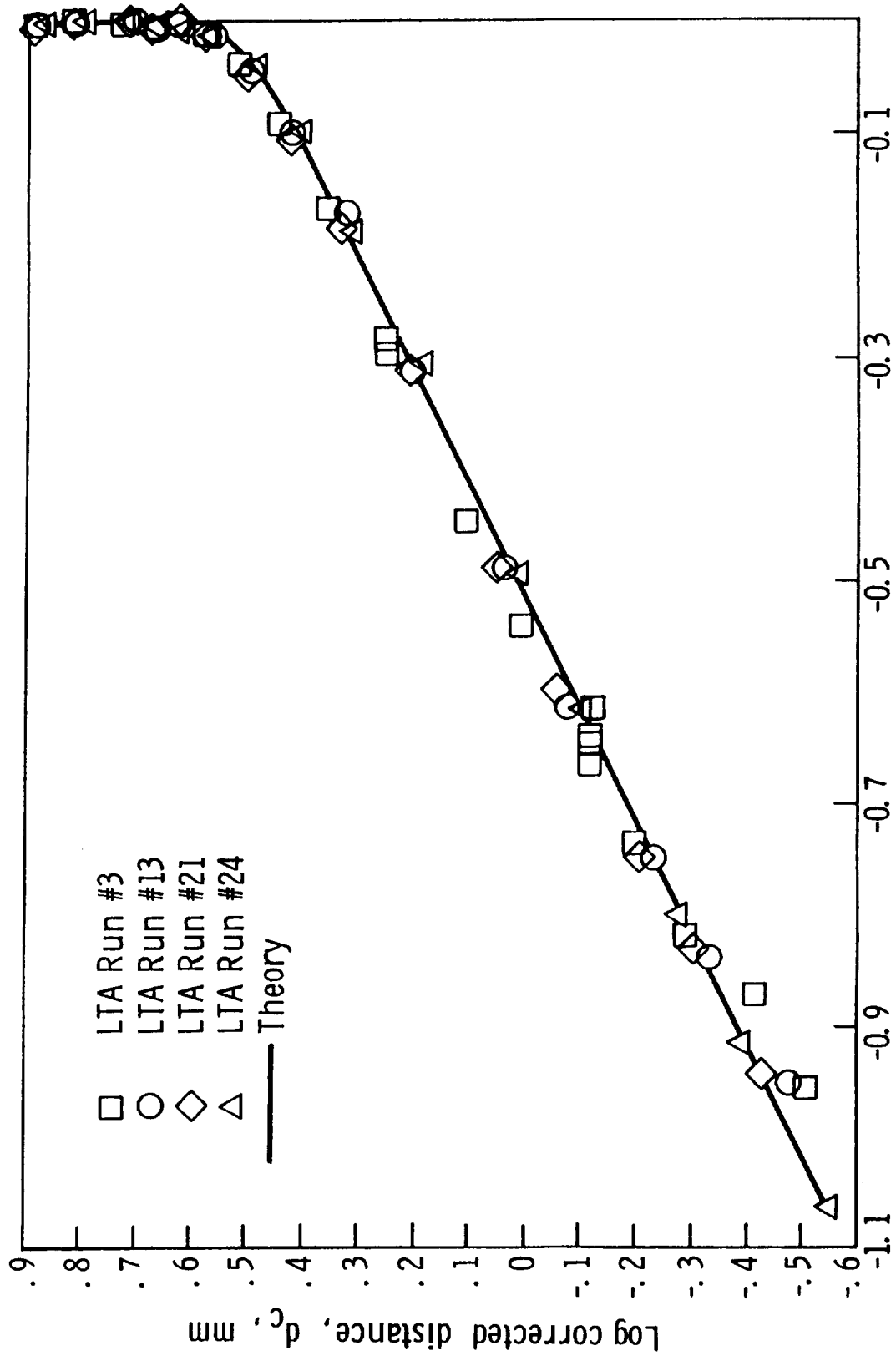

Figure 4. - Log-Log graph of LTA measurement and tricone theory data for velocity profiles in the laminar boundary layer using corrected LTA distance measurements.

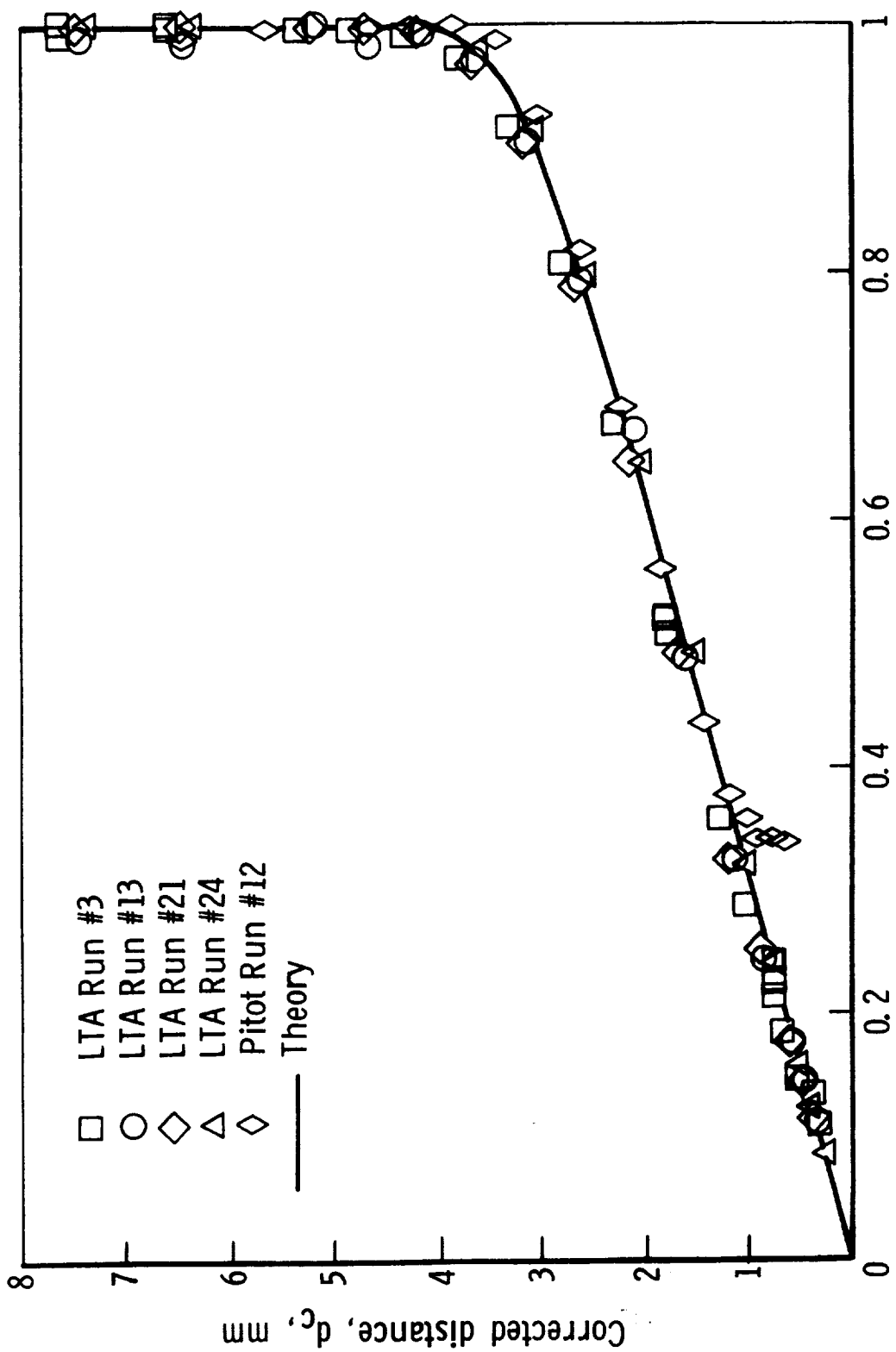

Figure 5. - Linear graph of LTA, pitot, and tricone theory data for velocity profiles in the laminar boundary layer using corrected LTA and pitot distance data.

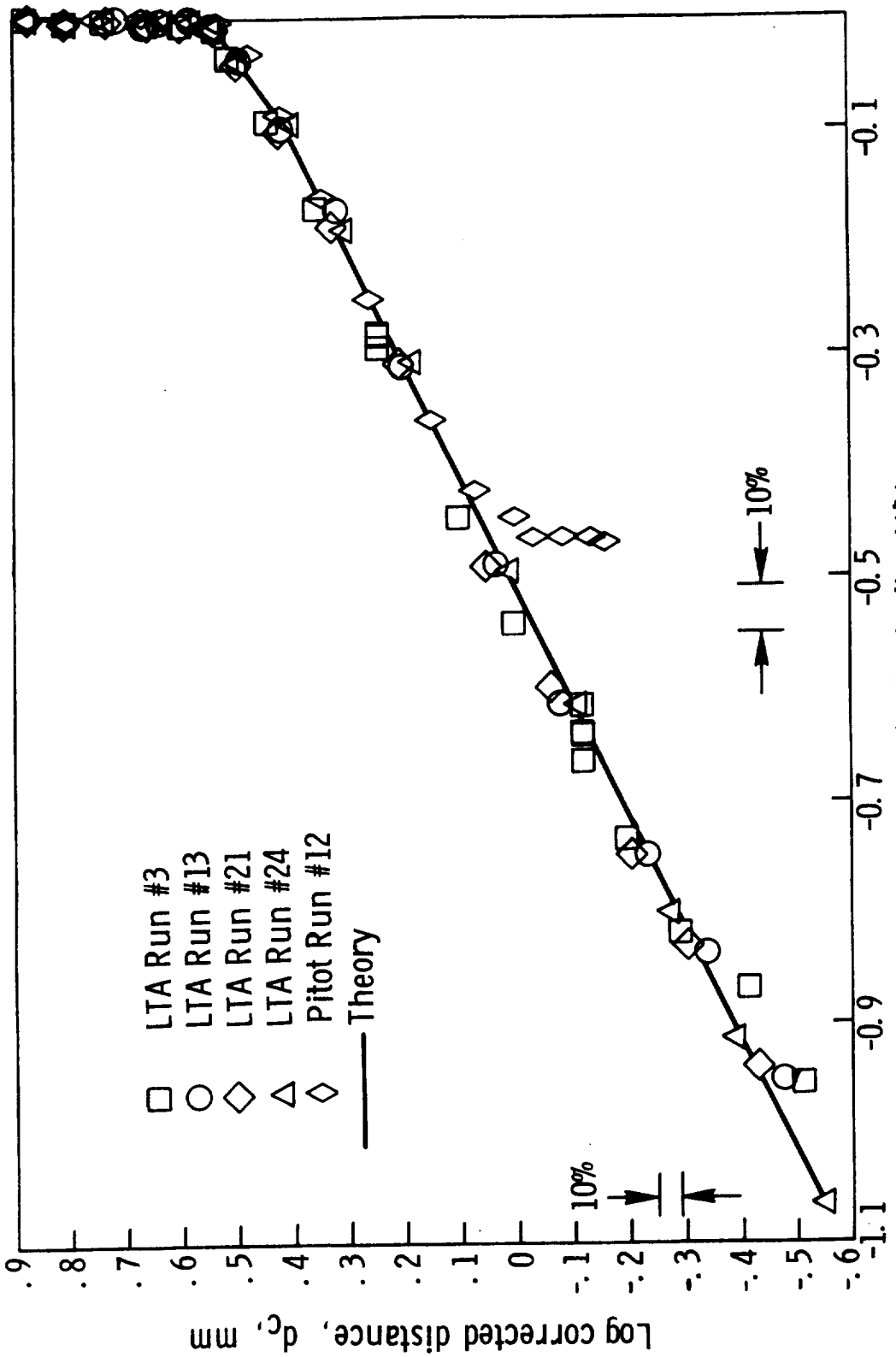

Figure 6. - Log-Log graph of LTA, pitot, and tricone theory data for velocity profiles in the laminar boundary layer using corrected LTA and pitot distance data.

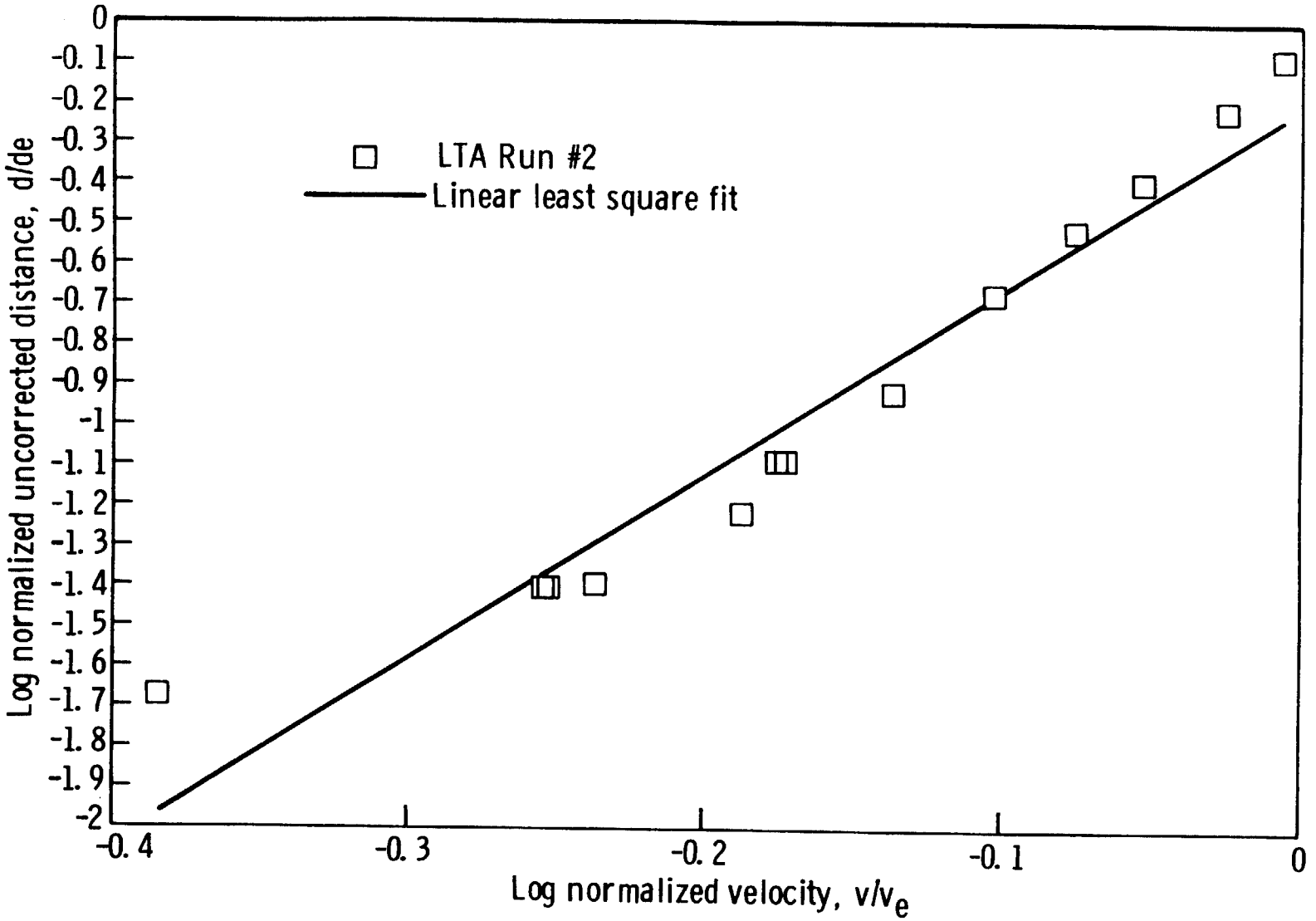

Figure 7. - Log-Log graph of LTA data Run #2 for velocity profile in the turbulent boundary layer using uncorrected distance measurements.

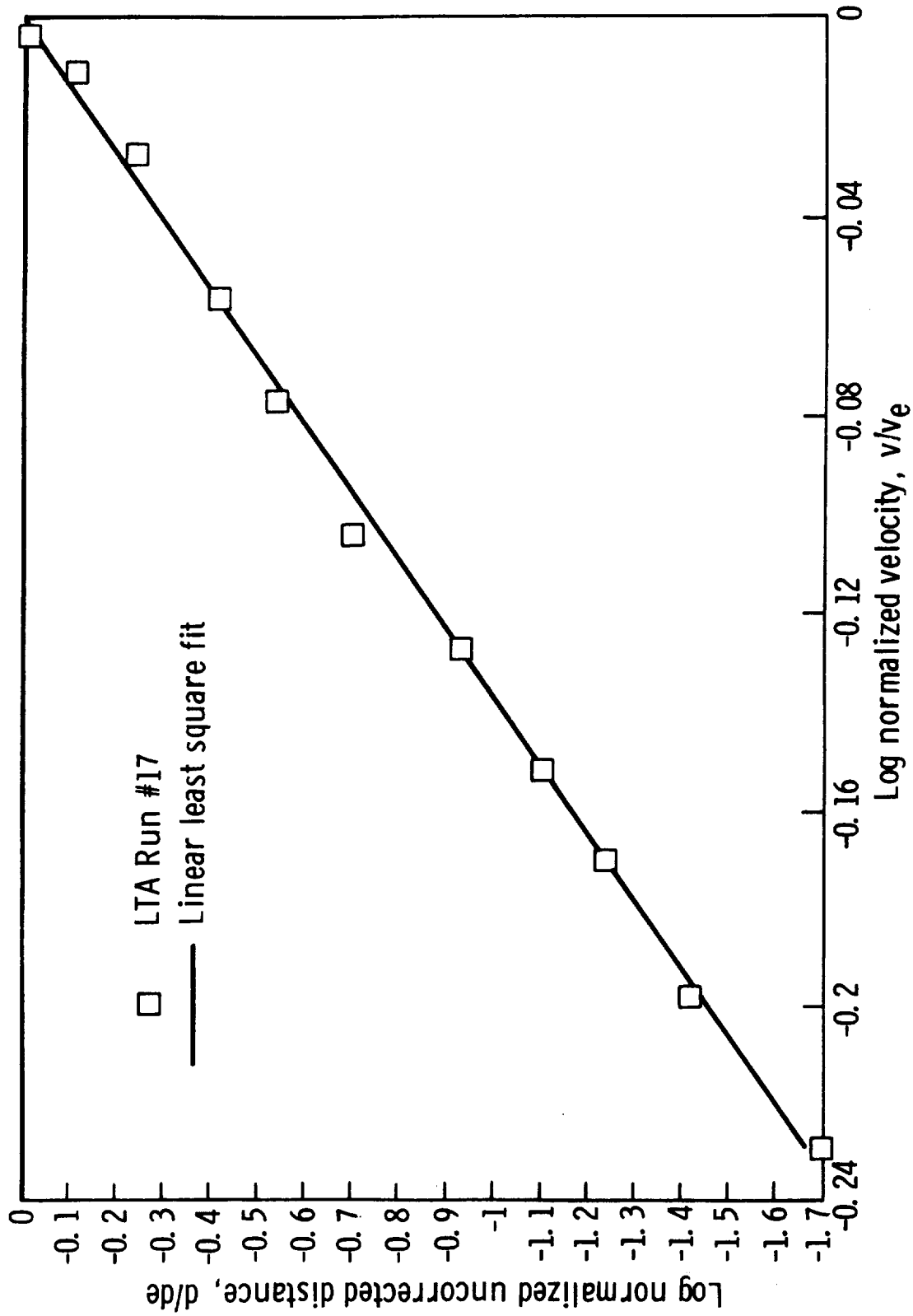

Figure 8.- Log-Log graph of LTA data Run # 17 for velocity profile in the turbulent boundary layer using uncorrected distance measurements.

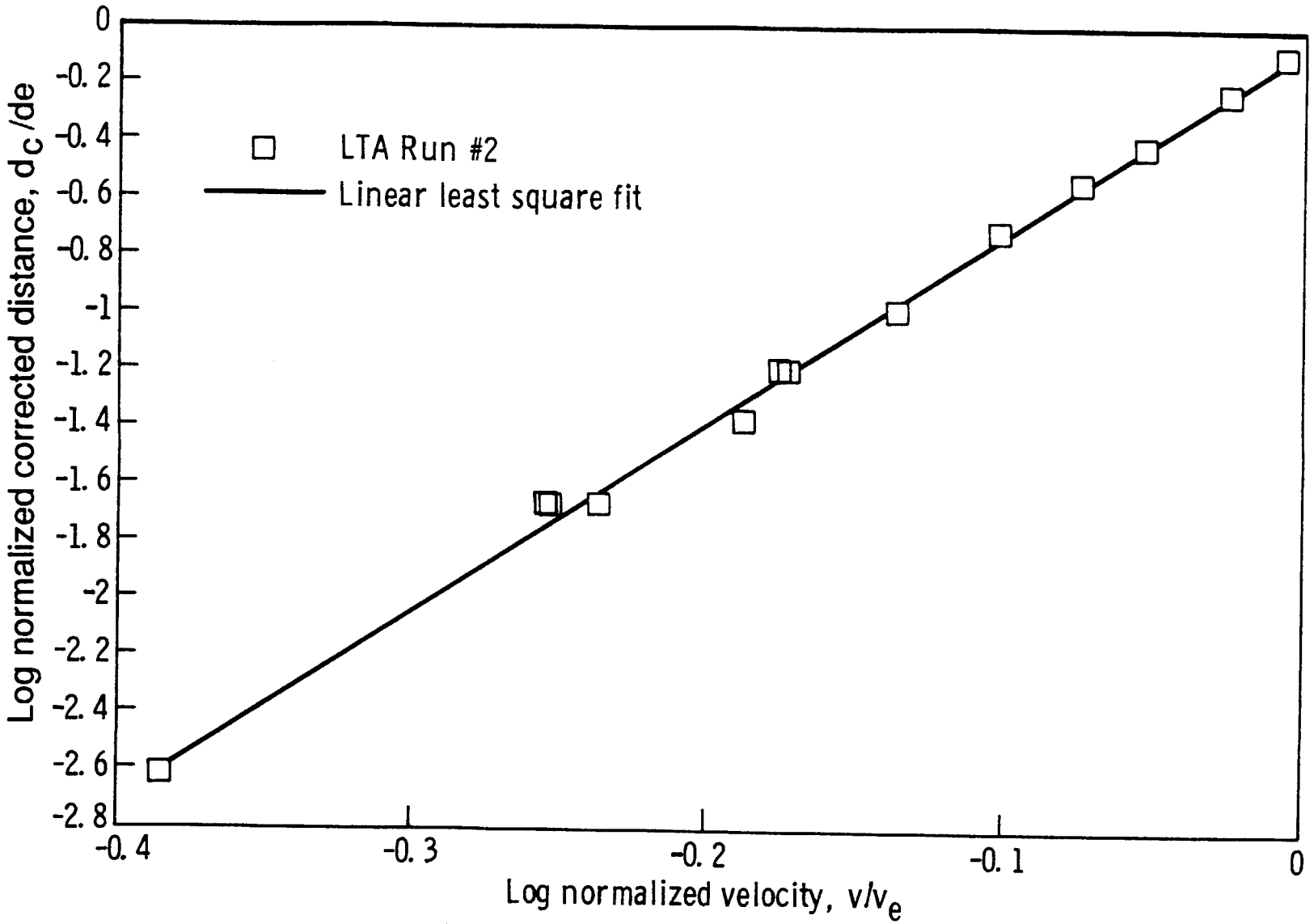

Figure 9. - Log-Log graph of LTA data Run #2 for velocity profile in the turbulent boundary layer using corrected distance measurements.

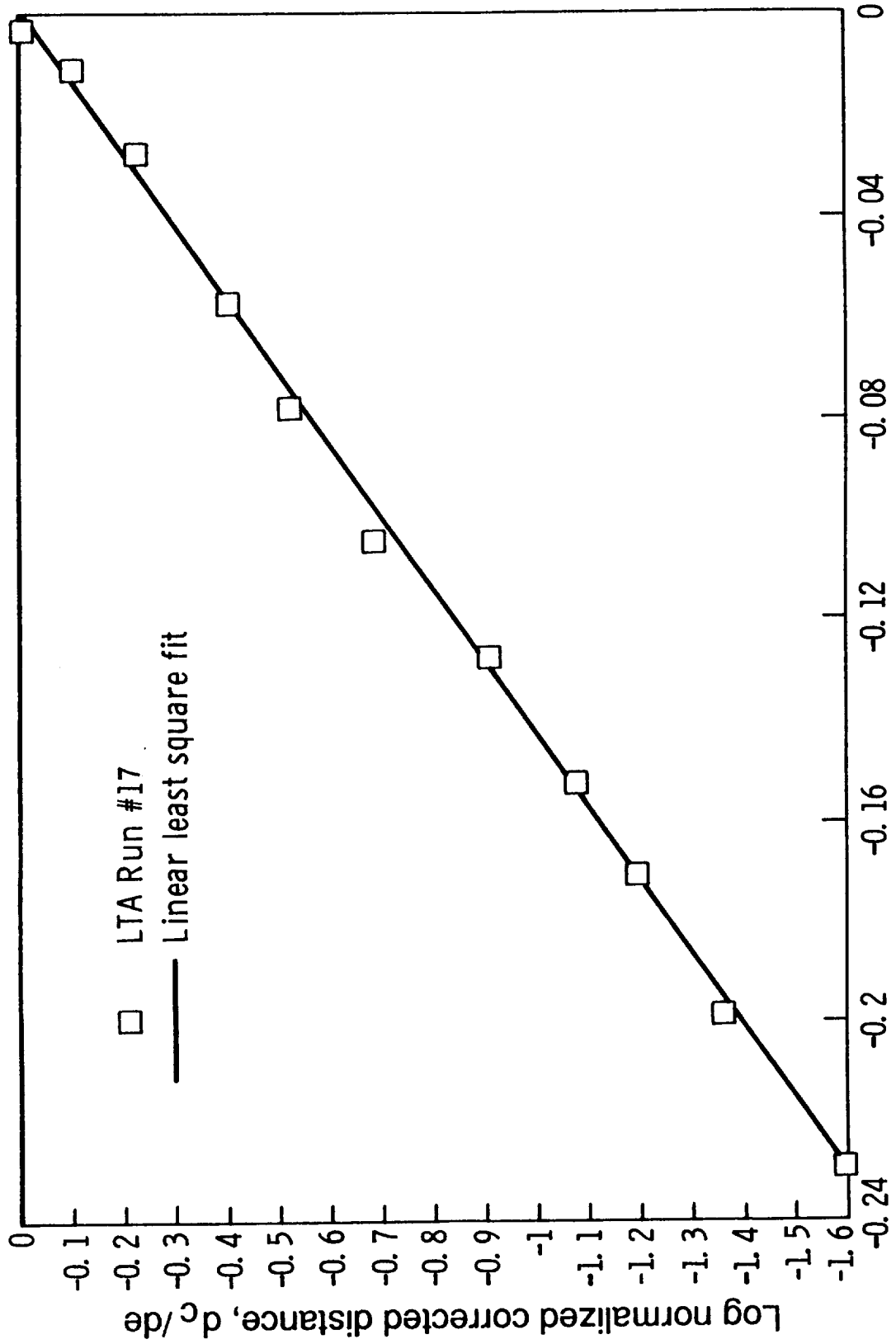

Figure 10. - Log-Log graph of LTA data Run # 17 for velocity profile in the turbulent boundary layer using corrected distance measurements.

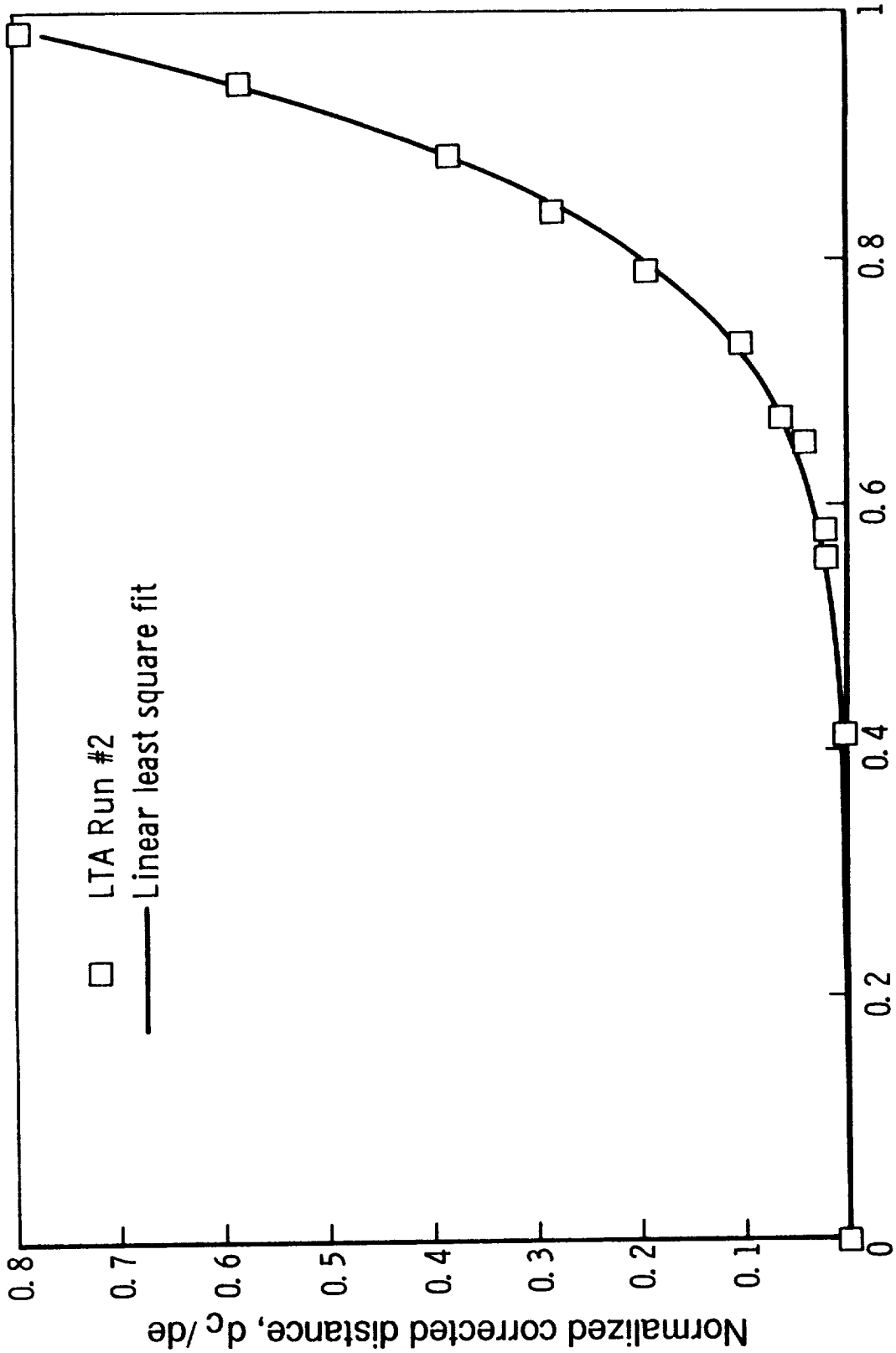

Figure 11. - Linear graph of LTA Data Run # 2 for velocity profile in the turbulent boundary layer using corrected distance measurements.

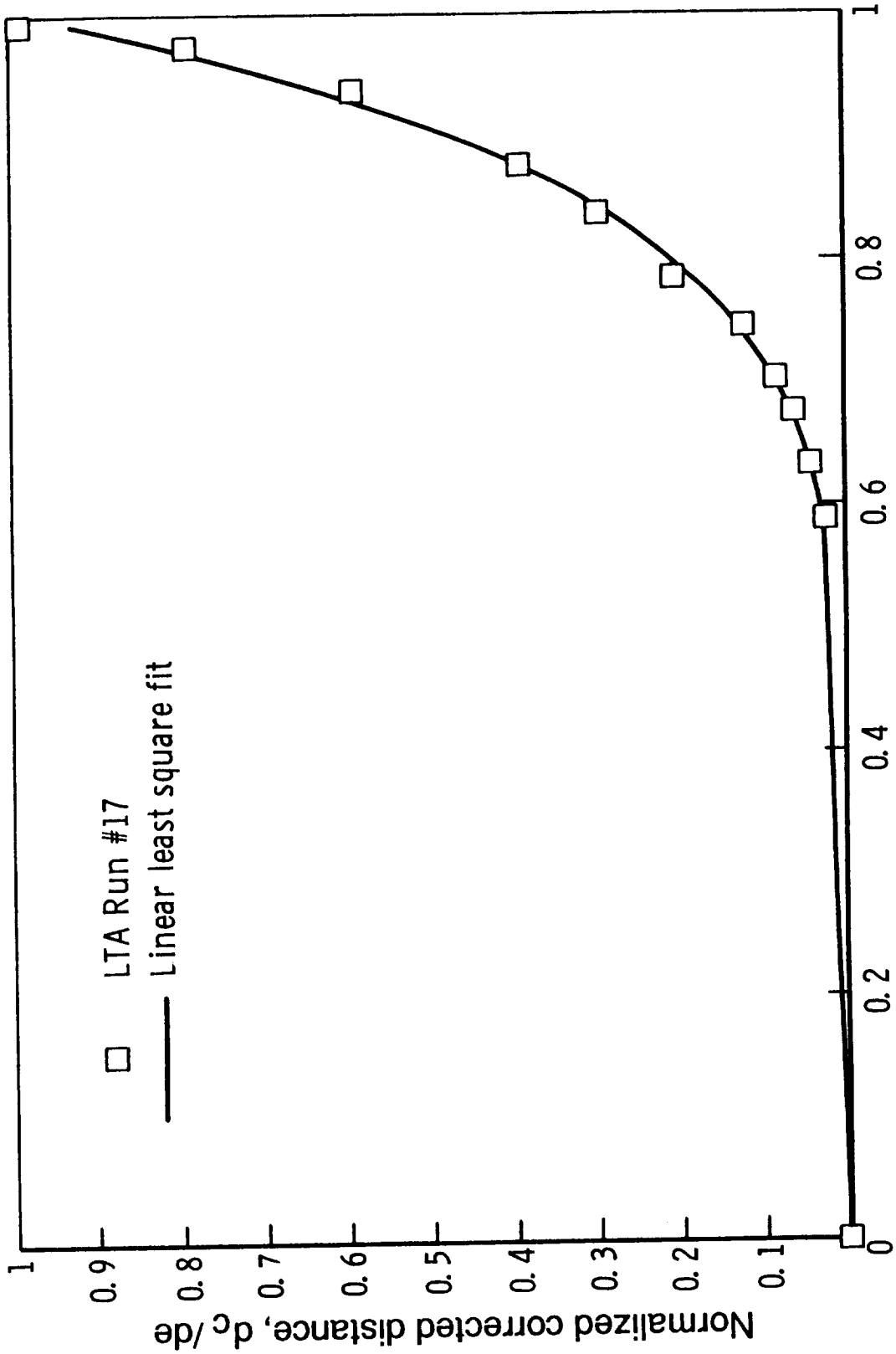

Figure 12. - Linear graph of LTA data Run # 17 for velocity profile in the turbulent boundary layer using corrected distance measurements.

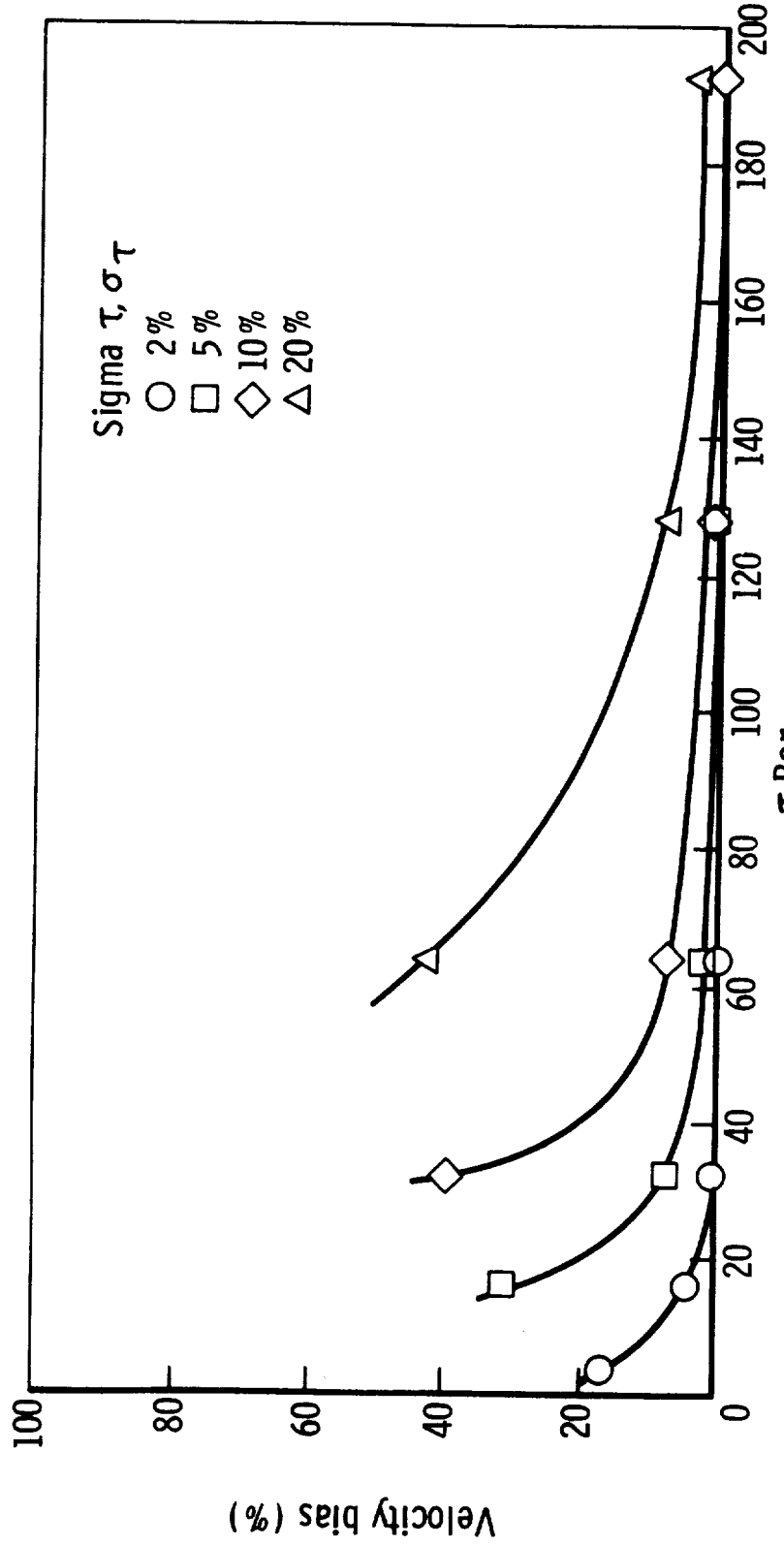

Figure 13. - Graph of velocity bias as a function of the mean transient time for standard deviation of mean transient time of 2, 5, 10, and 20 percent.

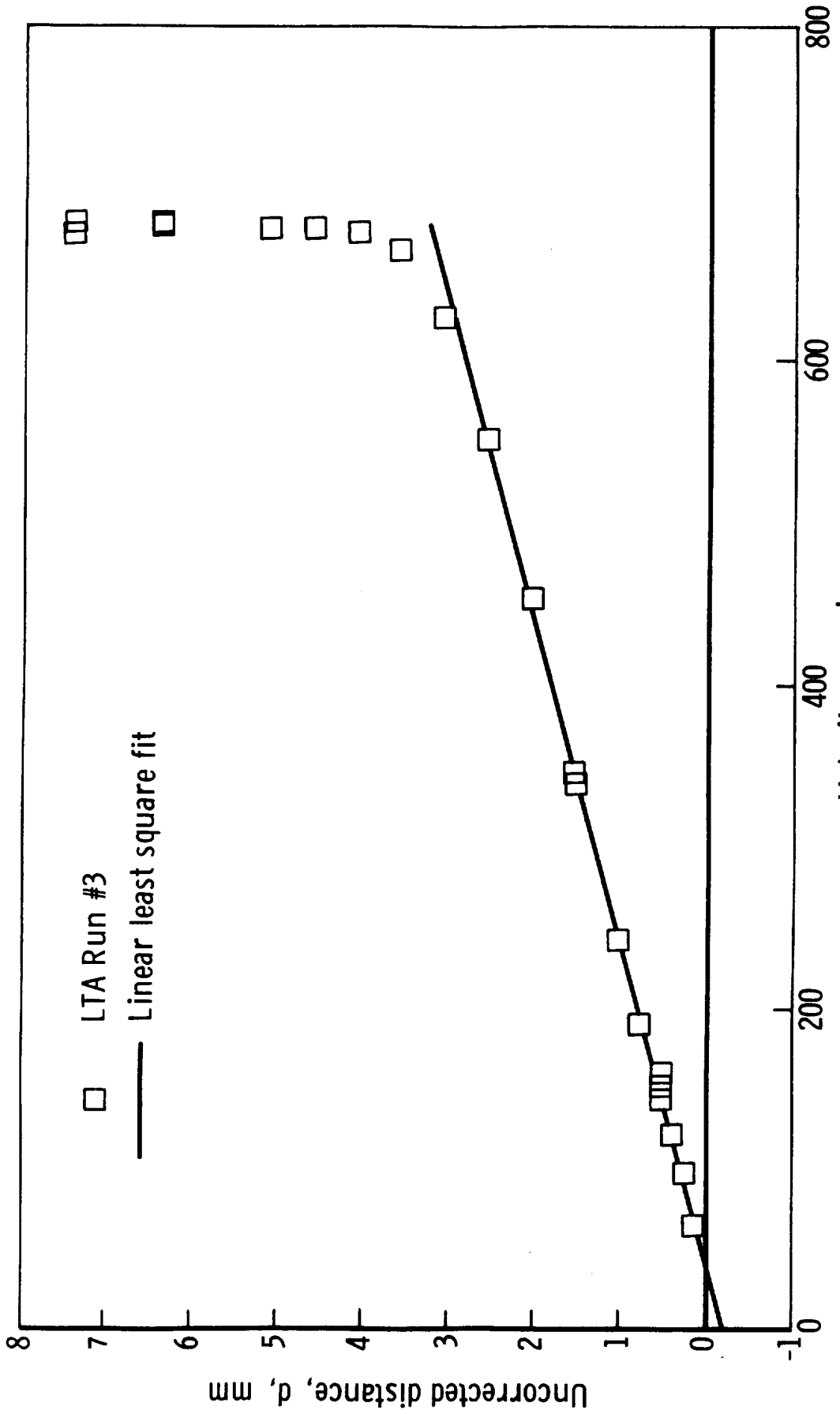

Figure 14. - Linear graph of LTA Run # 3 for velocity profile in the laminar boundary layer using uncorrected distance measurements.

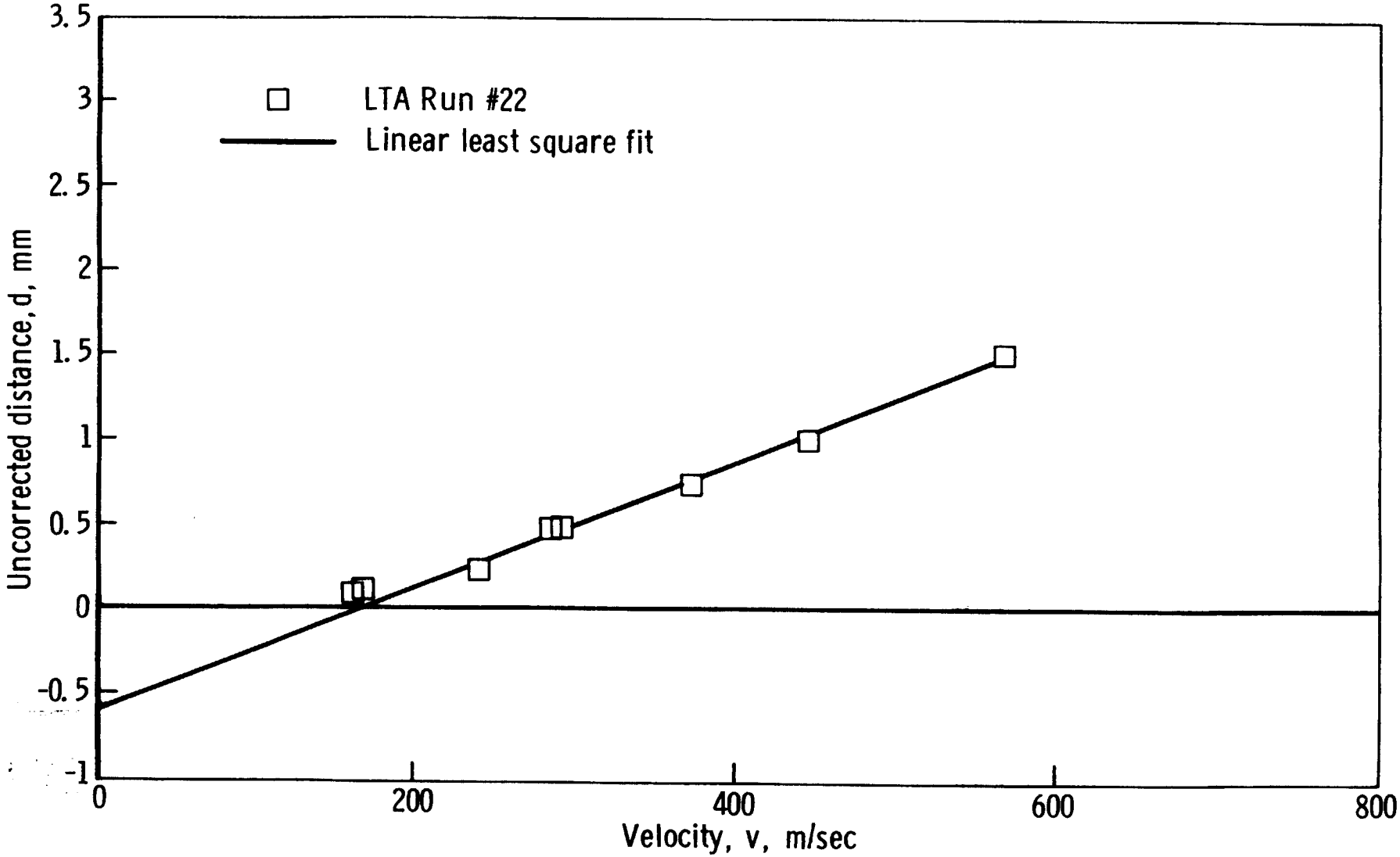

Figure 15. - Linear graph of LTA Run # 22 for velocity profile in the laminar boundary layer using uncorrected distance measurements.

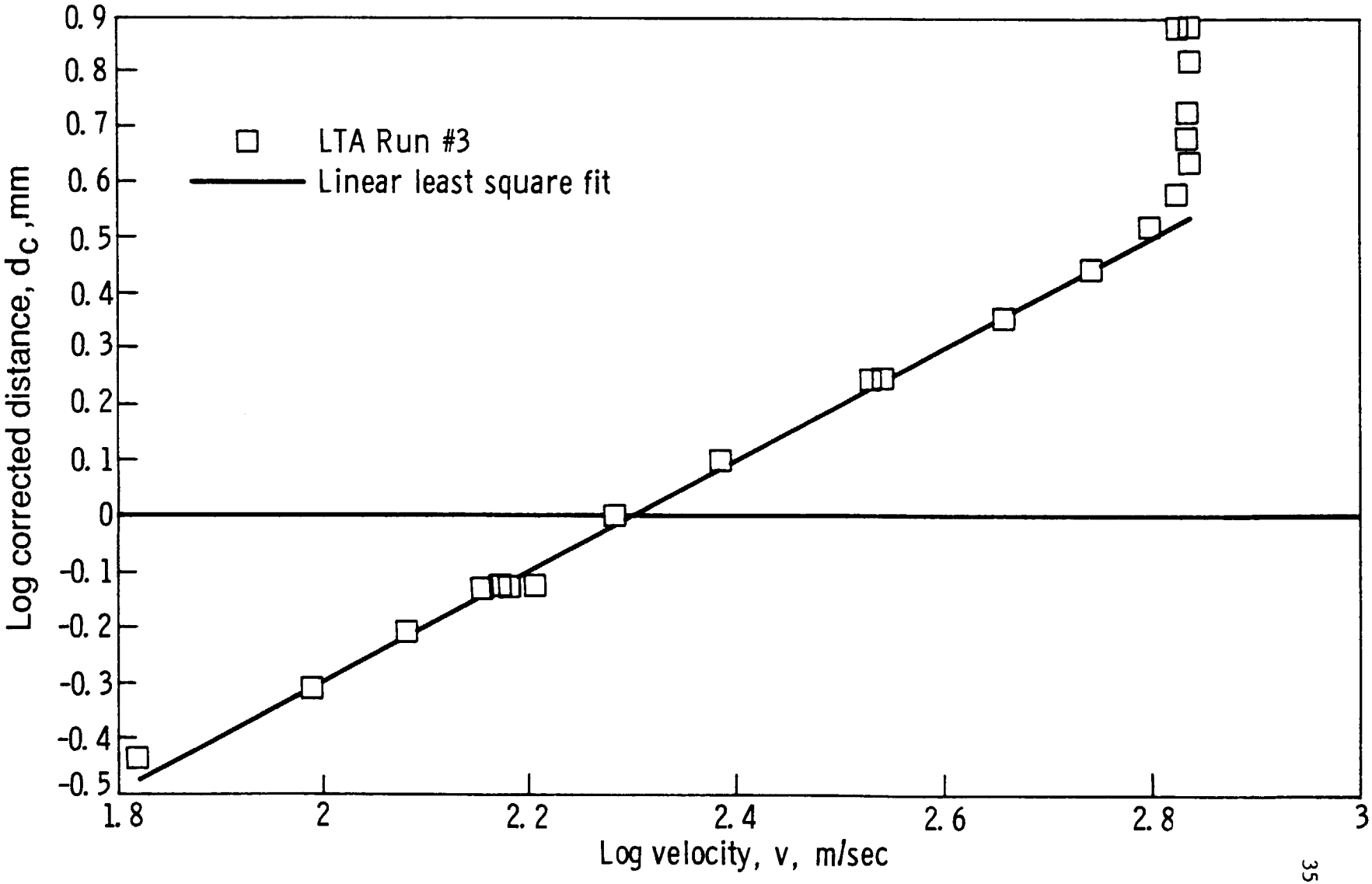

Figure 16. - Log-Log graph of LTA Run # 3 for velocity profile in the laminar boundary layer using corrected distance measurements. Results of velocity space analyses.

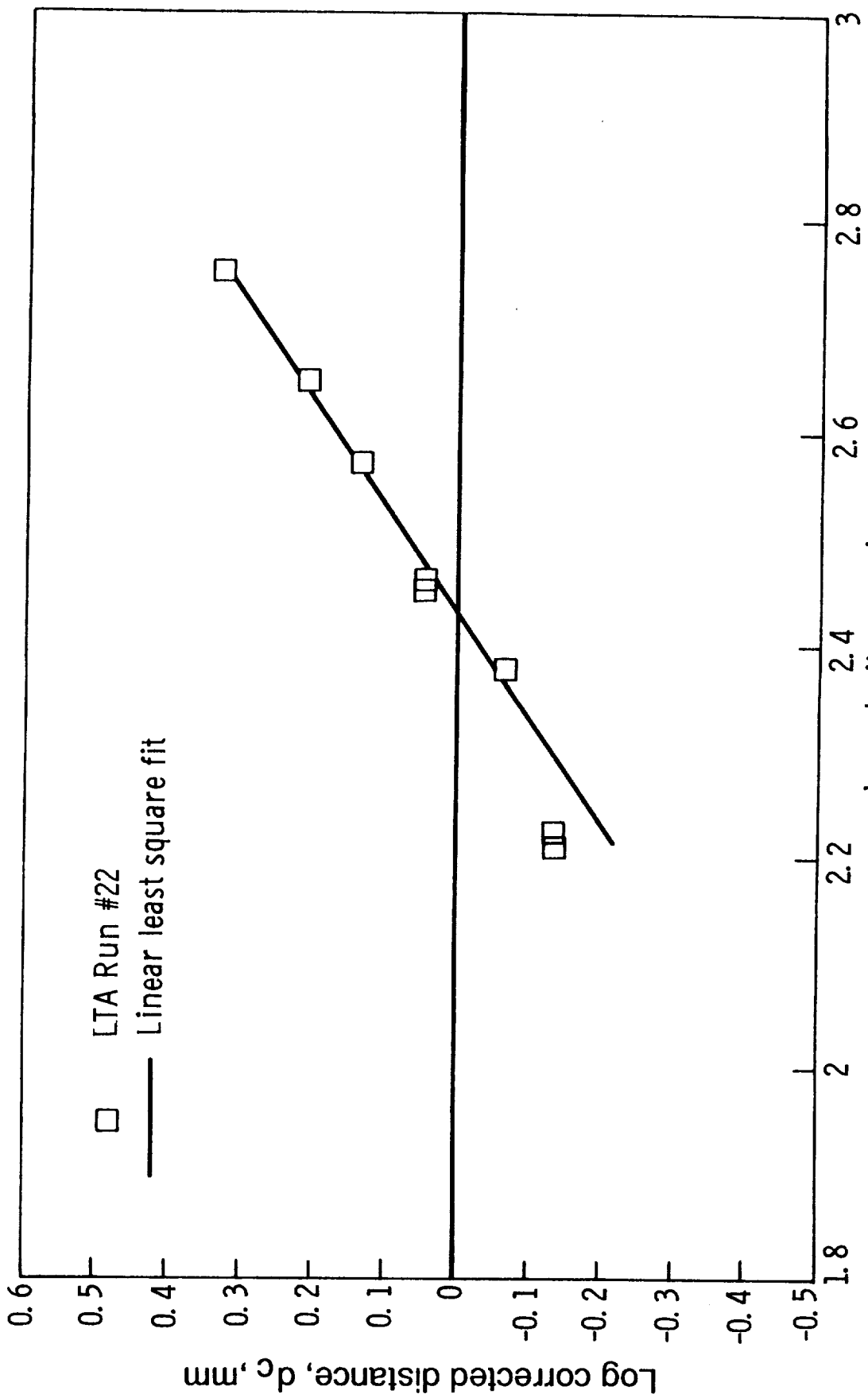

Figure 17. - Log-Log graph of LTA Run # 22 for velocity profile in the laminar boundary layer using corrected distance measurements. Results of velocity space analyses.

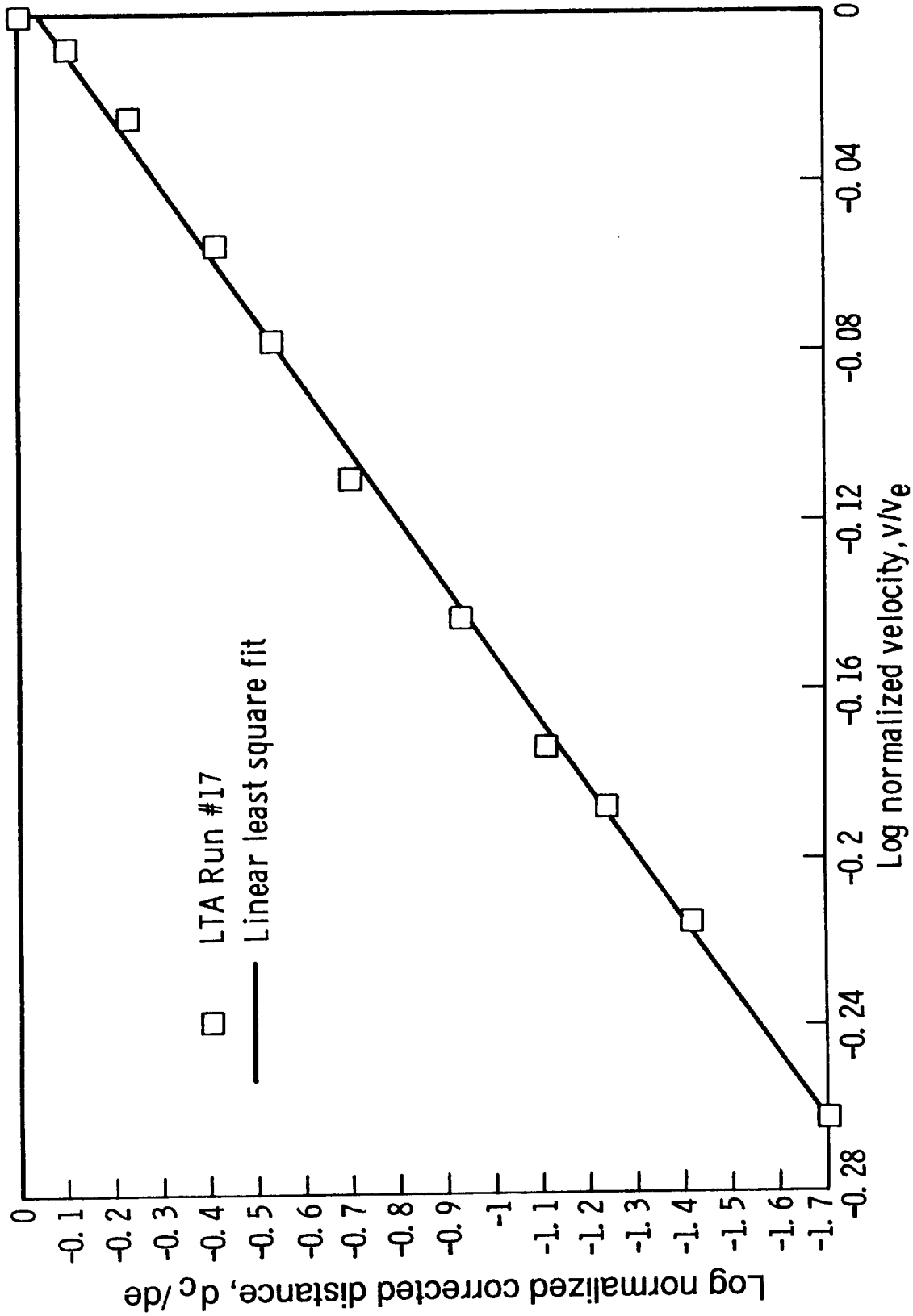

Figure 13. - Log-Log graph of LTA Run # 17 for velocity profile in the turbulent boundary layer using corrected distance measurements. Results of velocity space analyses.

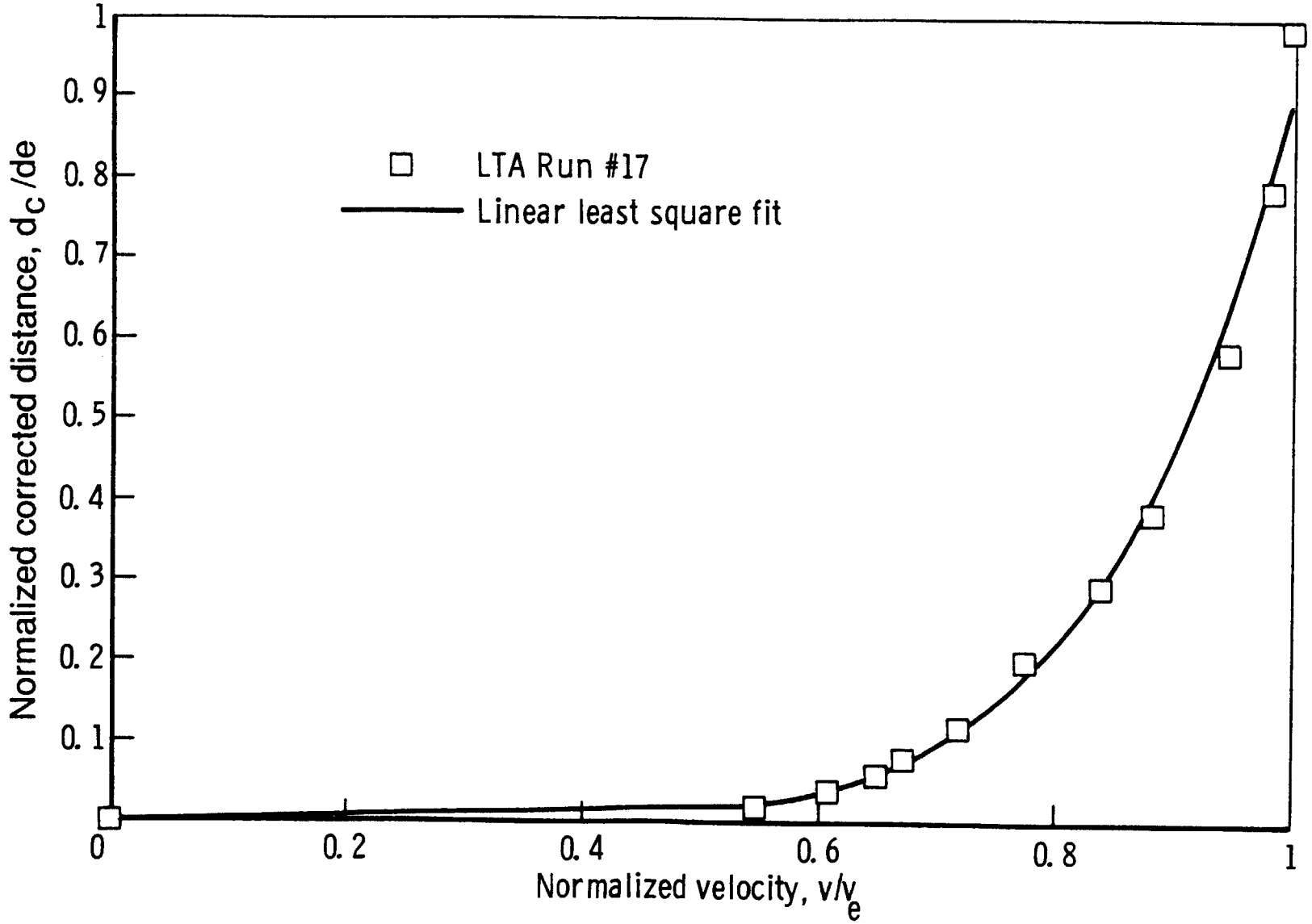

Figure 19. - Linear graph of LTA Run # 17 for velocity profile in the turbulent boundary layer using corrected distance measurements. Results of velocity space analyses.

APPENDICES

Appendices A, B, and C contain Tau space correlograms of run numbers 3, 22, and 17 respectively. Each appendix incorporates a tabulation of the calculated mean velocity values determined from Tau and velocity space data. Each result in the listing includes the uncorrected distance above the model and an experiment number. Following the tabulations, correlograms of data obtained in Tau space and the companion transformed velocity space correlograms are presented. These correlograms are keyed to the tabulations by noting the experiment number shown in the ordinate axis description of the Tau space results, e.g., "NO. OF EVENTS (204.020)." Tau space ordinate values are the number of correlated measurements per period of time. The abscissa description of the Tau space correlograms shows the counting time interval. The correlogram at the bottom of each page is the weighted velocity space representations.

APPENDIX A

Table A

	EXP. NO.	Z-POS (mm)	VEL (τ)	VEL (V)
AEDC	204.001	7.37	679.2	678.5
	.008	7.37	685.2	684.3
	.009	6.35	685.2	684.4
	.010	6.35	684.2	683.4
	.011	6.35	683.0	682.1
	.012	5.08	683.1	682.2
	.013	4.57	682.6	681.7
	.014	4.06	680.6	679.6
	.015	3.56	668.1	667.5
	.016	3.05	629.0	627.4
	.017	2.54	554.3	551.2
	.018	2.03	464.4	455.1
	.019	1.52	349.9	343.5
	.020	1.52	355.7	343.0
	.021	1.52	356.8	546.3
	.022	1.02	245.6	243.5
	.023	.76	197.4	192.3
	.024	.51	147.9	144.1
	.025	.38	126.0	121.2
	.026	.25	103.9	97.6
	.027	.13	89.6	66.3
	.029	.51	156.4	151.6
	.030	.51	155.5	152.6
	.033	.51	166.3	160.9

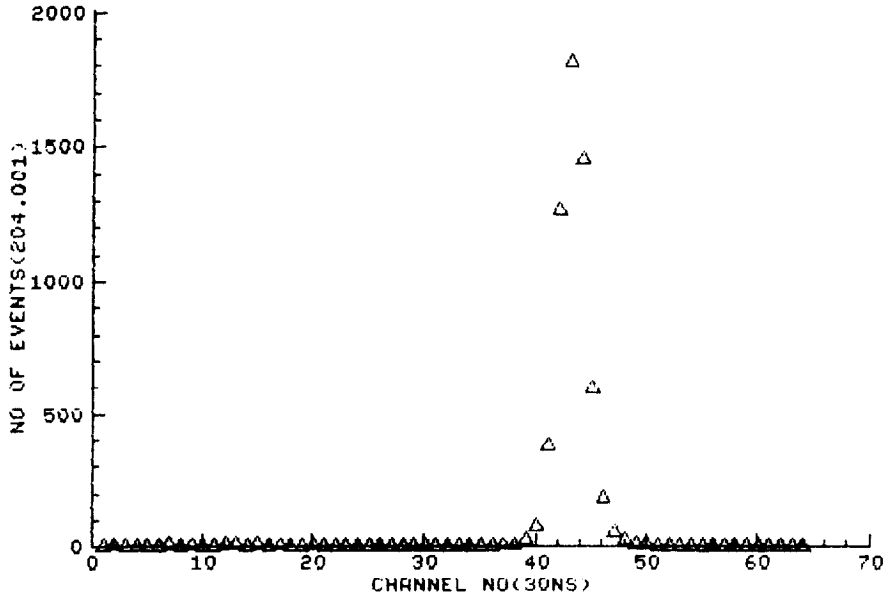
2000
1500
1000
500
0
NO OF EVENTS(204.001)
0
10
20
30
40
50
60
70
CHANNEL NO(30NS)

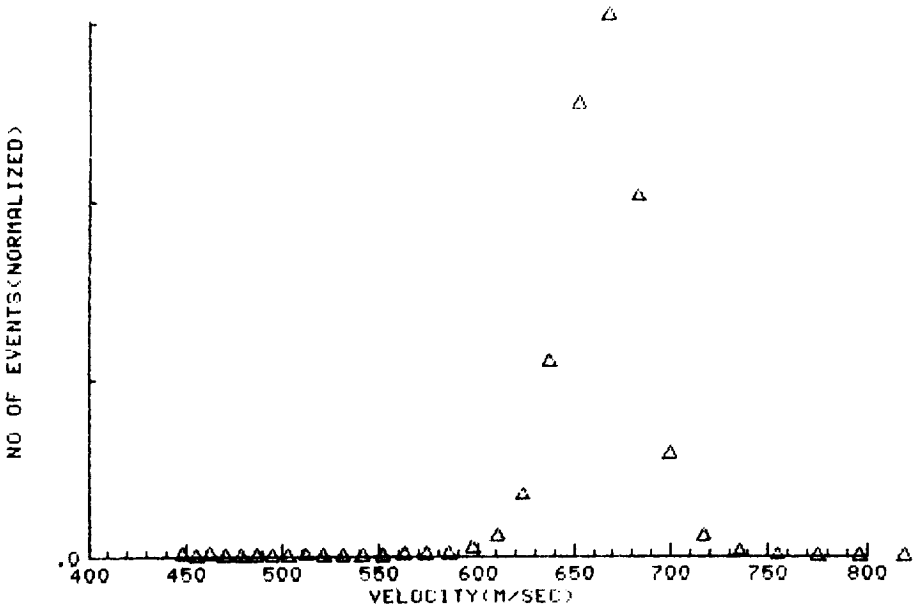
NO OF EVENTS(NORMALIZED)
.0
400
450
500
550
600
650
700
750
800
VELOCITY(M/SEC)

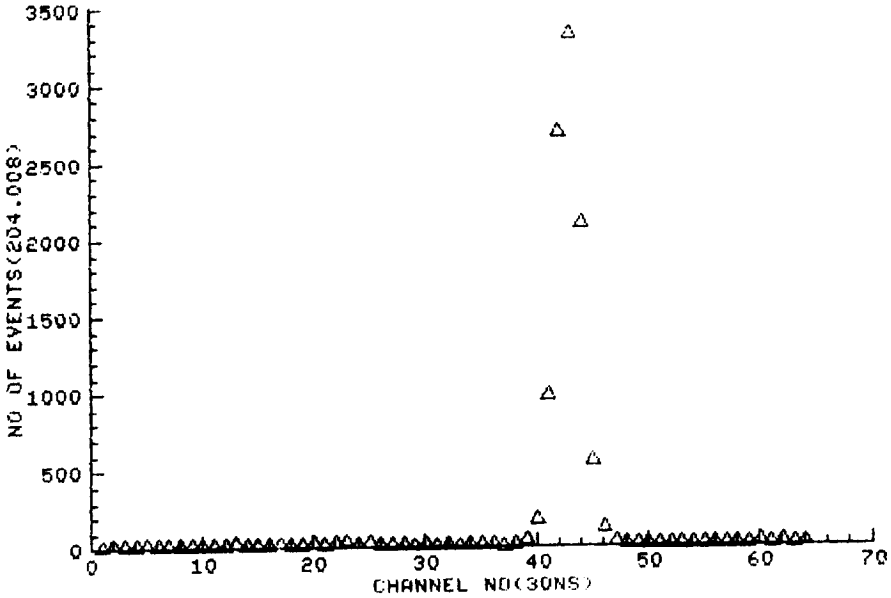
NO OF EVENTS(204.008)
3500
3000
2500
2000
1500
1000
500
0
0
10
20
30
40
50
60
70
CHANNEL NO(30NS)

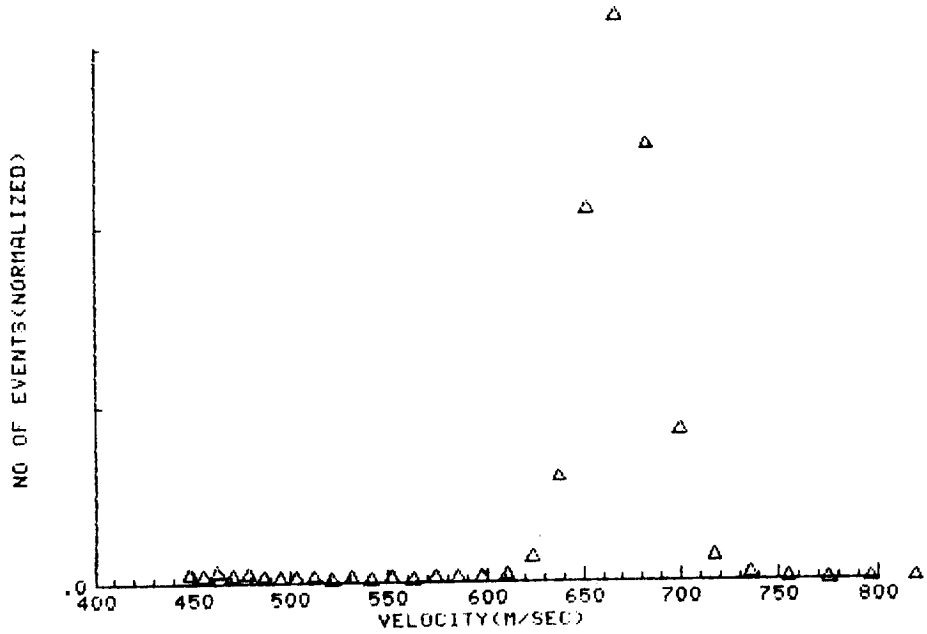
NO OF EVENTS(NORMALIZED)
.0
400
450
500
550
600
650
700
750
800
VELOCITY(M/SEC)

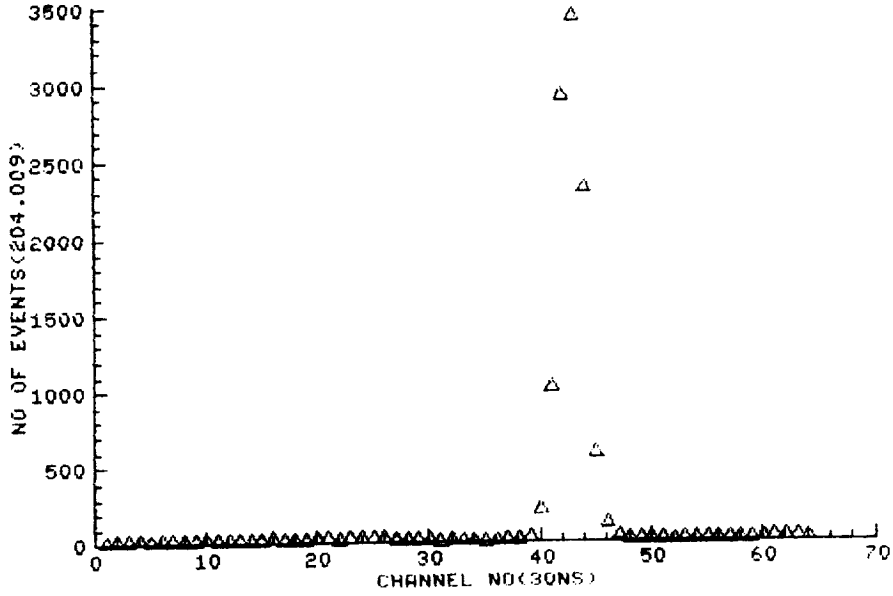
NO OF EVENTS(204.009)
3500
3000
2500
2000
1500
1000
500
0
0
10
20
30
40
50
60
70
CHANNEL NO(30NS)

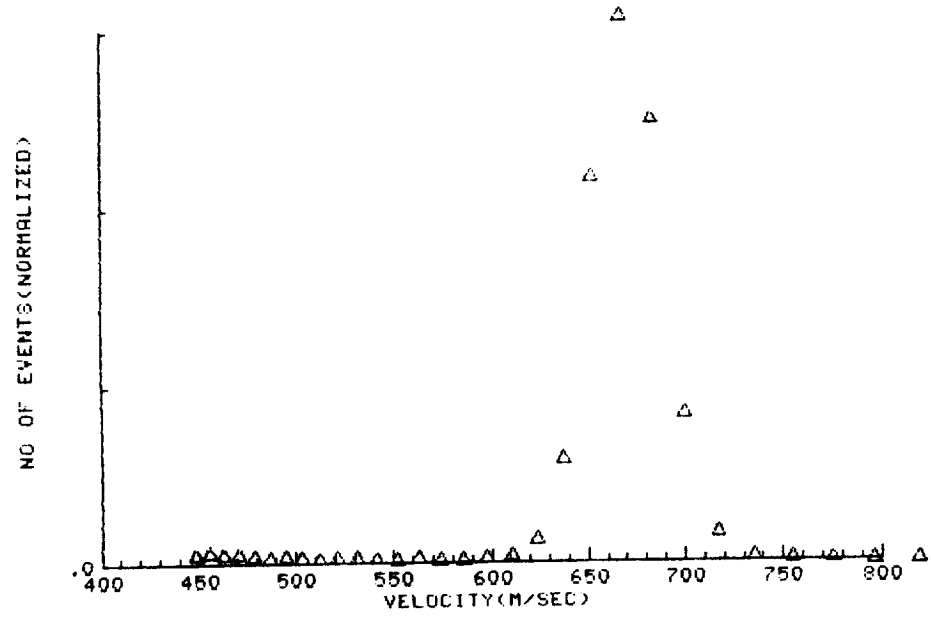
NO OF EVENTS(NORMALIZED)
.0
400
450
500
550
600
650
700
750
800
VELOCITY(M/SEC)

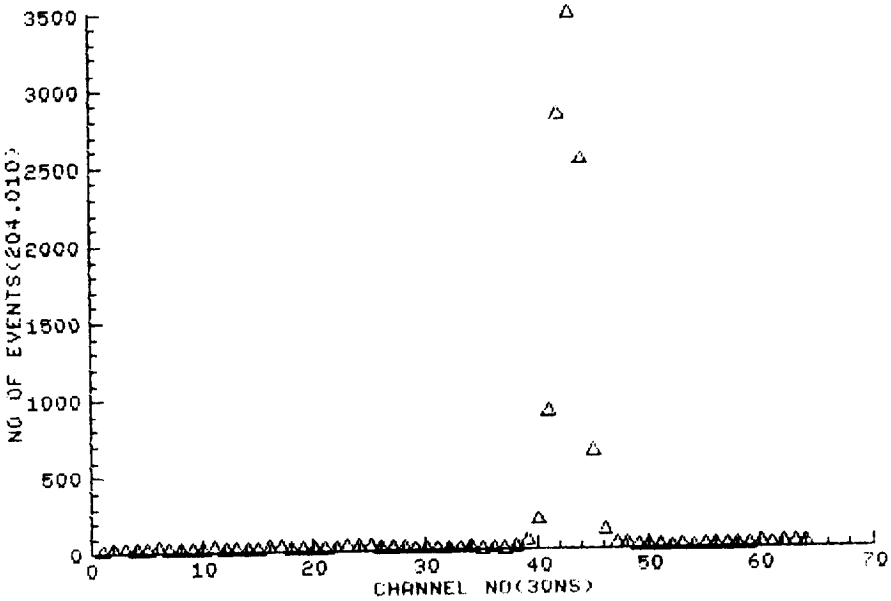
NO OF EVENTS(204.010)
3500
3000
2500
2000
1500
1000
500
0
0
10
20
30
40
50
60
70
CHANNEL NO(30NS)

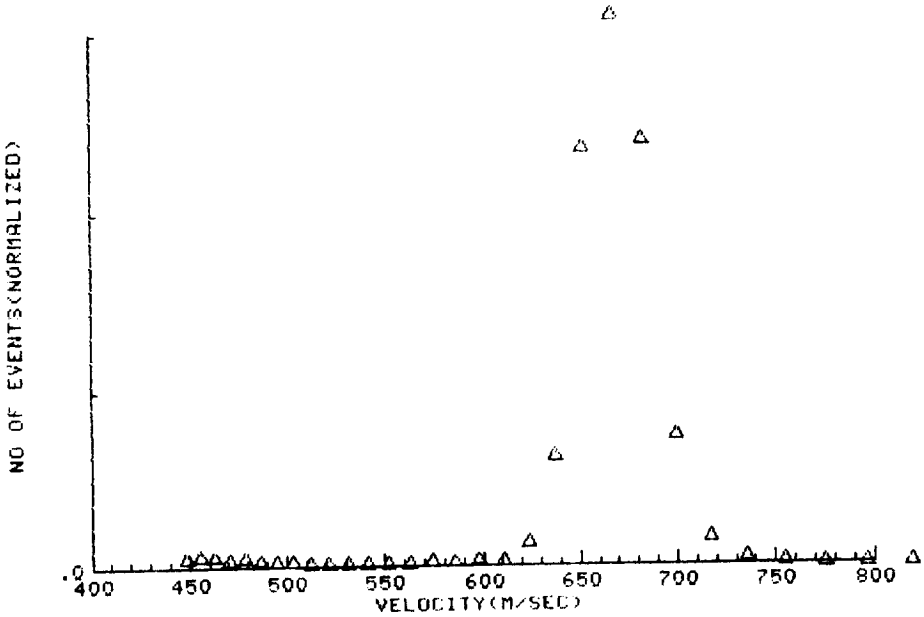
NO OF EVENTS(NORMALIZED)
.0
400
450
500
550
600
650
700
750
800
VELOCITY(M/SEC)

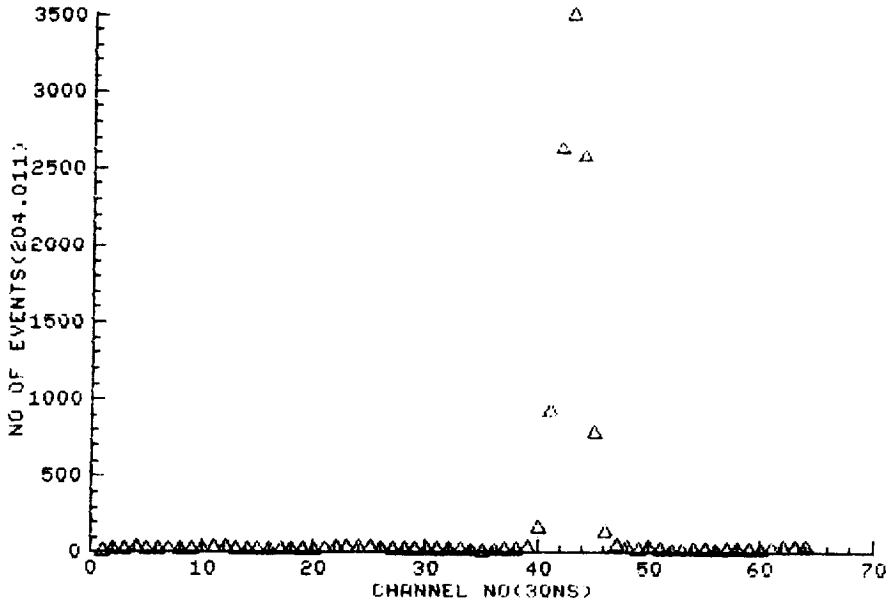
3500
3000
2500
2000
1500
1000
500
0
NO OF EVENTS(204.011)
0
10
20
30
40
50
60
70
CHANNEL NO(30NS)

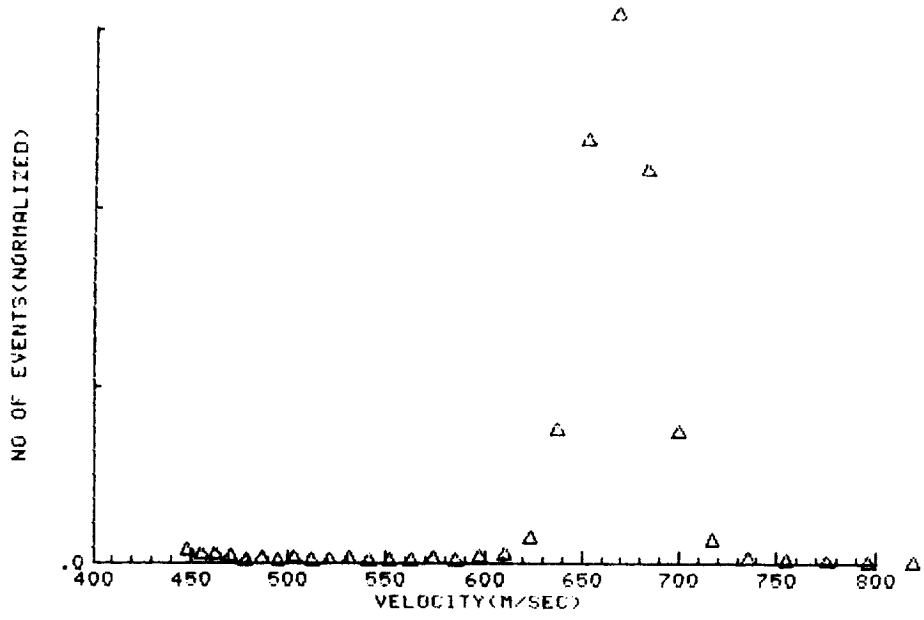
NO OF EVENTS(NORMALIZED)
.0
400
450
500
550
600
650
700
750
800
VELOCITY(M/SEC)

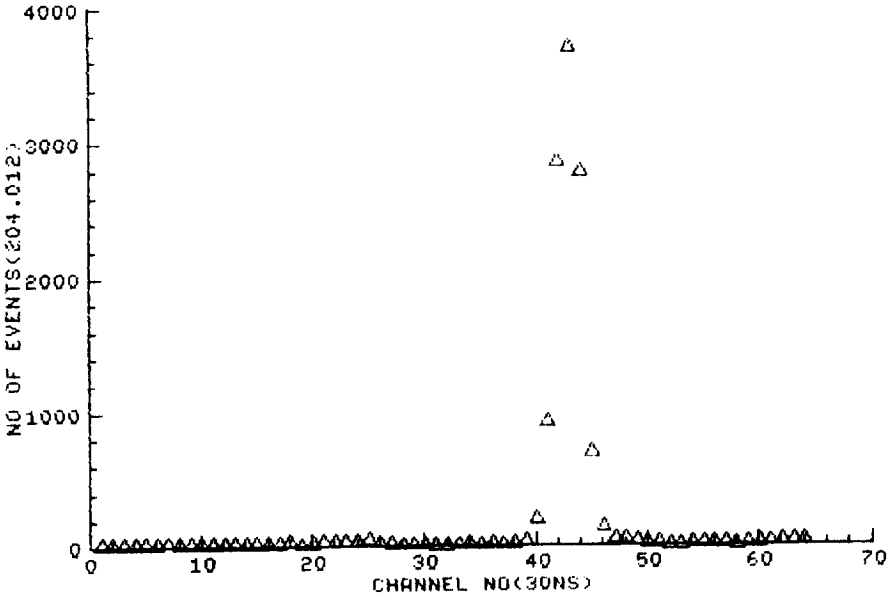
4000
3000
2000
1000
0
NO OF EVENTS(204.012)
0
10
20
30
40
50
60
70
CHANNEL NO(30NS)

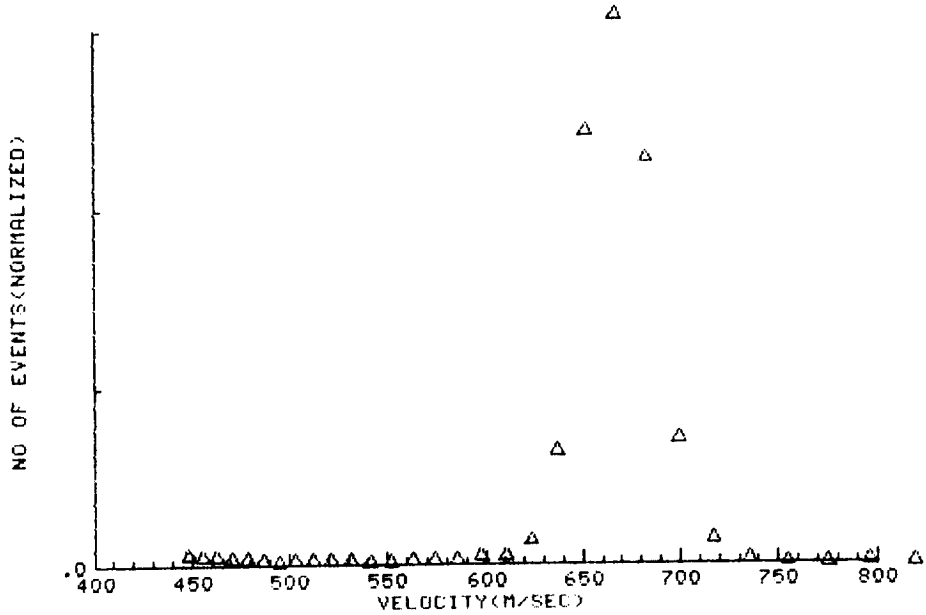
NO OF EVENTS(NORMALIZED)
.0
400
450
500
550
600
650
700
750
800
VELOCITY(M/SEC)

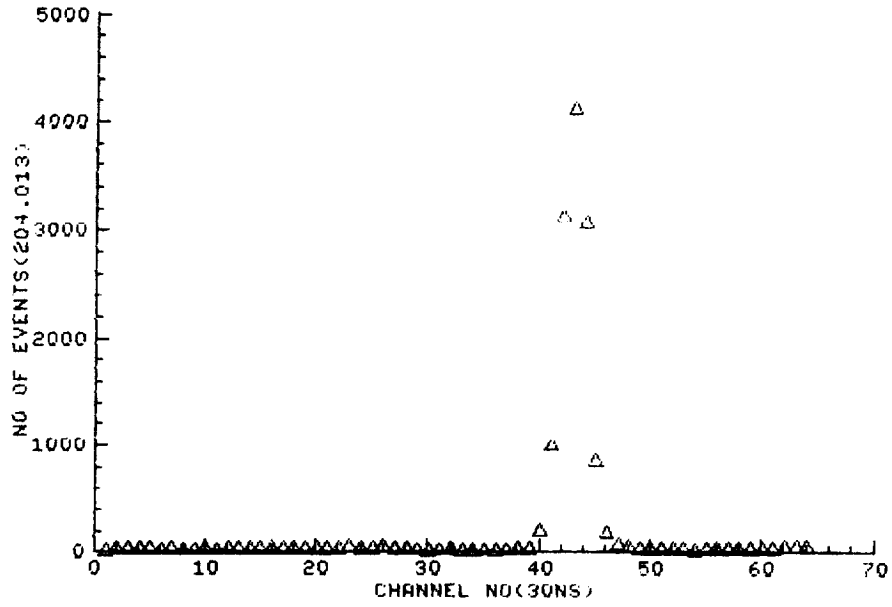
5000
4000
3000
2000
1000
0
NO OF EVENTS(204.013)
0
10
20
30
40
50
60
70
CHANNEL NO(30NS)

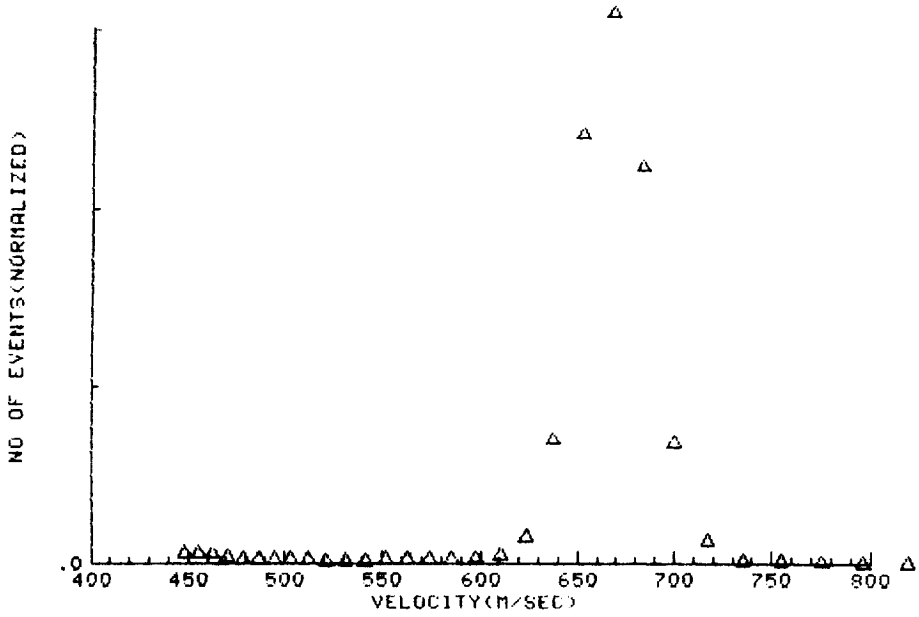
NO OF EVENTS(NORMALIZED)
.0
400
450
500
550
600
650
700
750
800
VELOCITY(M/SEC)

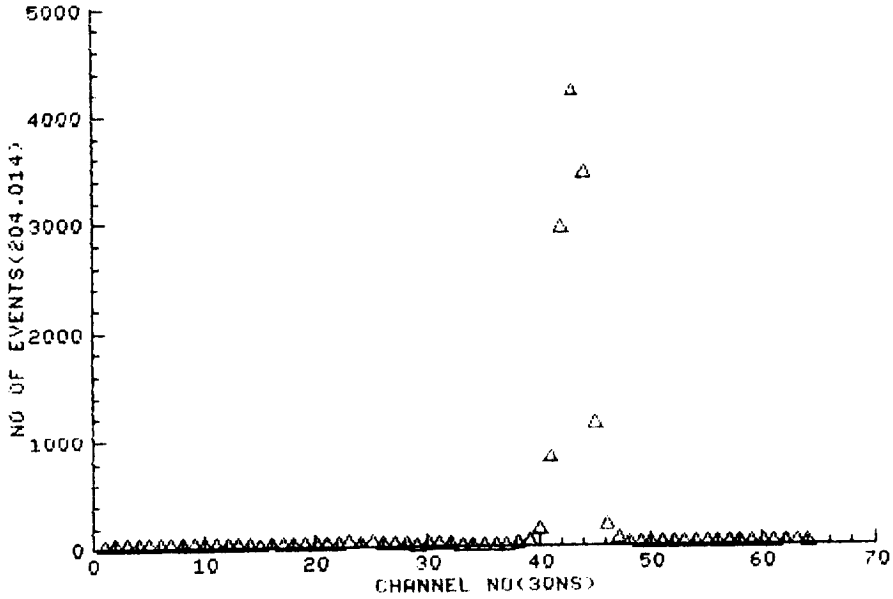
5000
4000
3000
2000
1000
0
NO OF EVENTS(204.014)
0
10
20
30
40
50
60
70
CHANNEL NO(30NS)

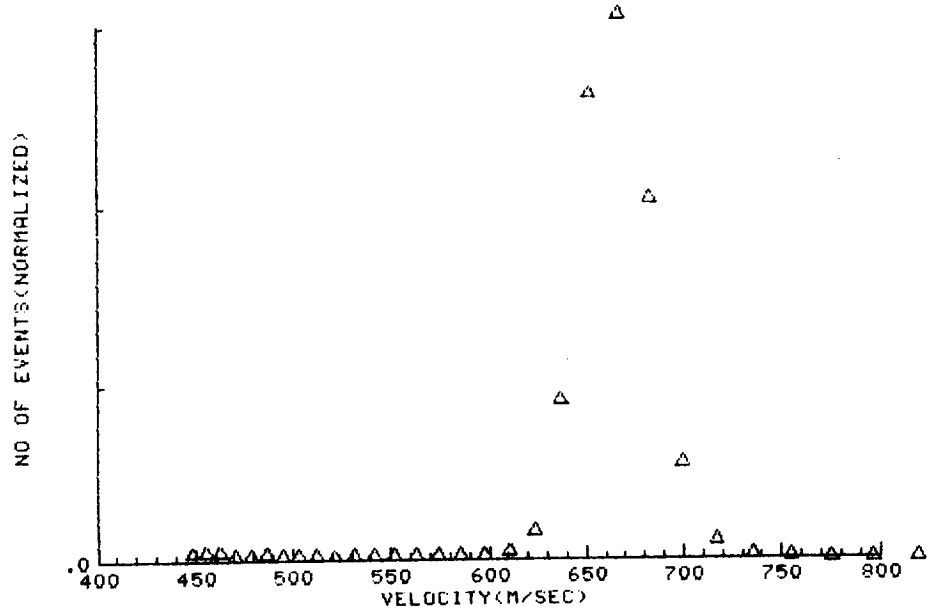
NO OF EVENTS(NORMALIZED)
.0
400
450
500
550
600
650
700
750
800
VELOCITY(M/SEC)

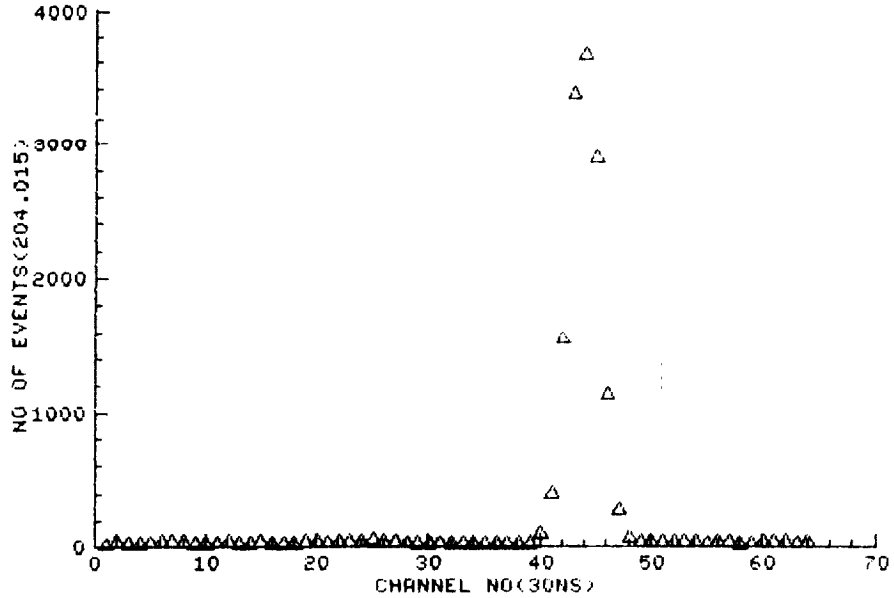
4000
3000
2000
1000
0
NO OF EVENTS(204.015)
0
10
20
30
40
50
60
70
CHANNEL NO(30NS)

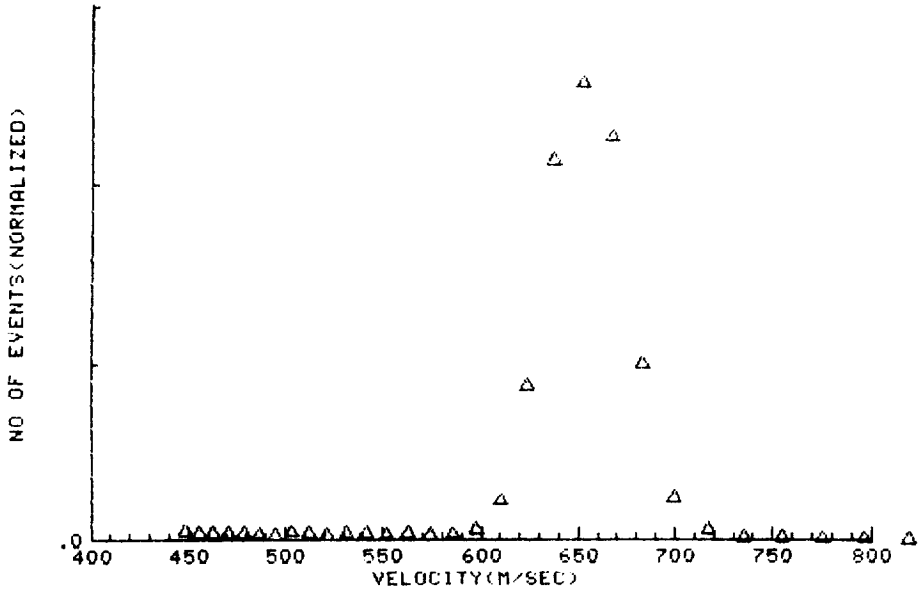
NO OF EVENTS(NORMALIZED)
.0
400
450
500
550
600
650
700
750
800
VELOCITY(M/SEC)

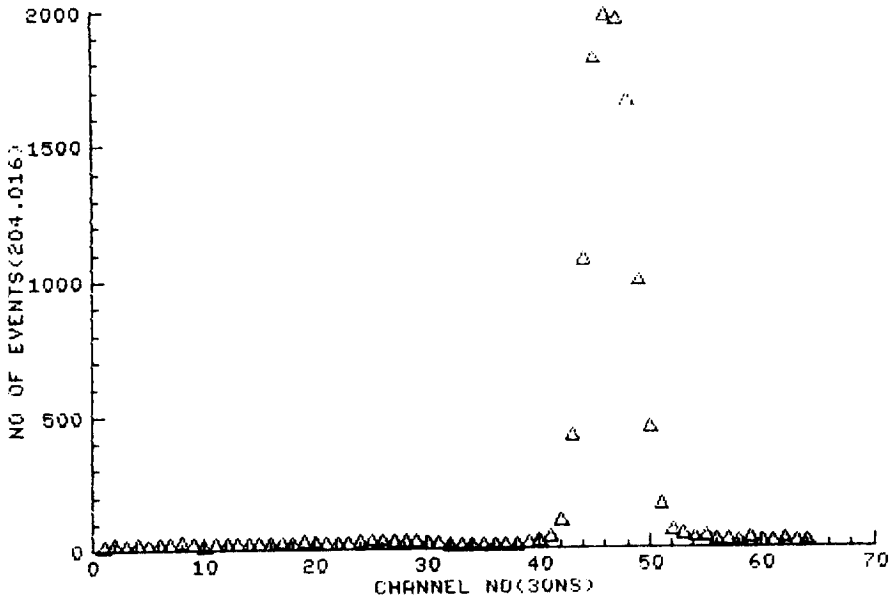
2000
1500
1000
500
0
NO OF EVENTS(204.016)
0
10
20
30
40
50
60
70
CHANNEL NO(30NS)

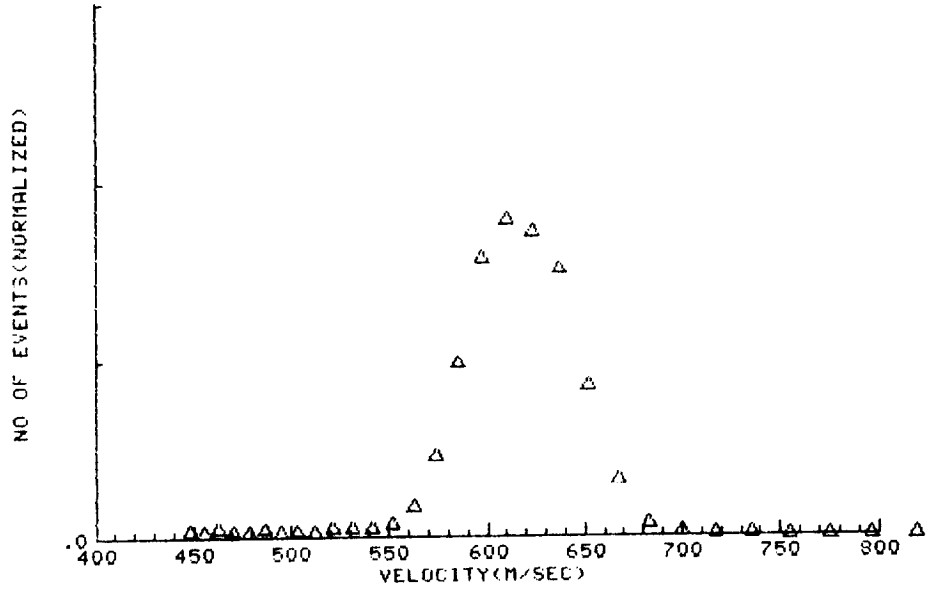
NO OF EVENTS(NORMALIZED)
.0
400
450
500
550
600
650
700
750
800
VELOCITY(M/SEC)

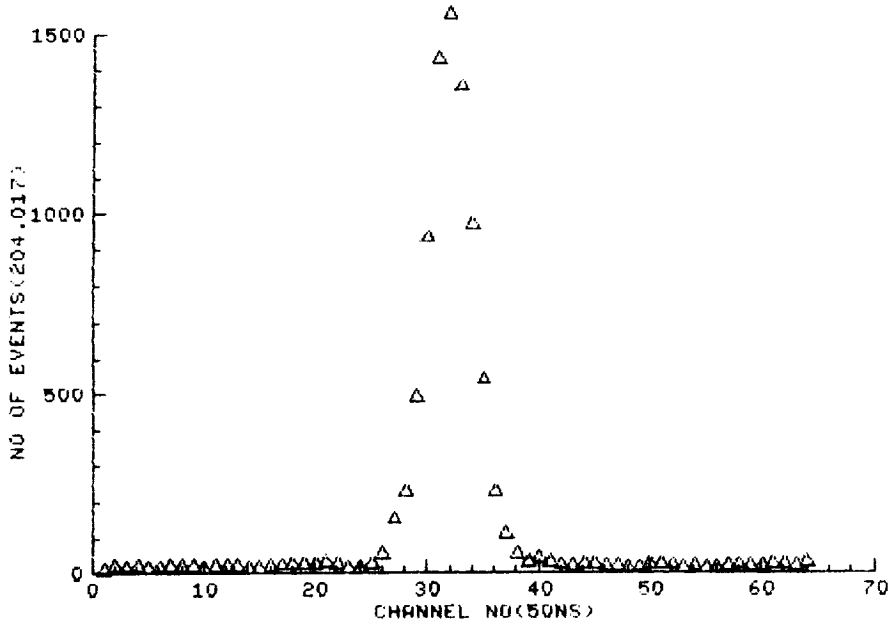
1500
1000
500
0
NO OF EVENTS(204.017)
0
10
20
30
40
50
60
70
CHANNEL NO(50NS)

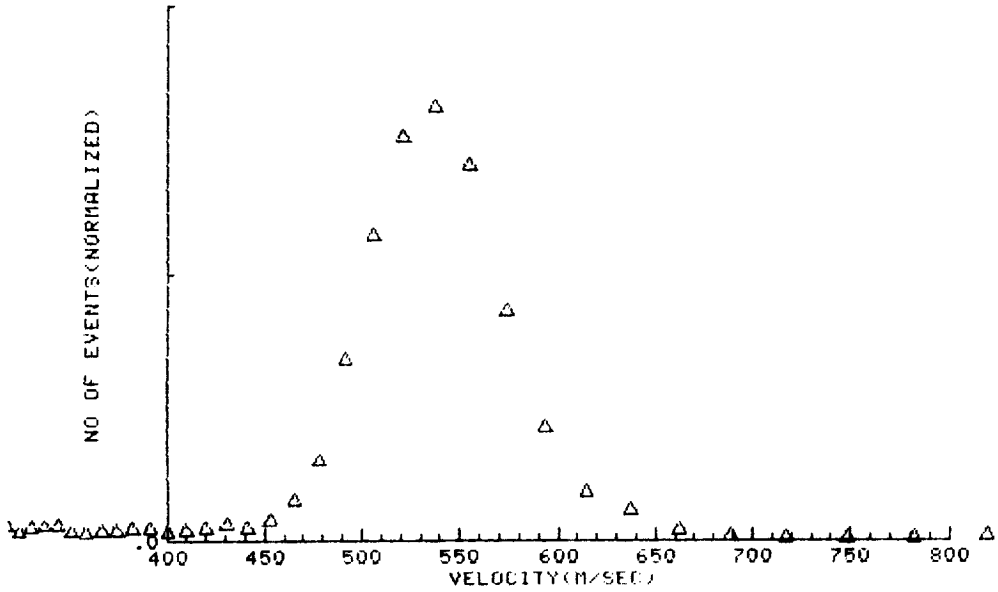
NO OF EVENTS(NORMALIZED)
0
400
450
500
550
600
650
700
750
800
VELOCITY(M/SEC)

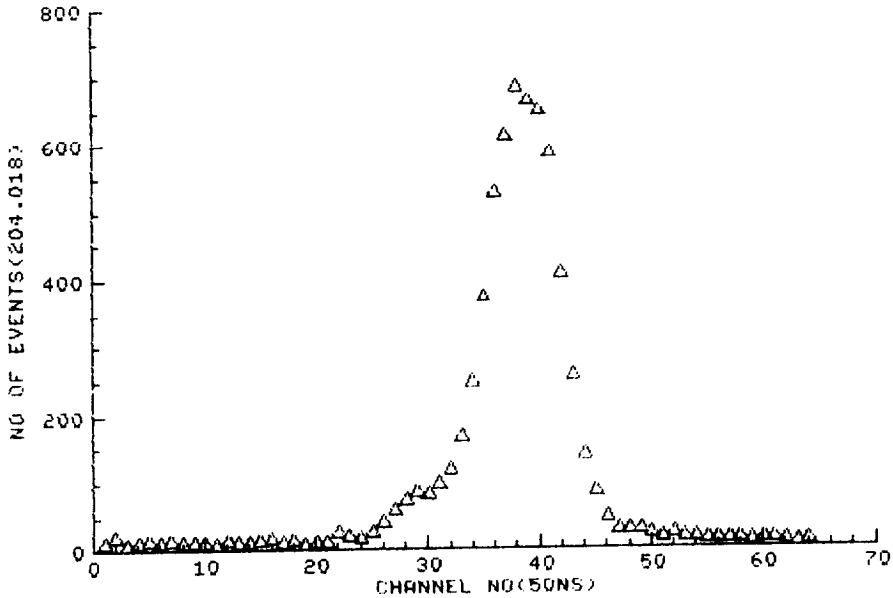
800
600
400
200
0
NO OF EVENTS(204.018)
0
10
20
30
40
50
60
70
CHANNEL NO(50NS)

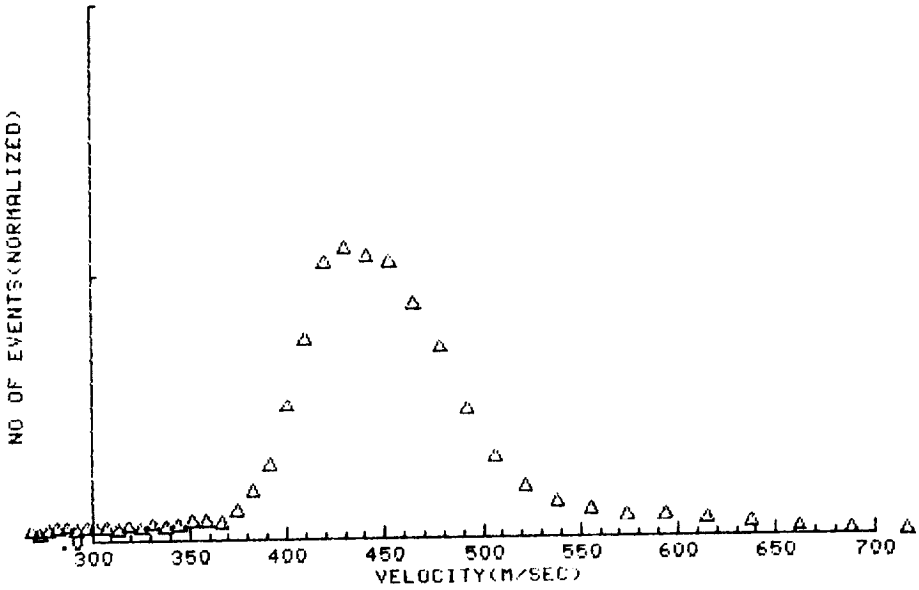
NO OF EVENTS(NORMALIZED)
300
350
400
450
500
550
600
650
700
VELOCITY(M/SEC)

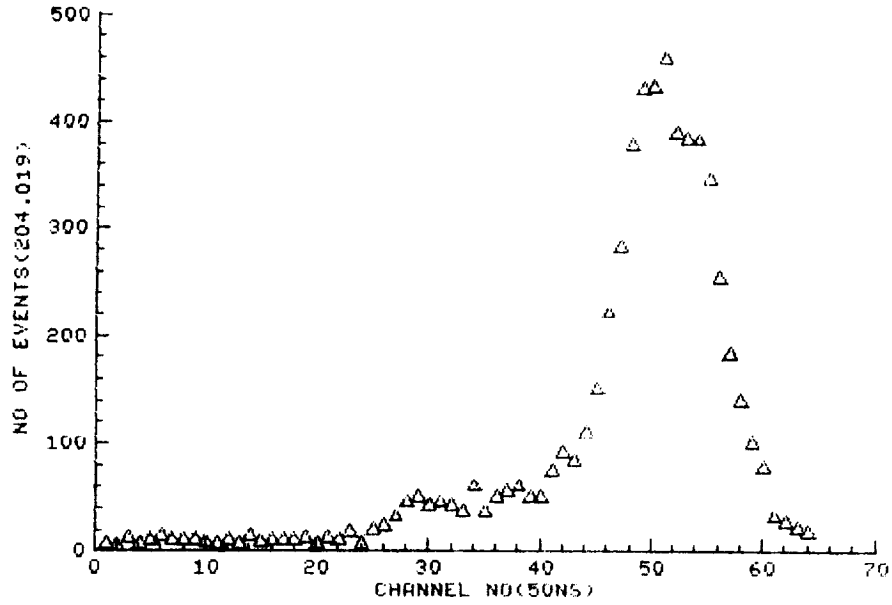
NO OF EVENTS(204.019)
500
400
300
200
100
0
0
10
20
30
40
50
60
70
CHANNEL NO(50NS)

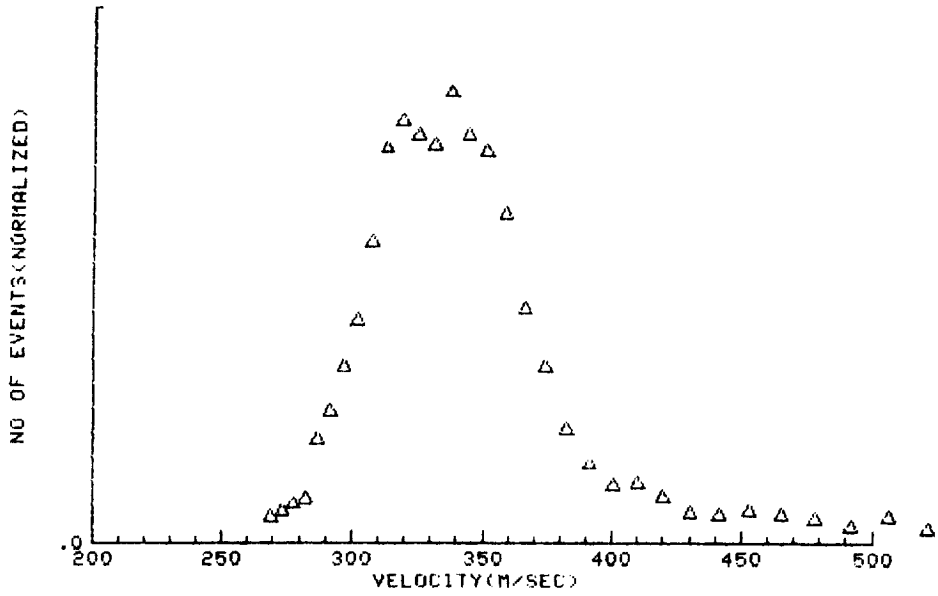
NO OF EVENTS(NORMALIZED)
.0
200
250
300
350
400
450
500
VELOCITY(M/SEC)

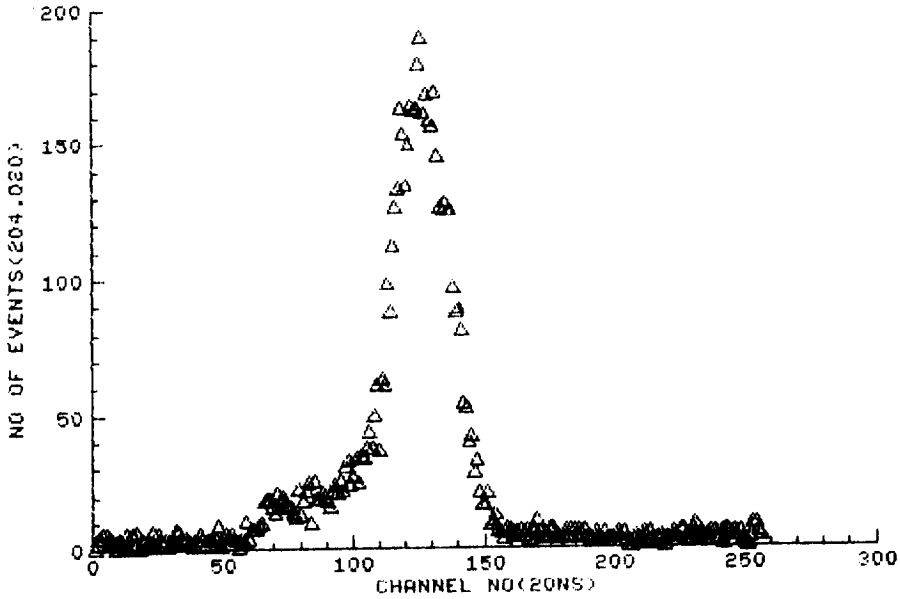
NO OF EVENTS(204.020)
200
150
100
50
0
0
50
100
150
200
250
300
CHANNEL NO(20NS)

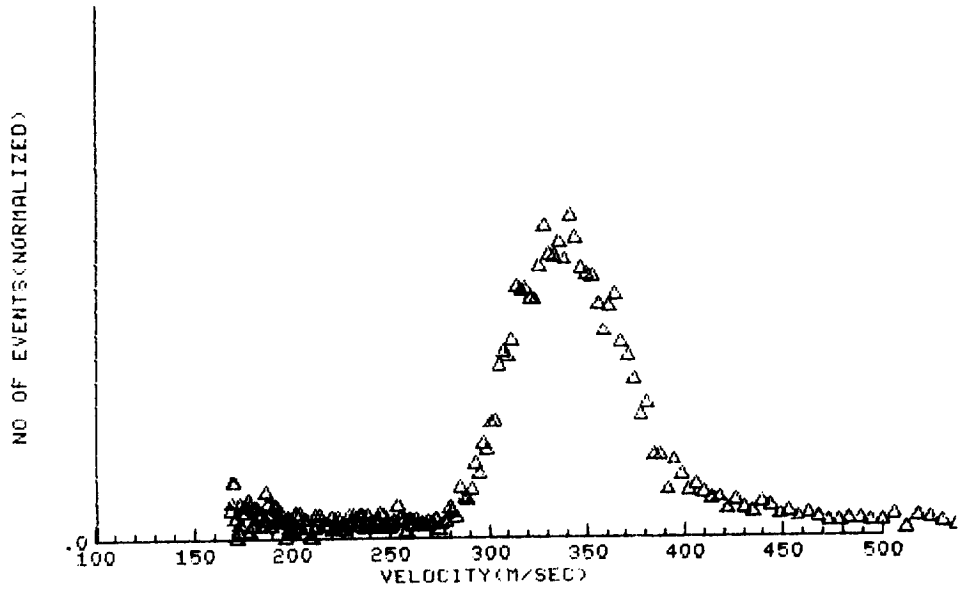
NO OF EVENTS(NORMALIZED)
0
100
150
200
250
300
350
400
450
500
VELOCITY(M/SEC)

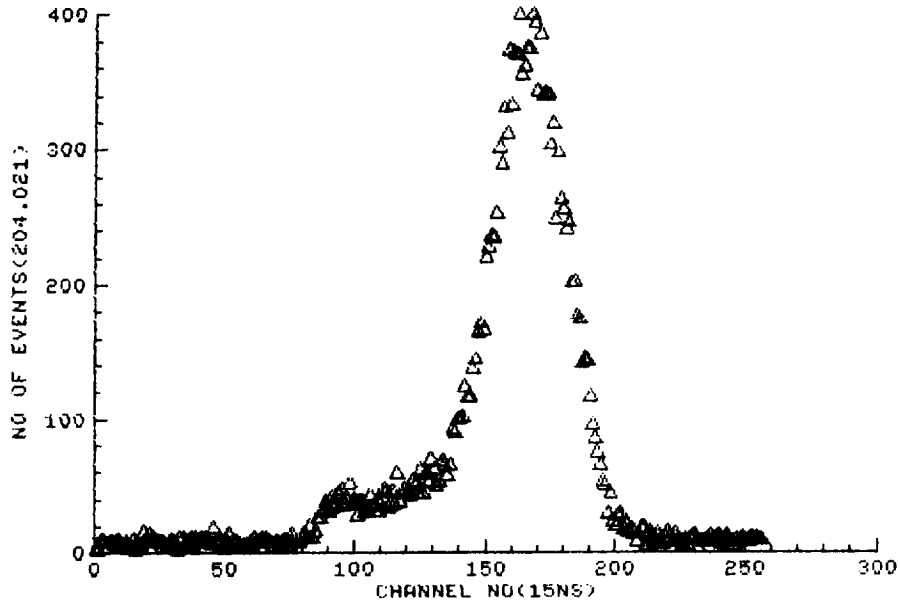
NO OF EVENTS(204.021)
400
300
200
100
0
0
50
100
150
200
250
300
CHANNEL NO(15NS)

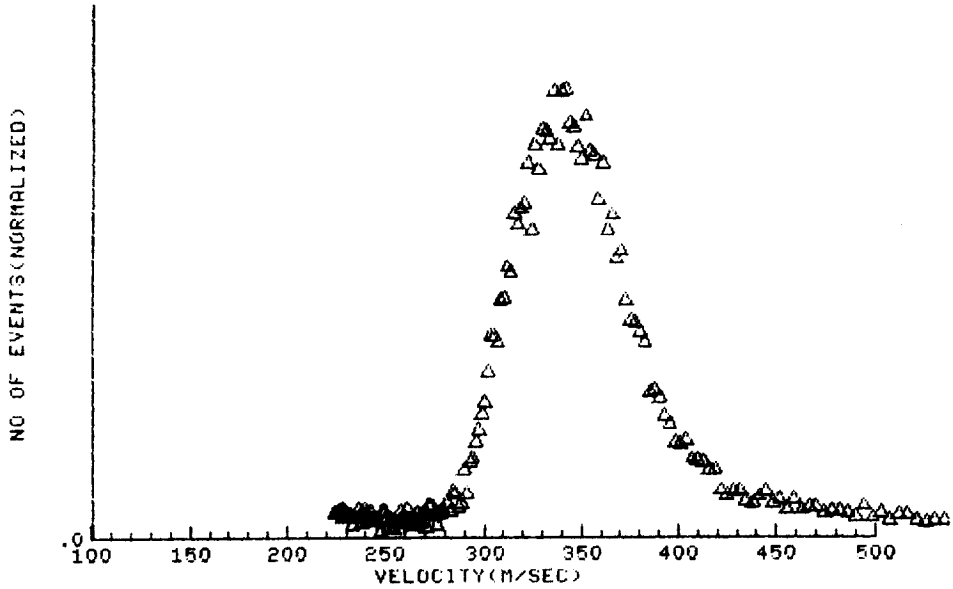
NO OF EVENTS(NORMALIZED)
.0
100
150
200
250
300
350
400
450
500
VELOCITY(M/SEC)

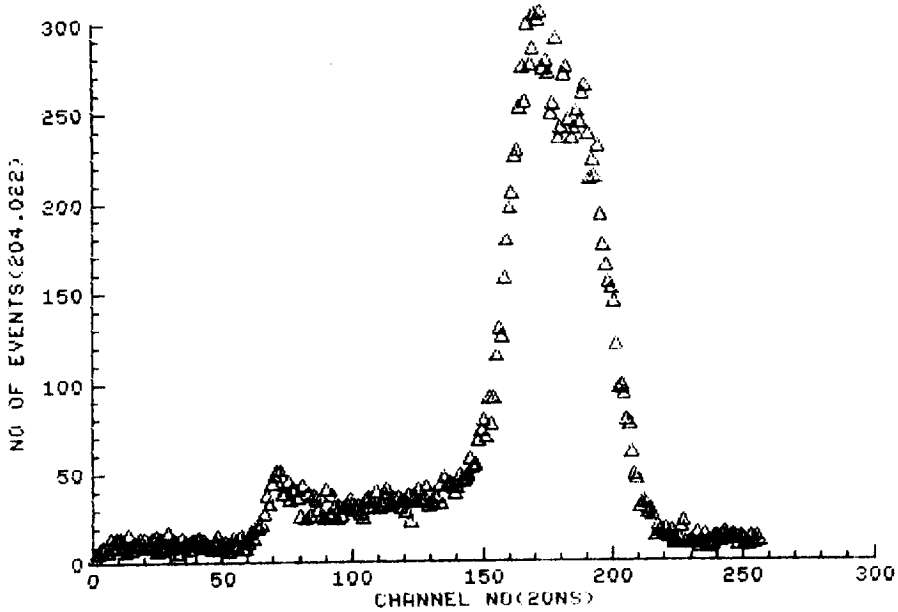
NO OF EVENTS(204.022)
300
250
200
150
100
50
0
0
50
100
150
200
250
300
CHANNEL NO(20NS)

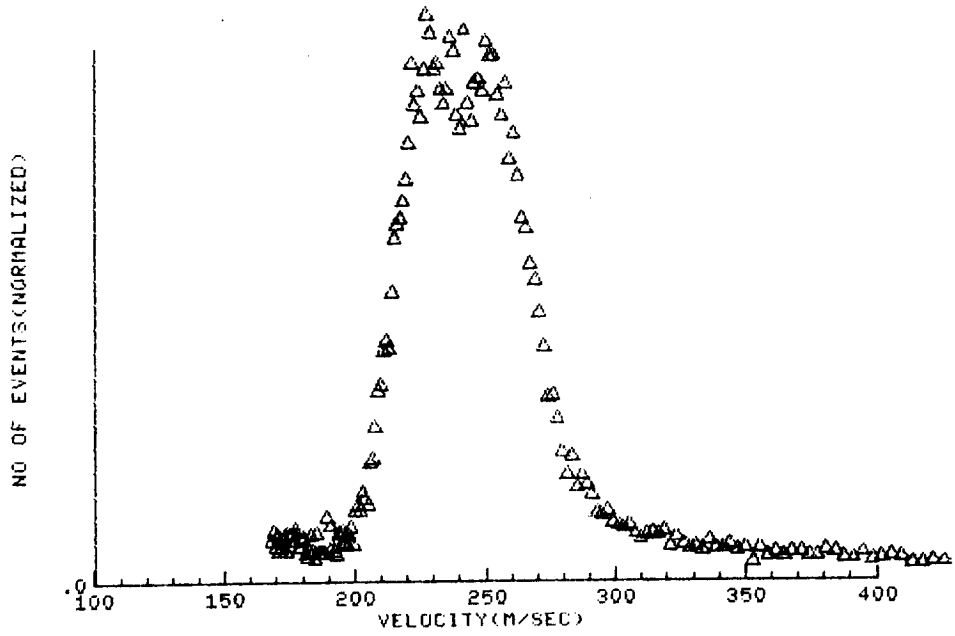
NO OF EVENTS(NORMALIZED)
.0
100
150
200
250
300
350
400
VELOCITY(M/SEC)

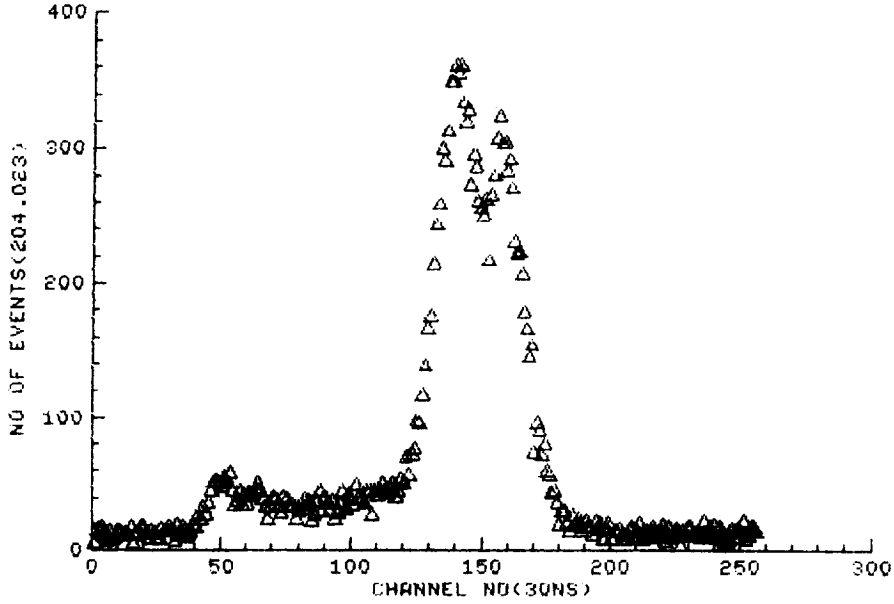
NO OF EVENTS(204.023)
400
300
200
100
0
0
50
100
150
200
250
300
CHANNEL NO(30NS)

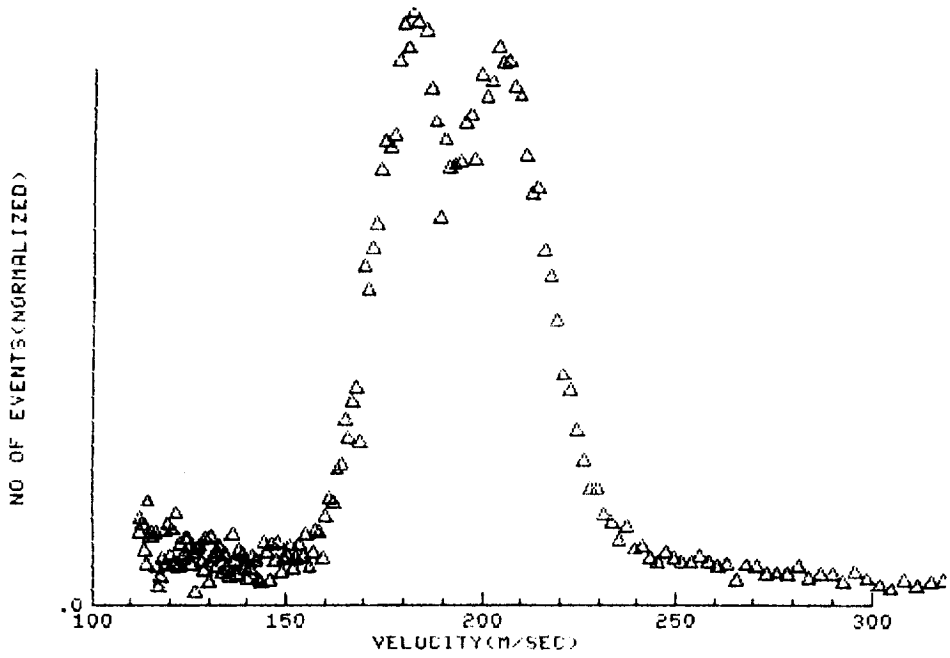
NO OF EVENTS(NORMALIZED)
.0
100
150
200
250
300
VELOCITY(M/SEC)

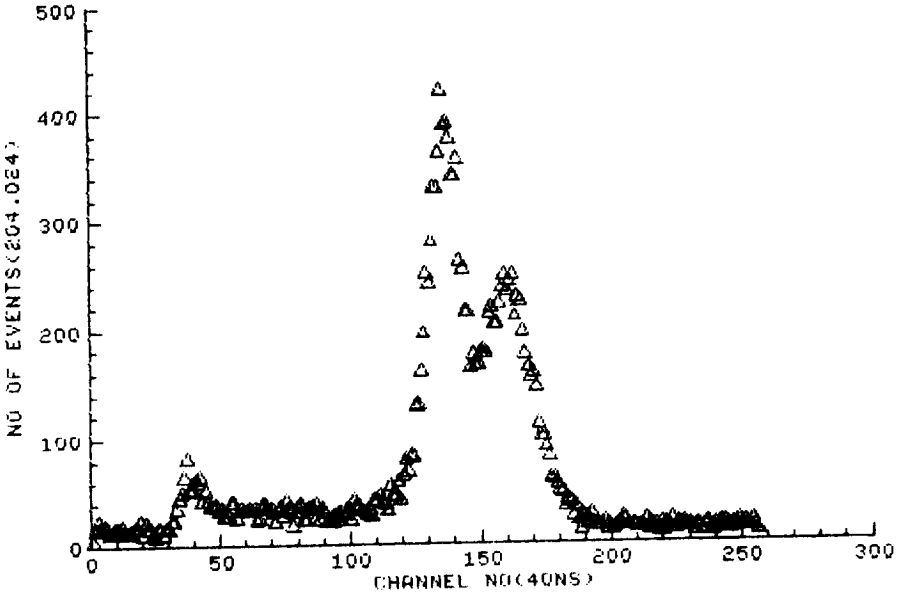
NO OF EVENTS(E04.0E4)
500
400
300
200
100
0
0
50
100
150
200
250
300
CHANNEL NO(40NS)

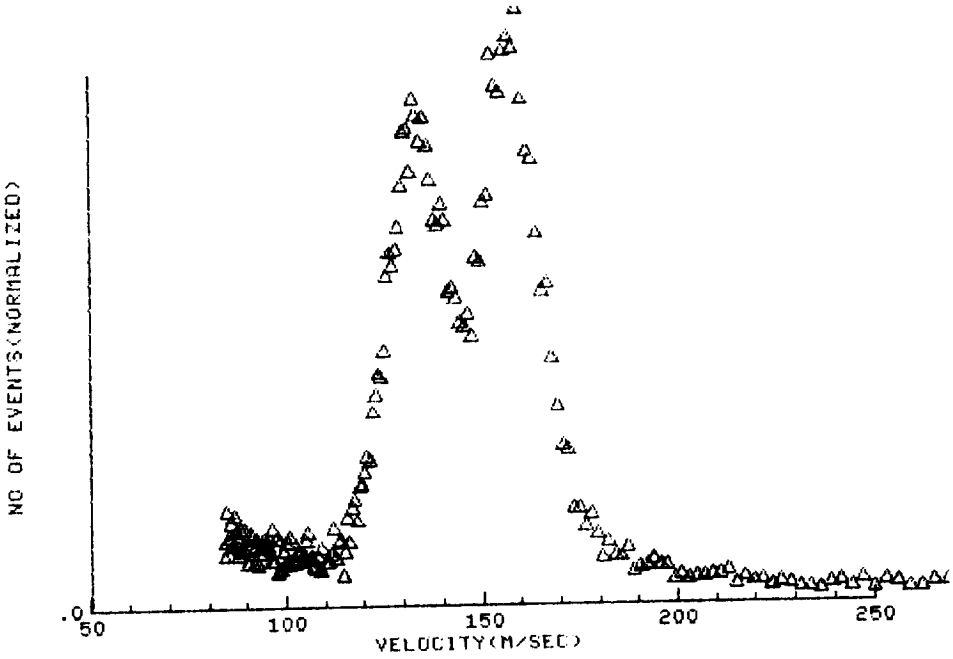
NO OF EVENTS(NORMALIZED)
.0
50
100
150
200
250
VELOCITY(M/SEC)

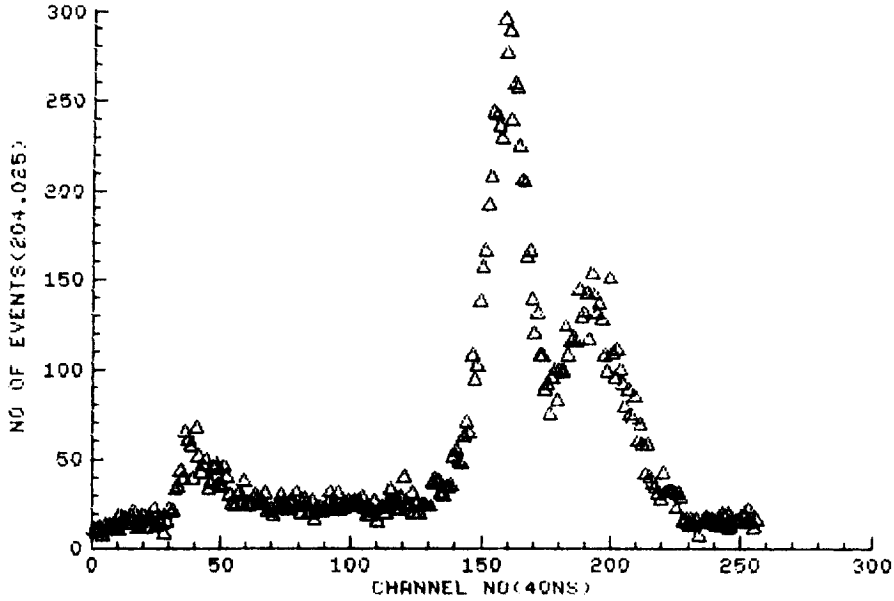
NO OF EVENTS(204.025)
300
250
200
150
100
50
0
0
50
100
150
200
250
300
CHANNEL NO(40NS)

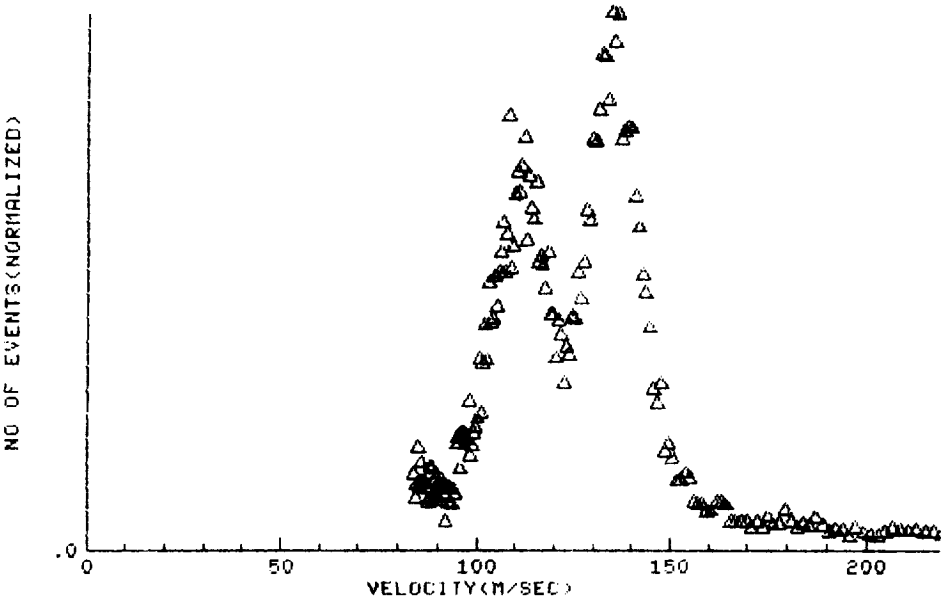
NO OF EVENTS(NORMALIZED)
.0
0
50
100
150
200
VELOCITY(M/SEC)

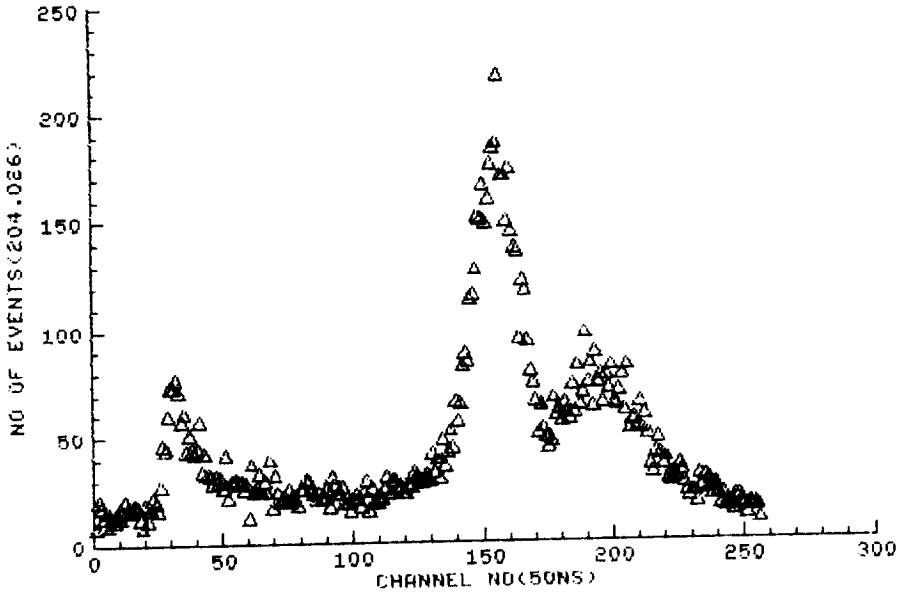
NO OF EVENTS(204.026)
250
200
150
100
50
0
0
50
100
150
200
250
300
CHANNEL NO(50NS)

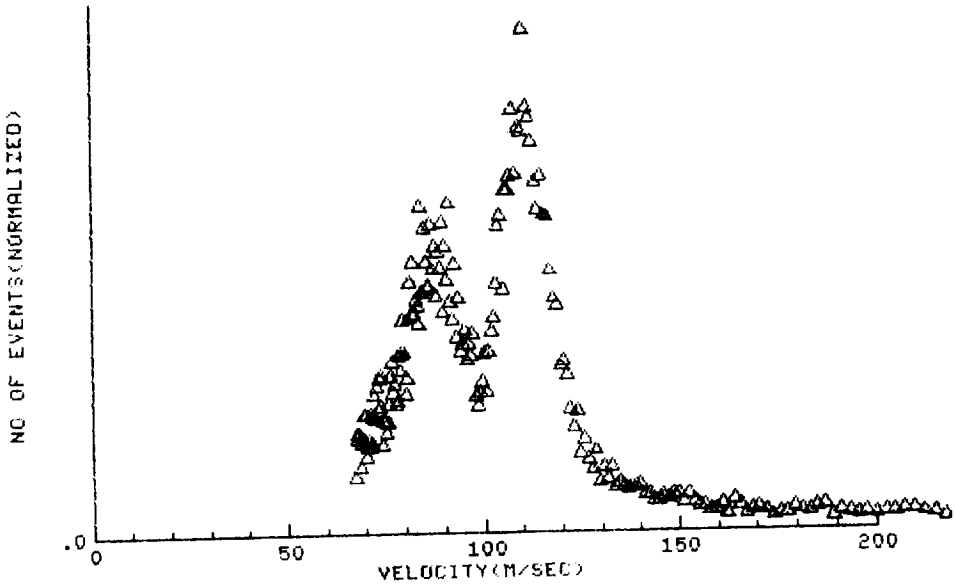
NO OF EVENTS(NORMALIZED)
.0
0
50
100
150
200
VELOCITY(M/SEC)

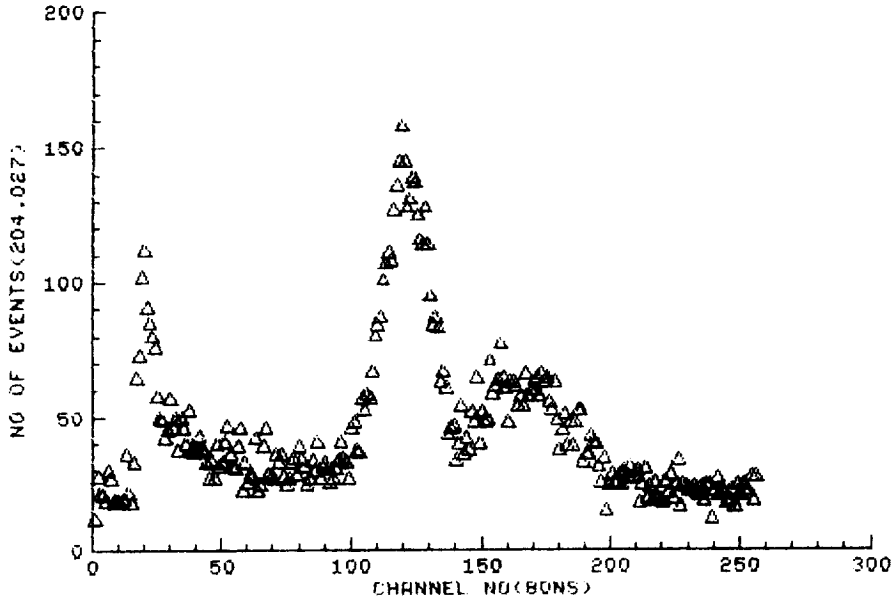
NO OF EVENTS(204.027)
200
150
100
50
0
0
50
100
150
200
250
300
CHANNEL NO(BINS)

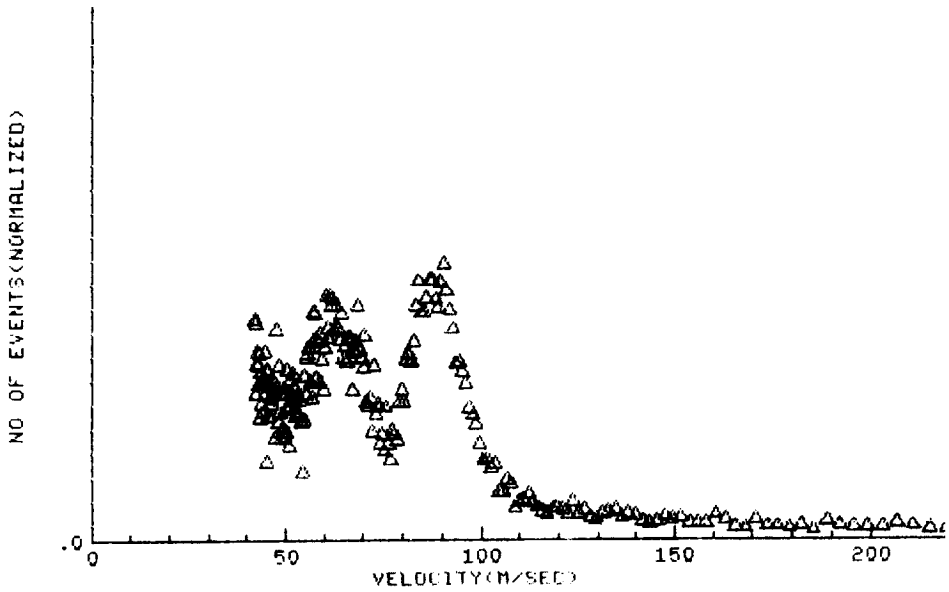
NO OF EVENTS(NORMALIZED)
.0
0
50
100
150
200
VELOCITY(M/SEC)

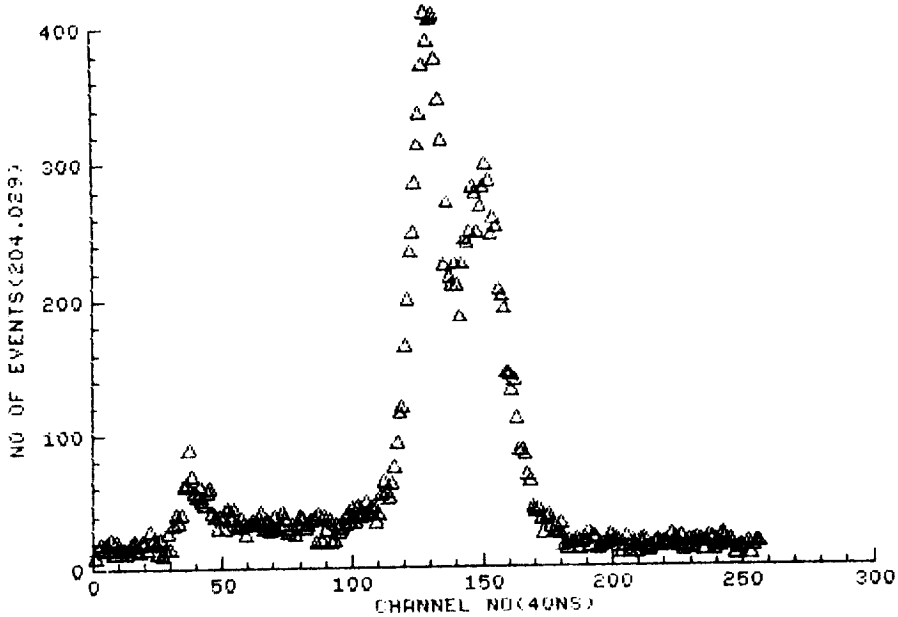
NO OF EVENTS(204.029)
400
300
200
100
0
0
50
100
150
200
250
300
CHANNEL NO(40NS)

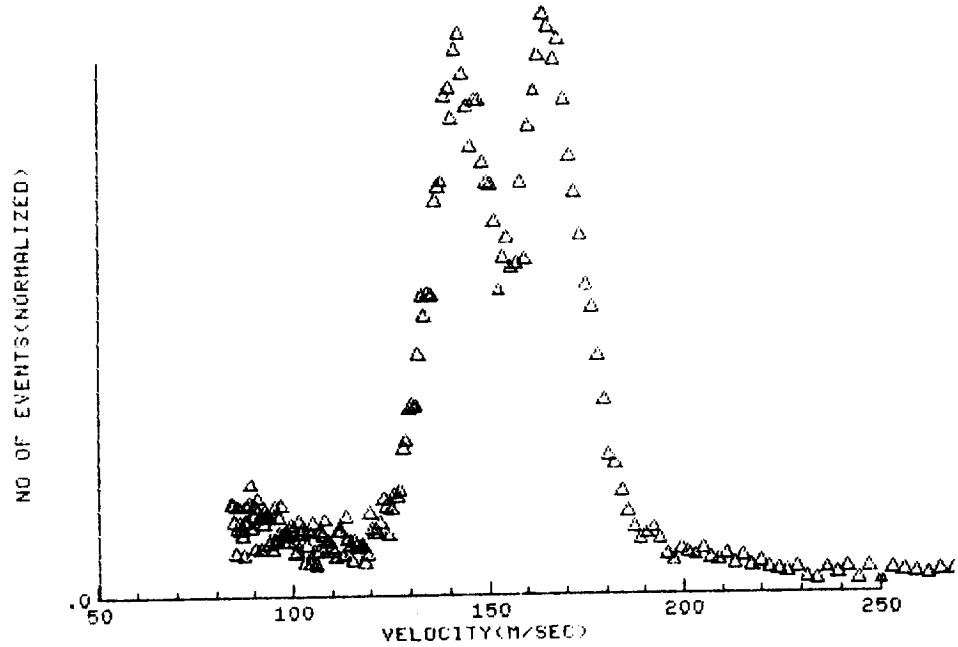
NO OF EVENTS(NORMALIZED)
.0
50
100
150
200
250
VELOCITY(M/SEC)

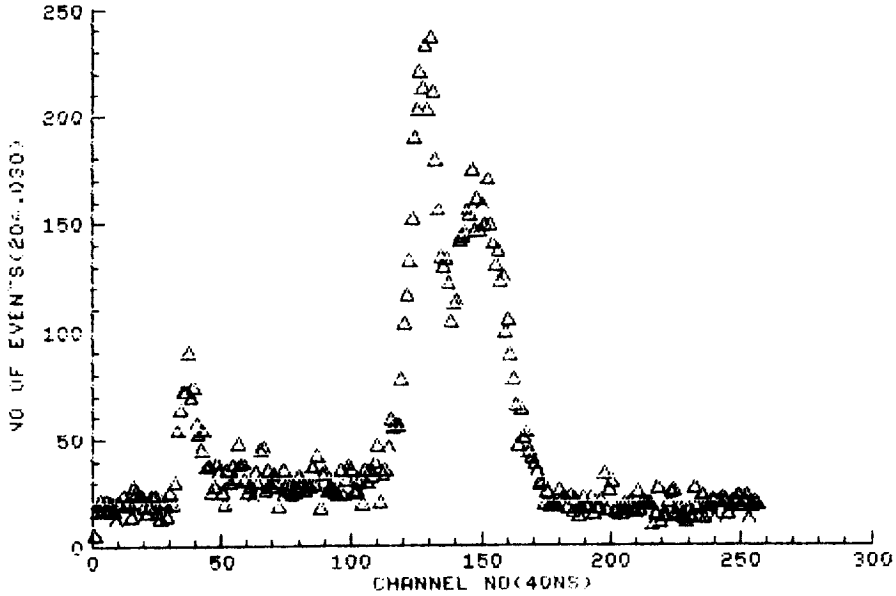
250
200
150
100
50
0
0
50
100
150
200
250
300
CHANNEL NO(40NS)

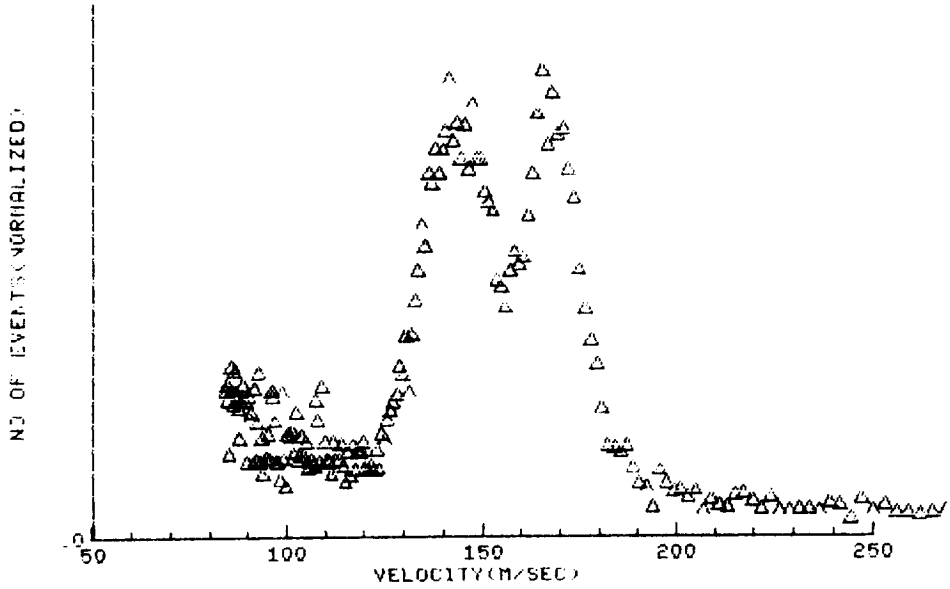
0
50
100
150
200
250
VELOCITY(M/SEC)

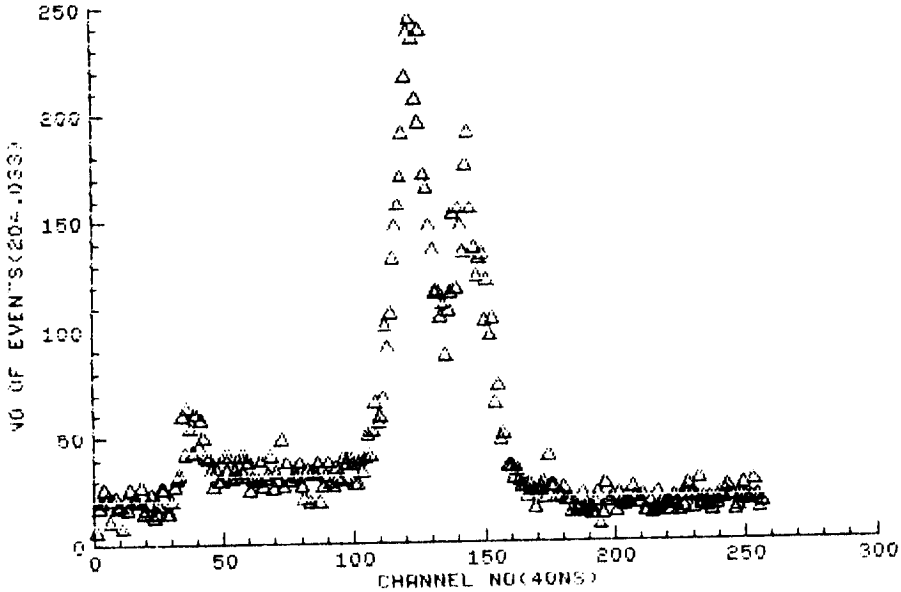
250
200
150
100
50
0
0
50
100
150
200
250
300
CHANNEL NO(40NS)

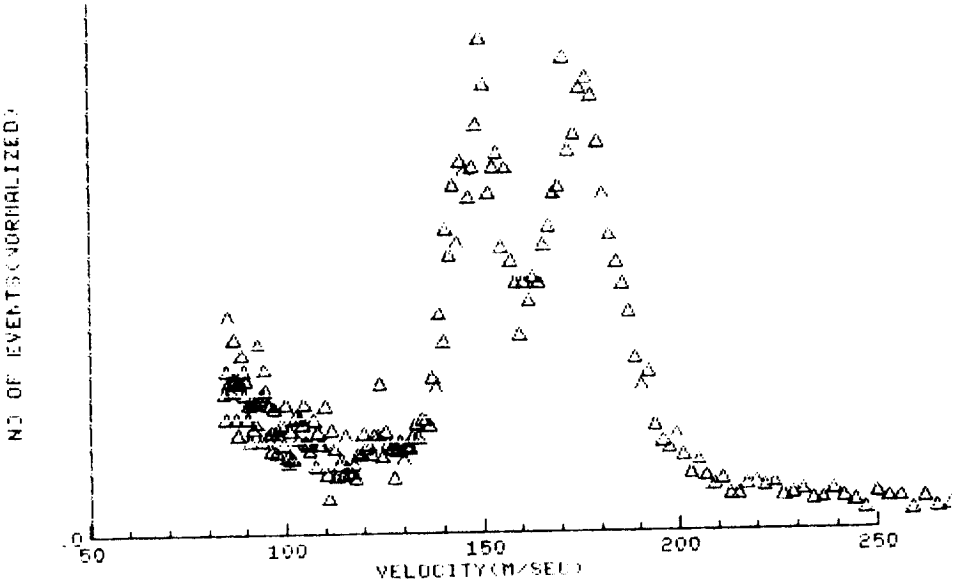
50
100
150
200
250
VELOCITY(M/SEC)

APPENDIX B

Table B

	EXP. NO.	Z-POS (mm)	VEL (τ)	VEL (V)
AEDC	208.020	1.524	585.4	567.8
	.021	1.016	501.4	446.0
	.024	.762	423.9	373.4
	.026	.508	397.9	291.5
	.028	.508	398.0	289.2
	.029	.254	442.8	239.8
	.030	.127	422.5	163.3
	.031	.127	395.4	167.2

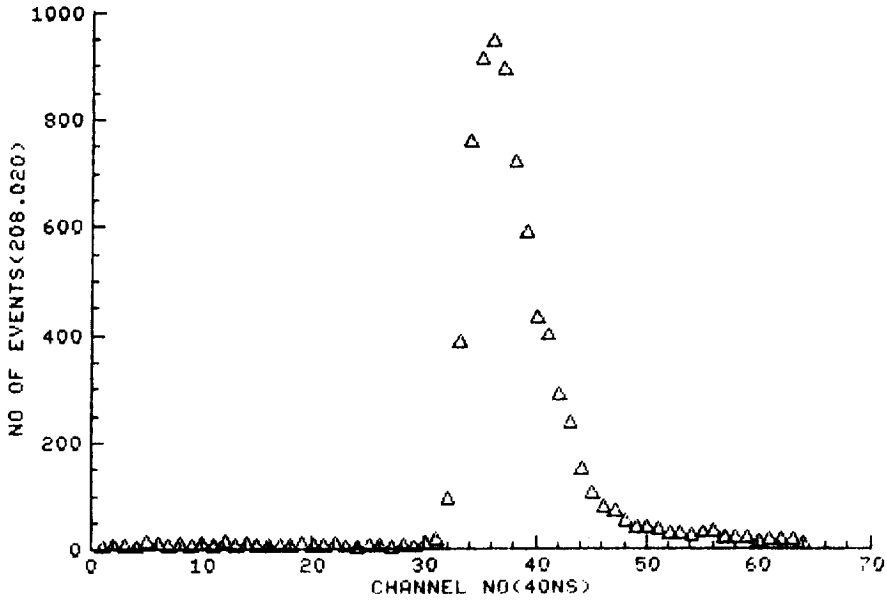
NO OF EVENTS(208.020)
1000
800
600
400
200
0
0
10
20
30
40
50
60
70
CHANNEL NO(40NS)

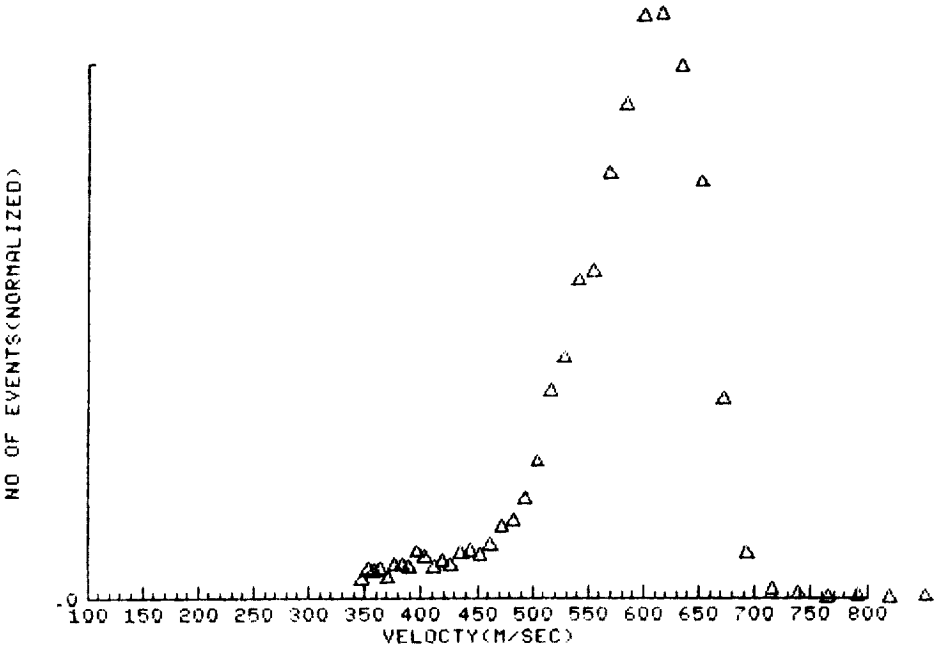
NO OF EVENTS(NORMALIZED)
0
100 150 200 250 300 350 400 450 500 550 600 650 700 750 800
VELOCTY(M/SEC)

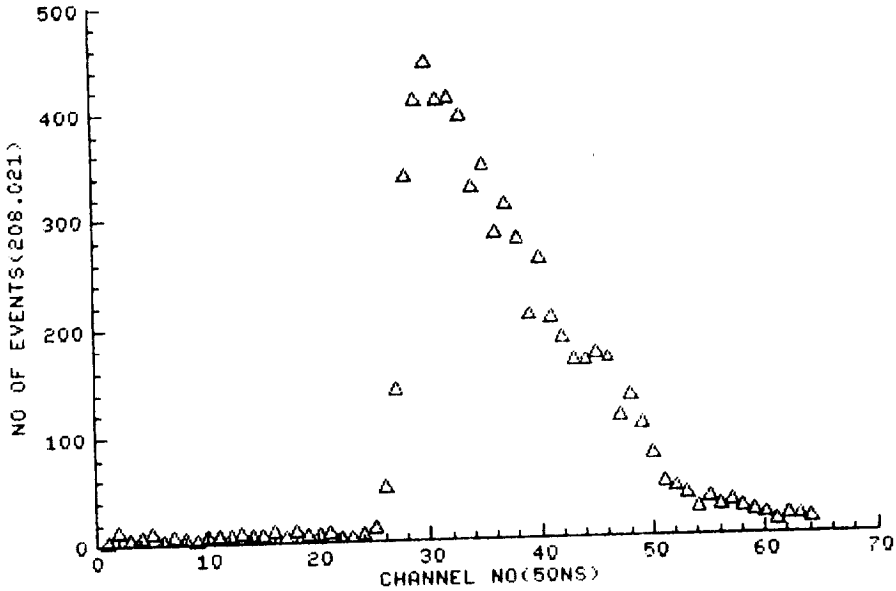
NO OF EVENTS(208.021)
500
400
300
200
100
0
0
10
20
30
40
50
60
70
CHANNEL NO(50NS)

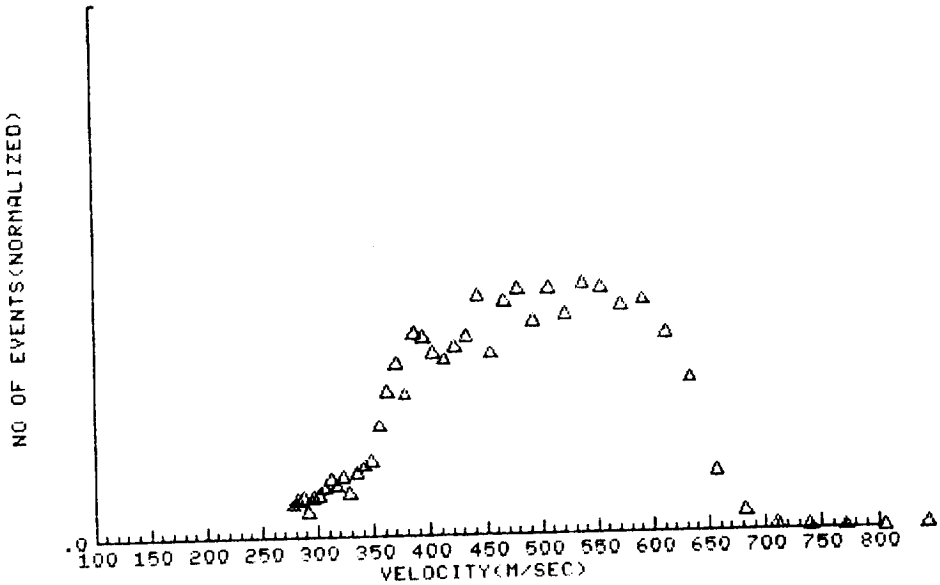
NO OF EVENTS(NORMALIZED)
.0
100 150 200 250 300 350 400 450 500 550 600 650 700 750 800
VELOCITY(M/SEC)

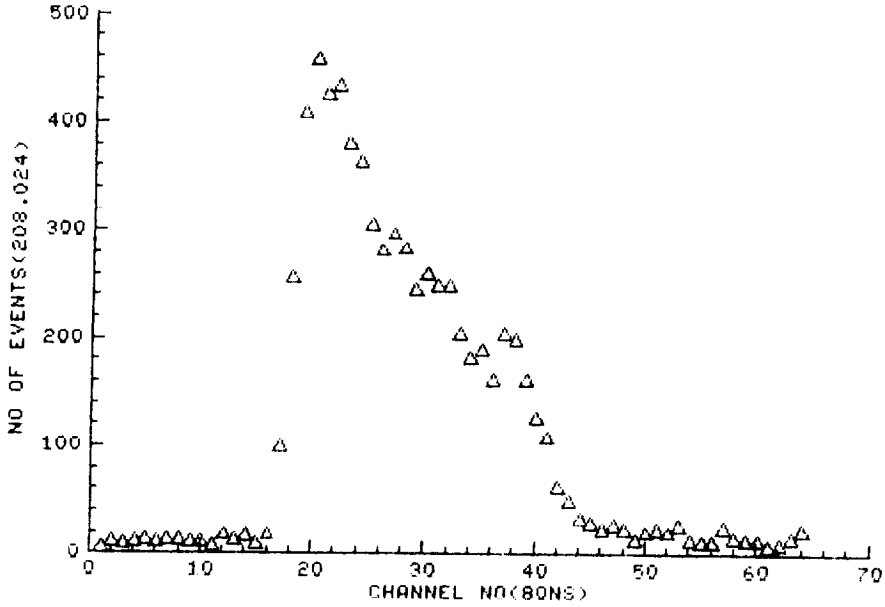
NO OF EVENTS(208.024)
500
400
300
200
100
0
0
10
20
30
40
50
60
70
CHANNEL NO(80NS)

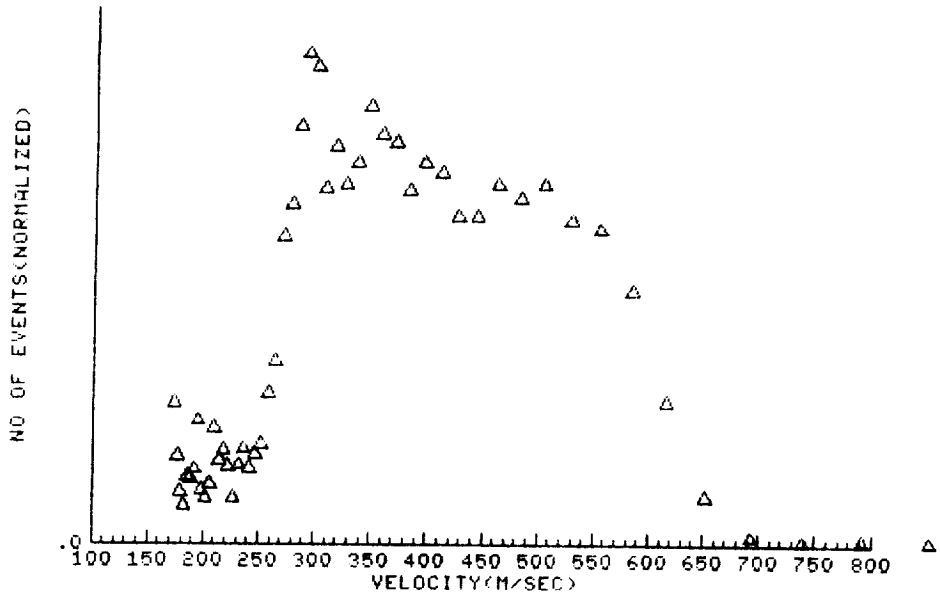
NO OF EVENTS(NORMALIZED)
.0
100 150 200 250 300 350 400 450 500 550 600 650 700 750 800
VELOCITY(M/SEC)

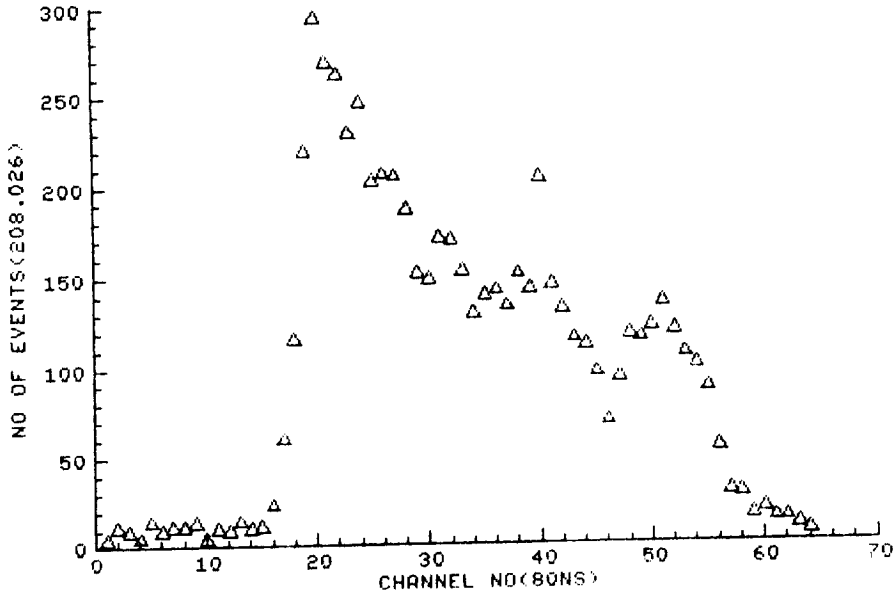
NO OF EVENTS(208.026)
300
250
200
150
100
50
0
0
10
20
30
40
50
60
70
CHANNEL NO(80NS)

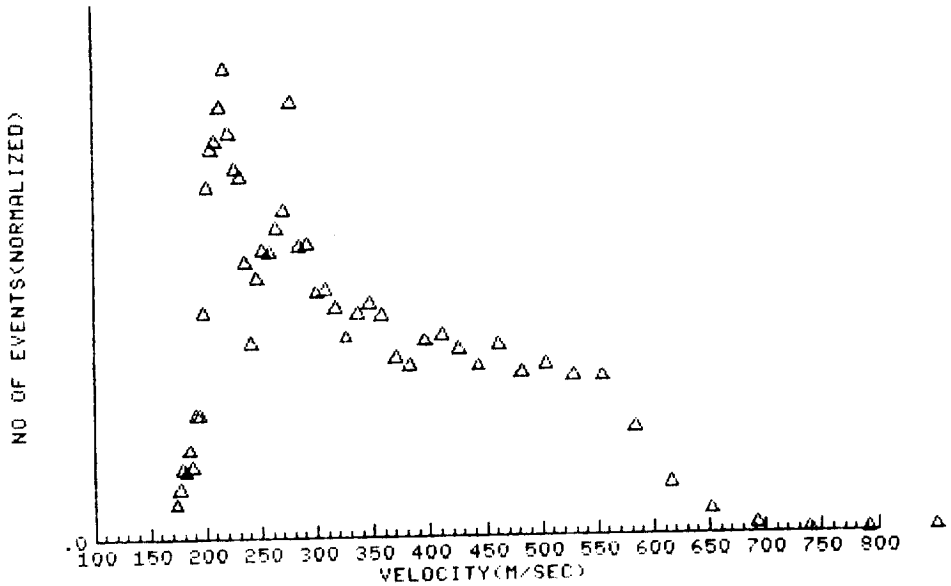
NO OF EVENTS(NORMALIZED)
.0
100 150 200 250 300 350 400 450 500 550 600 650 700 750 800
VELOCITY(M/SEC)

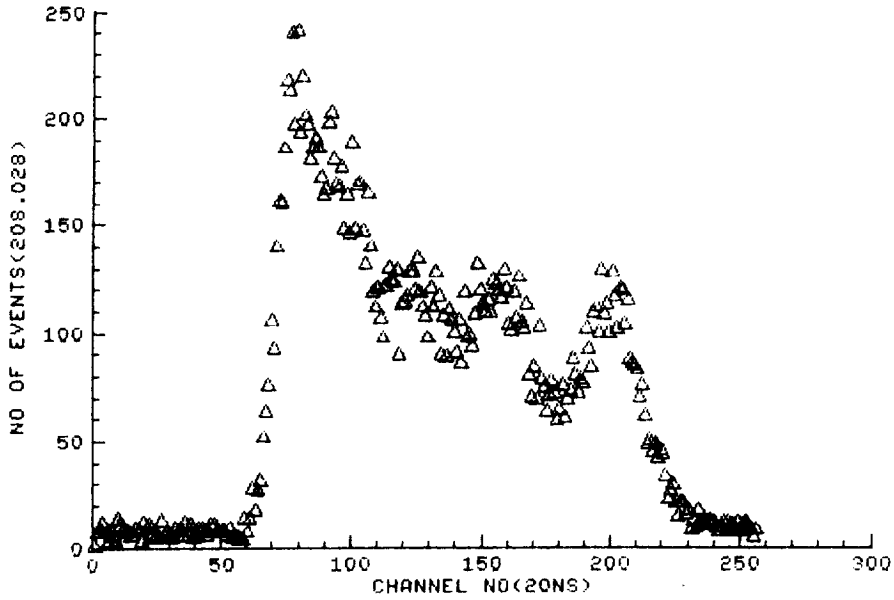
NO OF EVENTS(208.028)
250
200
150
100
50
0
0
50
100
150
200
250
300
CHANNEL NO(20NS)

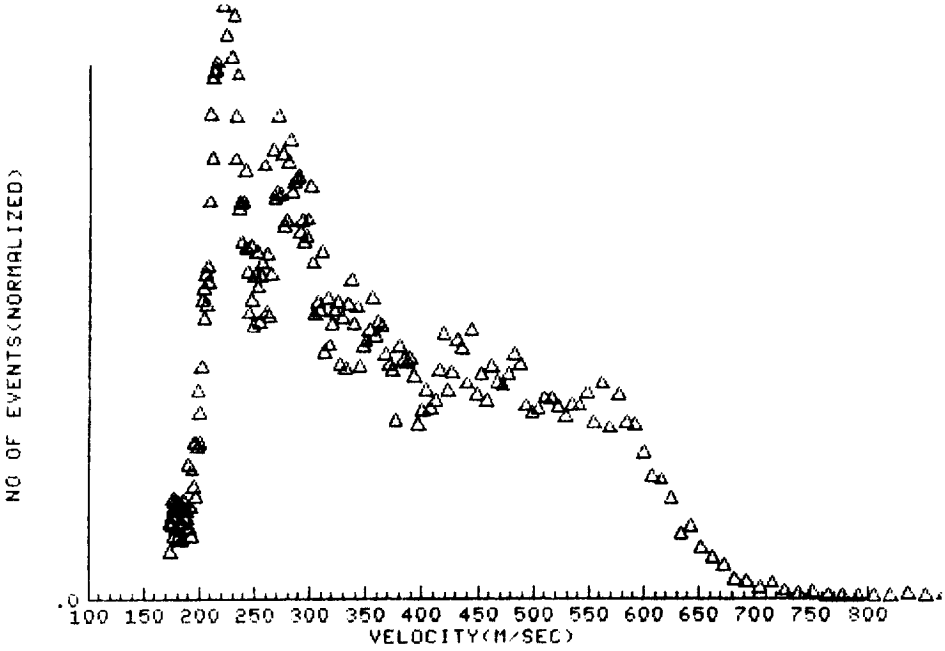
NO OF EVENTS(NORMALIZED)
.0
100 150 200 250 300 350 400 450 500 550 600 650 700 750 800
VELOCITY(M/SEC)

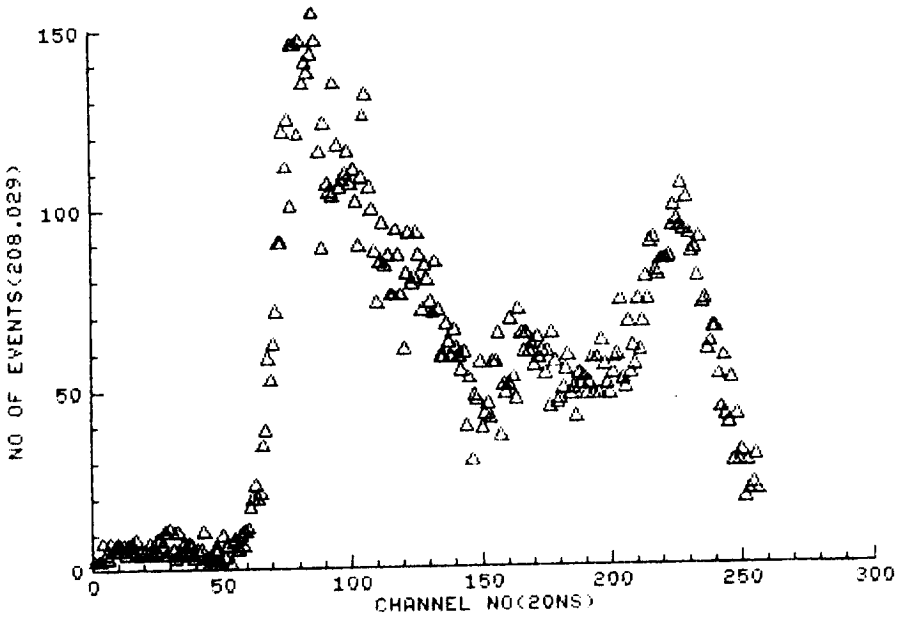
NO OF EVENTS(208.029)
150
100
50
0
0
50
100
150
200
250
300
CHANNEL NO(20NS)

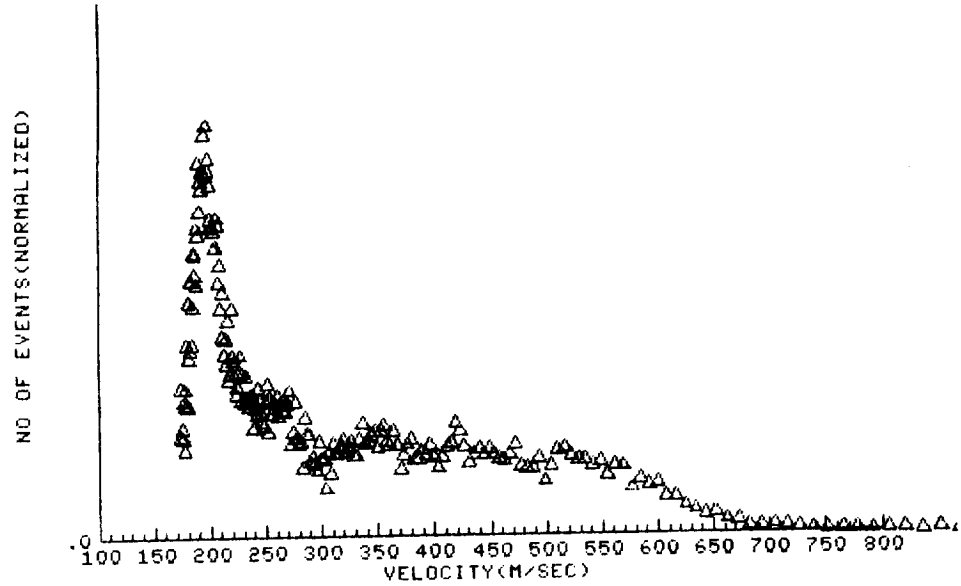
NO OF EVENTS(NORMALIZED)
0
100 150 200 250 300 350 400 450 500 550 600 650 700 750 800
VELOCITY(M/SEC)

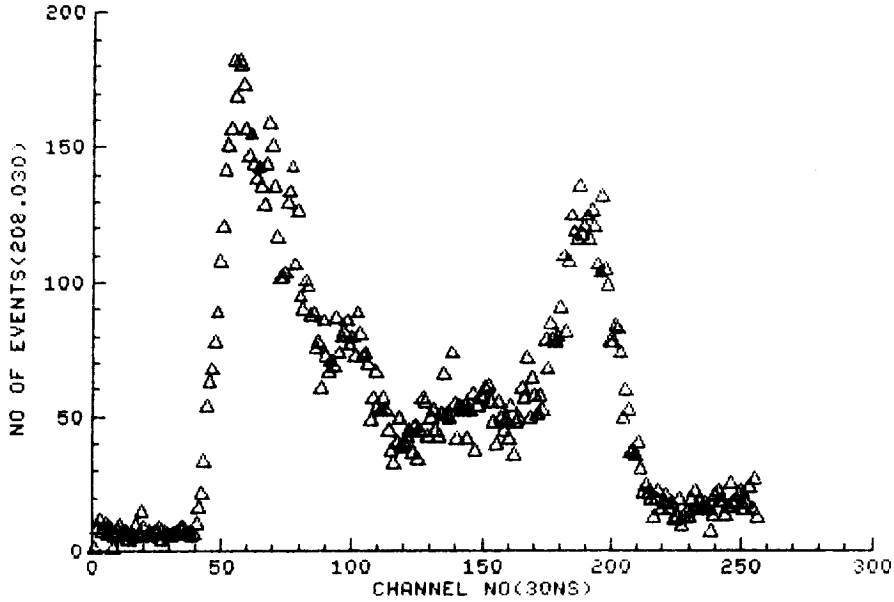
NO OF EVENTS(208.030)
200
150
100
50
0
0
50
100
150
200
250
300
CHANNEL NO(30NS)

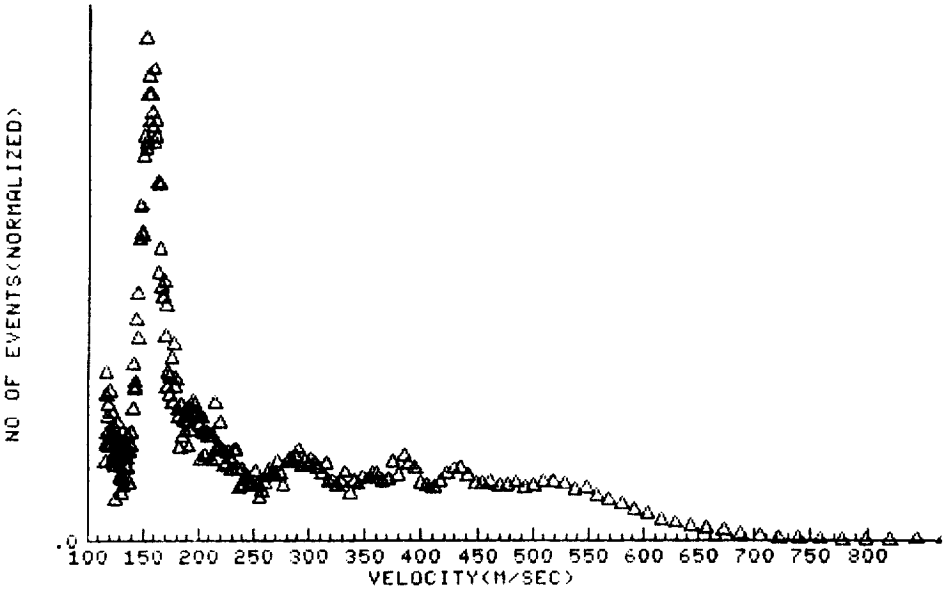
NO OF EVENTS(NORMALIZED)
.0
100 150 200 250 300 350 400 450 500 550 600 650 700 750 800
VELOCITY(M/SEC)

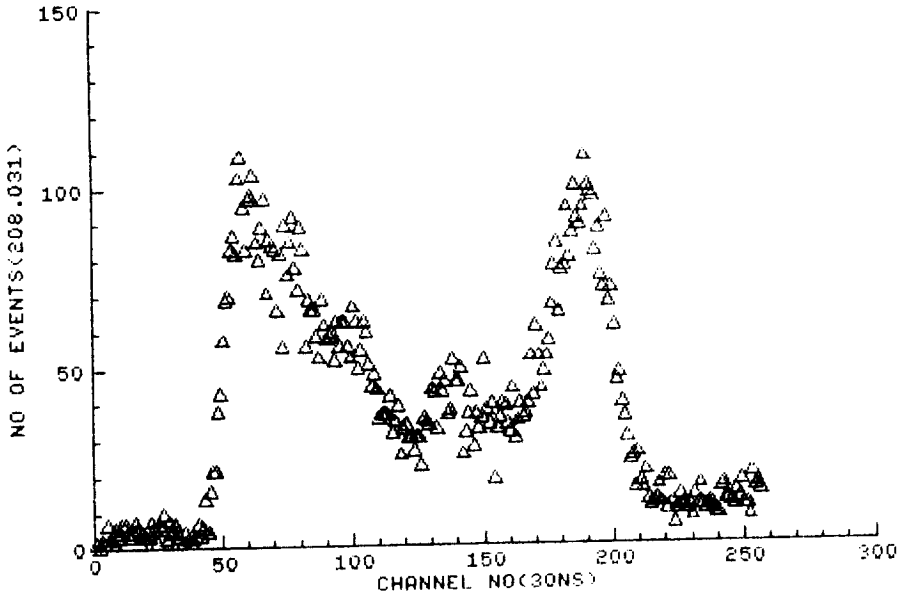
NO OF EVENTS(208.031)
150
100
50
0
0
50
100
150
200
250
300
CHANNEL NO(30NS)

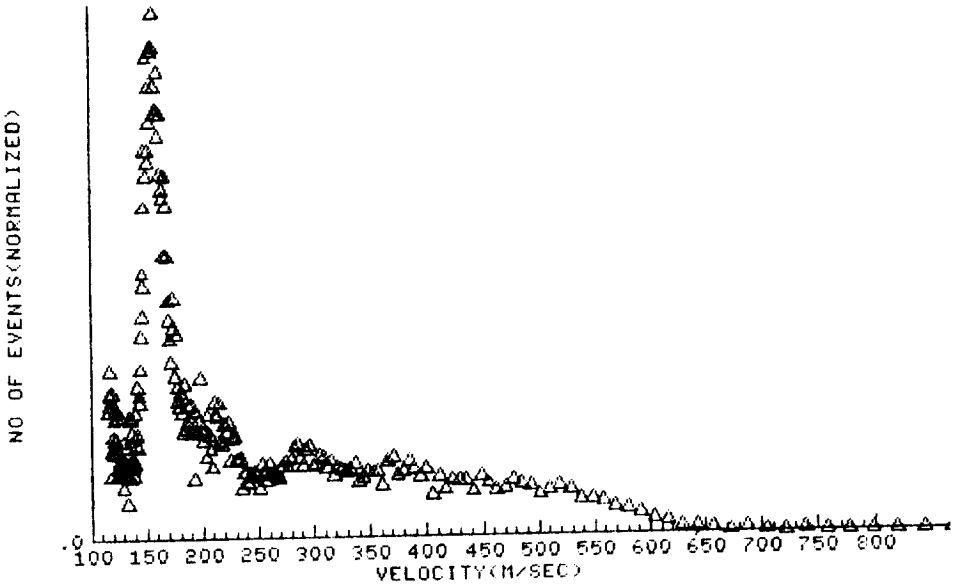
NO OF EVENTS(NORMALIZED)
.0
100 150 200 250 300 350 400 450 500 550 600 650 700 750 800
VELOCITY(M/SEC)

APPENDIX C

Table C

	EXP. NO.	Z-POS (mm)	VEL (τ)	VEL (V)
AEDC	206.034	15.0	692.6	691.9
	.035	12.7	692.0	694.1
	.036	10.2	691.7	694.5
	.038	7.6	689.7	690.0
	.039	6.4	686.5	683.6
	.040	5.1	673.9	672.9
	.041	3.8	649.3	647.6
	.042	2.5	607.7	603.9
	.043	1.9	579.6	574.2
	.044	1.3	544.4	532.4
	.045	.76	510.6	493.2
	.046	.51	487.2	460.0
	.047.	.38	467.2	445.1
	.048	.25	438.5	417.5
	.049	.13	407.9	375.0

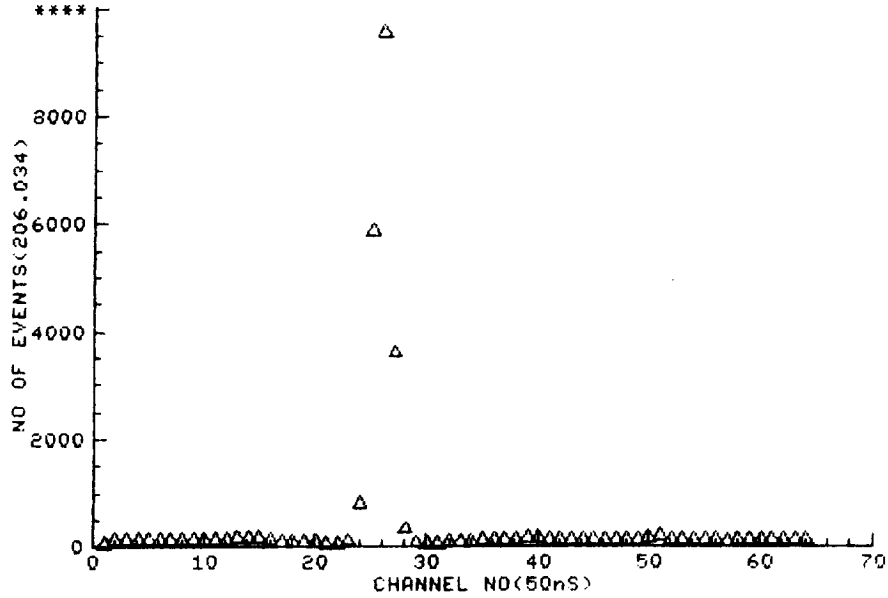
****
8000
6000
4000
2000
0
NO OF EVENTS(206.034)
0
10
20
30
40
50
60
70
CHANNEL NO(50nS)

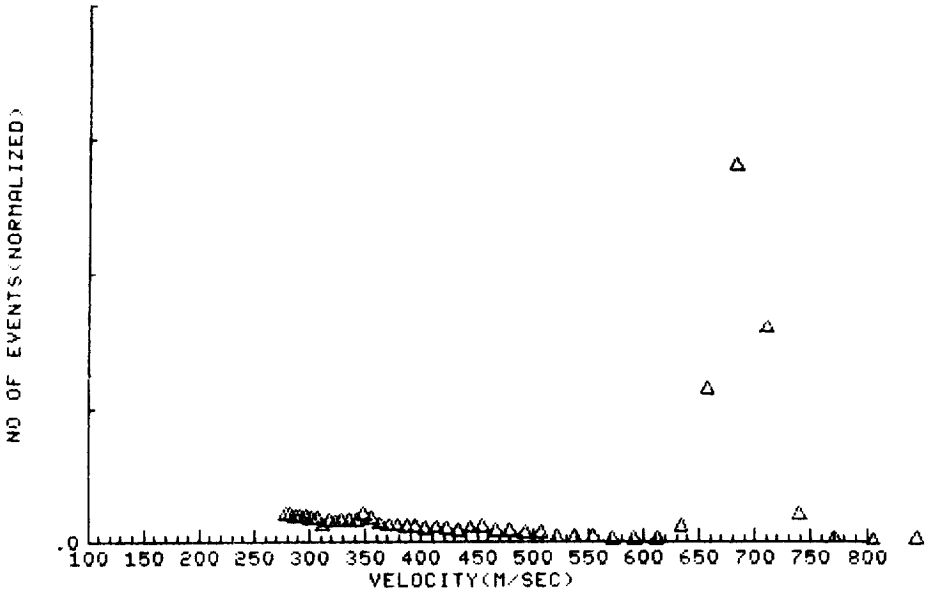
NO OF EVENTS(NORMALIZED)
.0
100 150 200 250 300 350 400 450 500 550 600 650 700 750 800
VELOCITY(M/SEC)

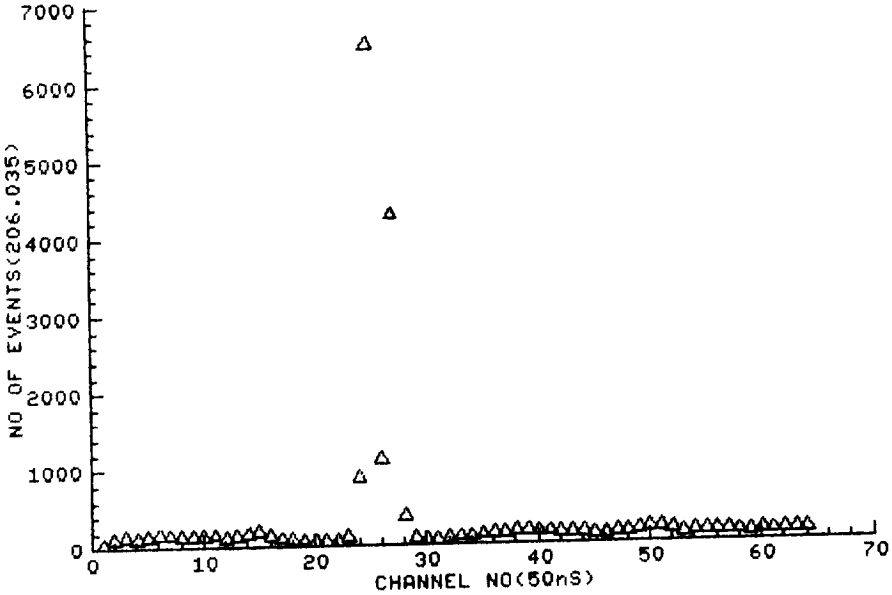
7000
6000
5000
4000
3000
2000
1000
0
NO OF EVENTS(206.035)
0
10
20
30
40
50
60
70
CHANNEL NO(50nS)

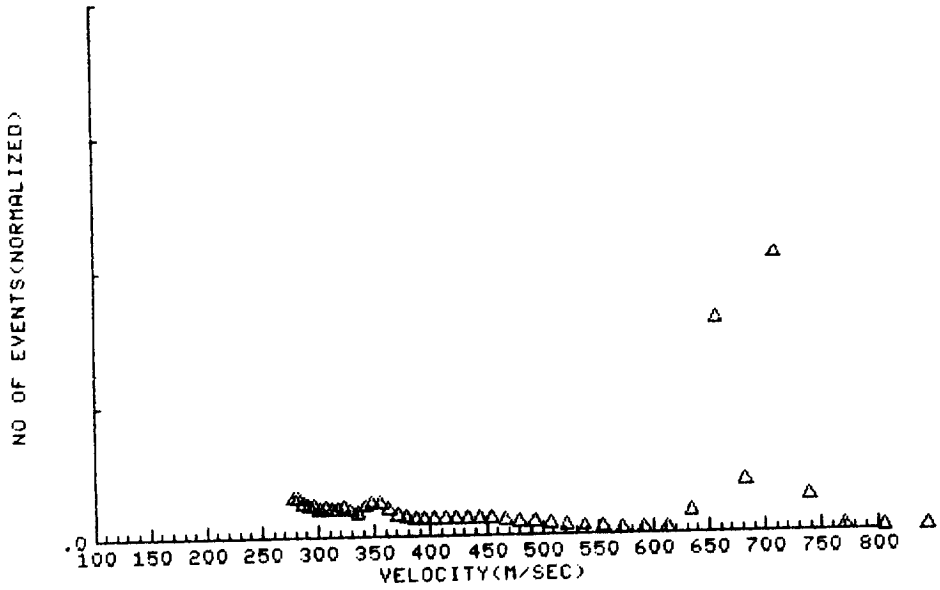
NO OF EVENTS(NORMALIZED)
.0
100 150 200 250 300 350 400 450 500 550 600 650 700 750 800
VELOCITY(M/SEC)

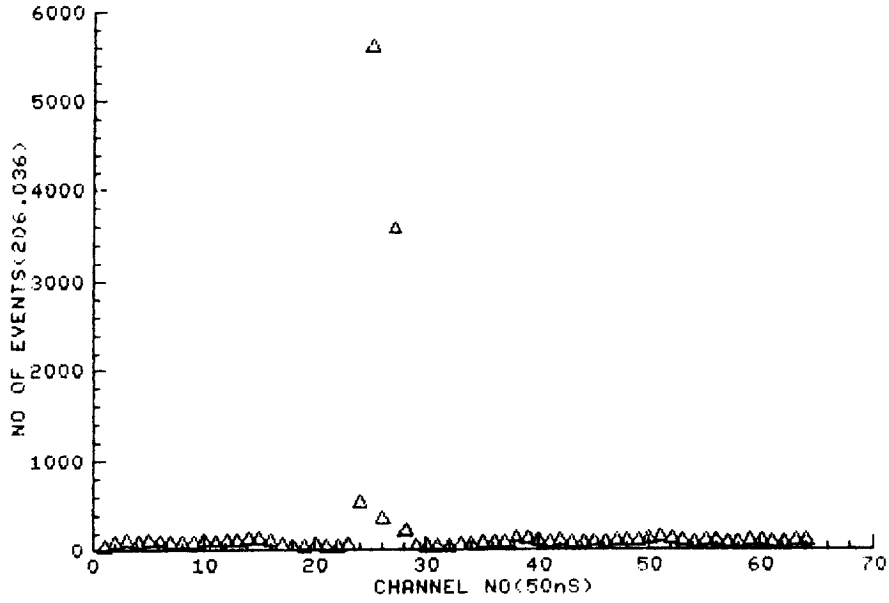
6000
5000
4000
3000
2000
1000
0
NO OF EVENTS(206.036)
0
10
20
30
40
50
60
70
CHANNEL NO(50nS)

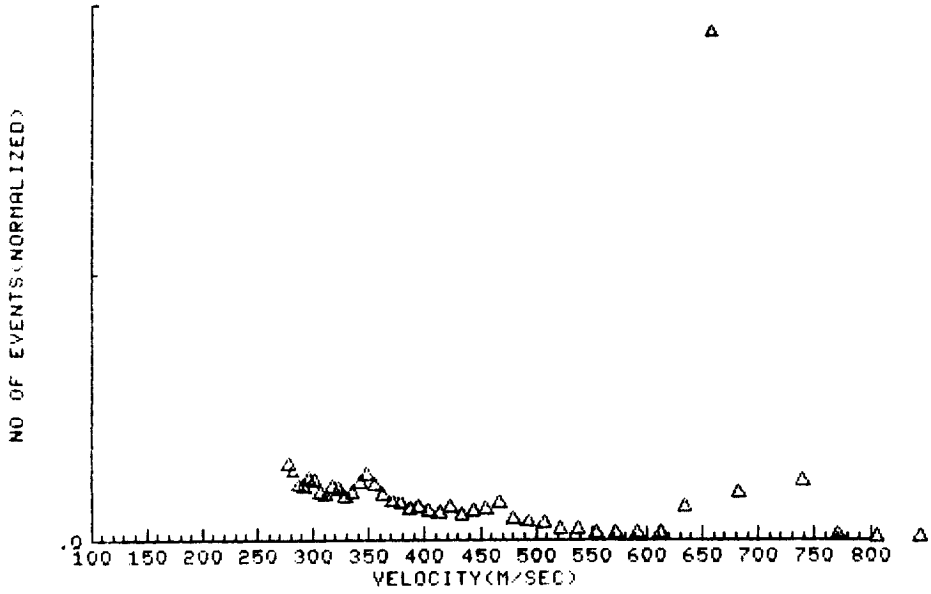
NO OF EVENTS(NORMALIZED)
0
100 150 200 250 300 350 400 450 500 550 600 650 700 750 800
VELOCITY(M/SEC)

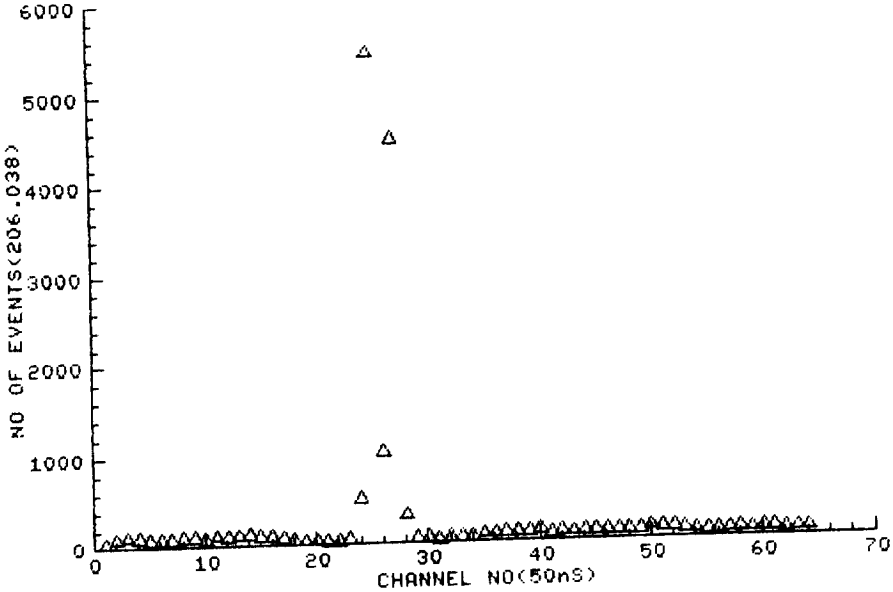
6000
5000
4000
3000
2000
1000
0
NO OF EVENTS(206.038)
0
10
20
30
40
50
60
70
CHANNEL NO(50nS)

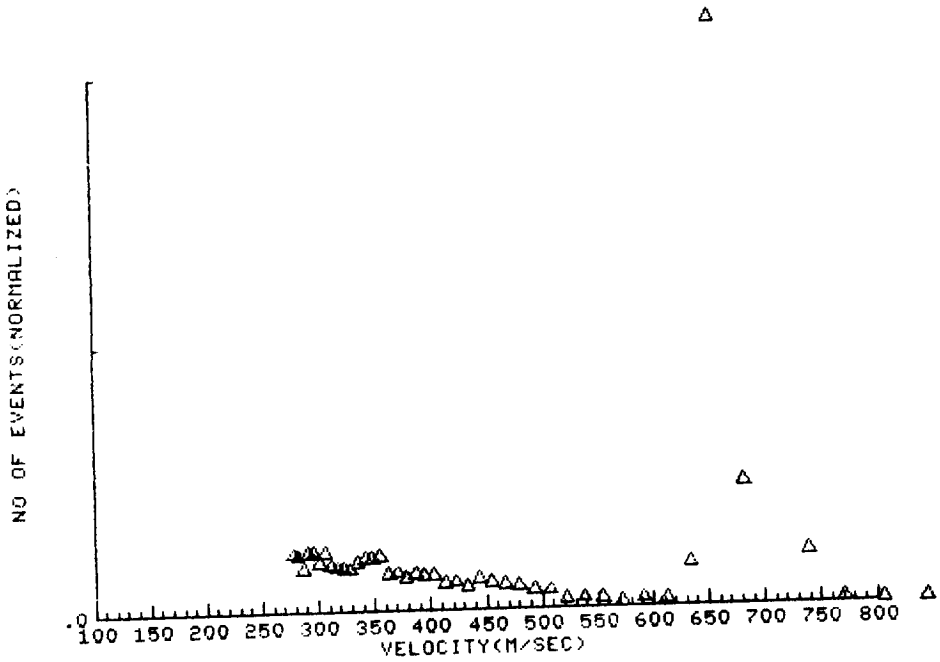
NO OF EVENTS(NORMALIZED)
0
100 150 200 250 300 350 400 450 500 550 600 650 700 750 800
VELOCITY(M/SEC)

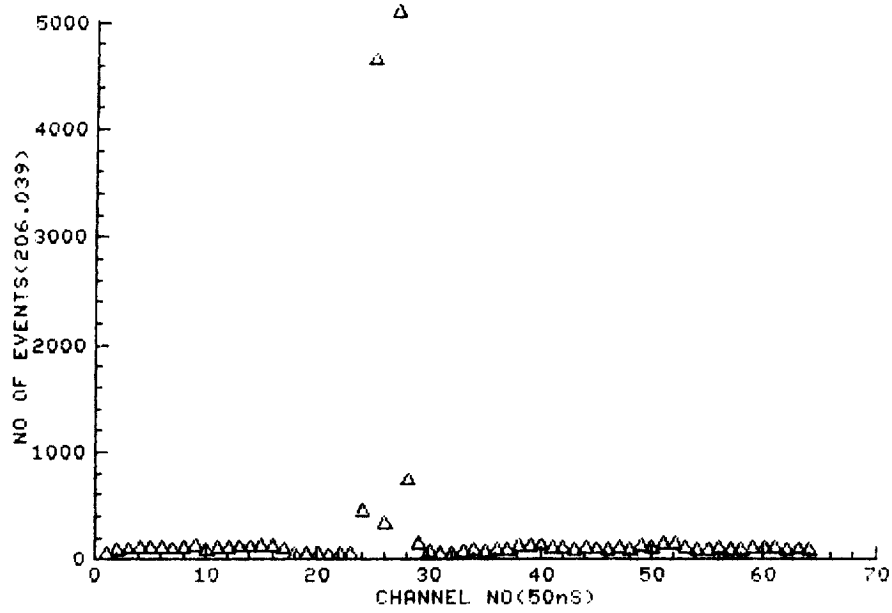
NO OF EVENTS(206.039)
5000
4000
3000
2000
1000
0
0
10
20
30
40
50
60
70
CHANNEL NO(50nS)

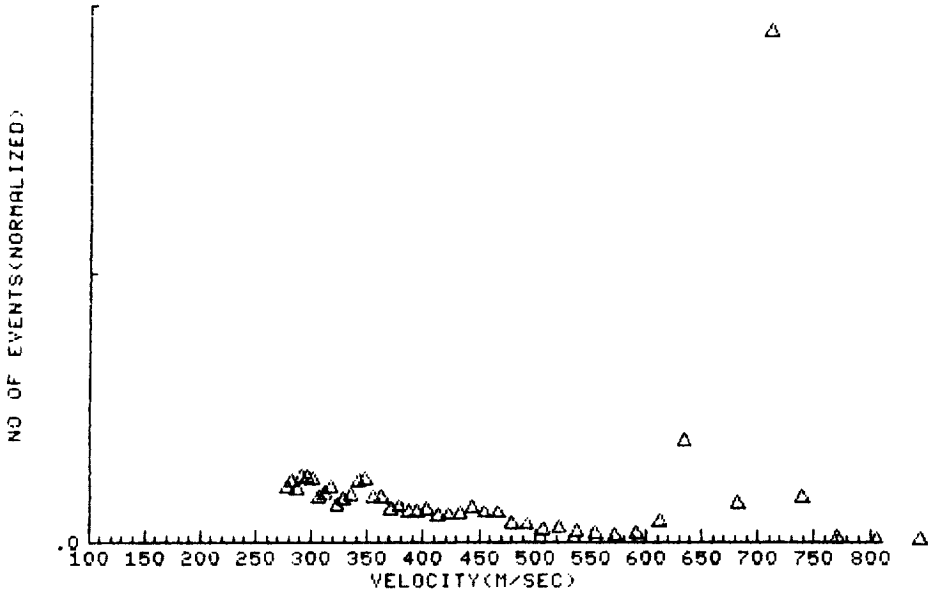
NO OF EVENTS(NORMALIZED)
.0
100 150 200 250 300 350 400 450 500 550 600 650 700 750 800
VELOCITY(M/SEC)

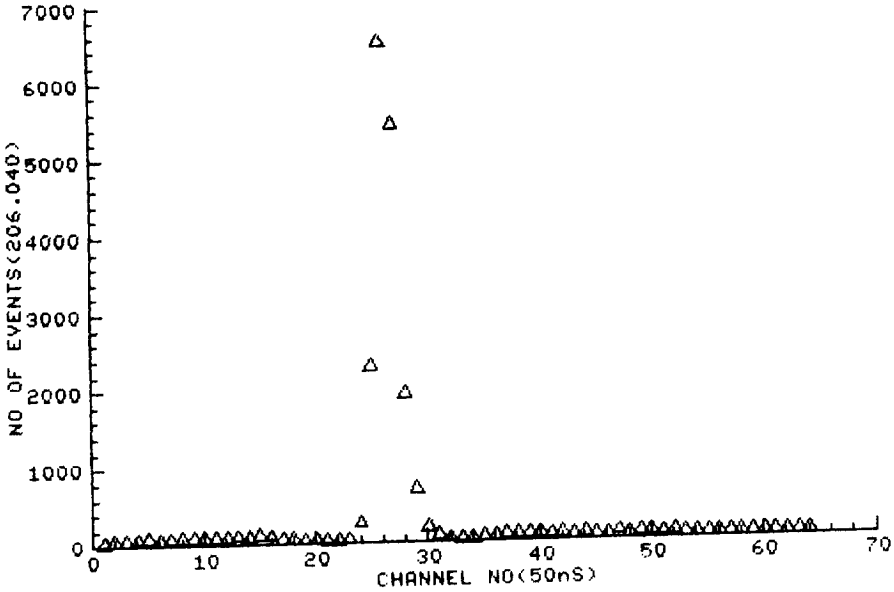
NO OF EVENTS(206.040)
7000
6000
5000
4000
3000
2000
1000
0
0
10
20
30
40
50
60
70
CHANNEL NO(50nS)

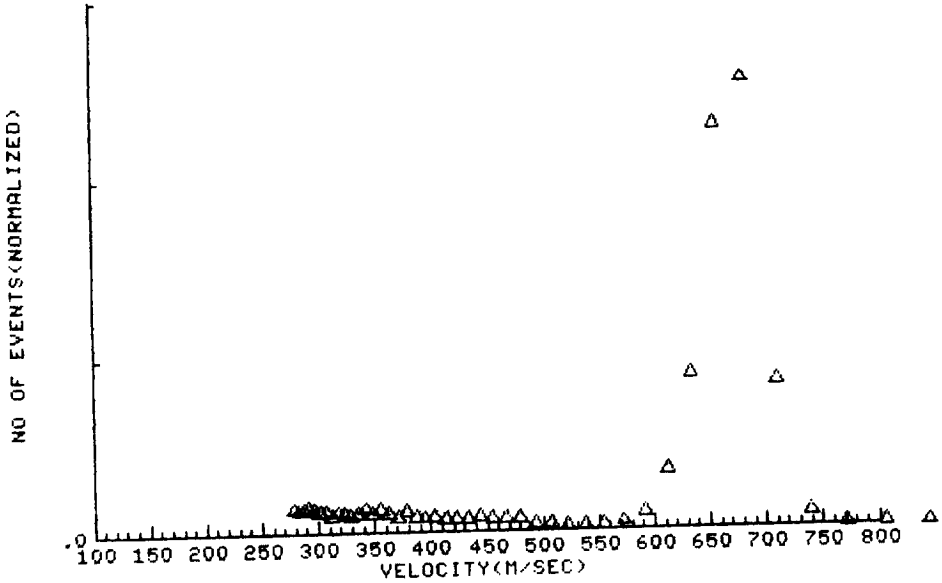
NO OF EVENTS(NORMALIZED)
.0
100 150 200 250 300 350 400 450 500 550 600 650 700 750 800
VELOCITY(M/SEC)

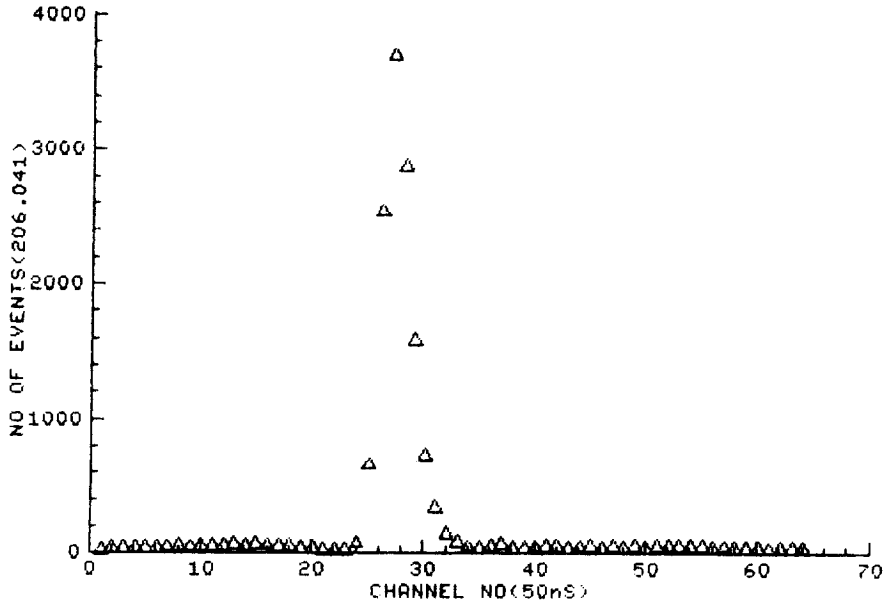
4000
3000
2000
1000
0
NO OF EVENTS(206.041)
0
10
20
30
40
50
60
70
CHANNEL NO(50nS)

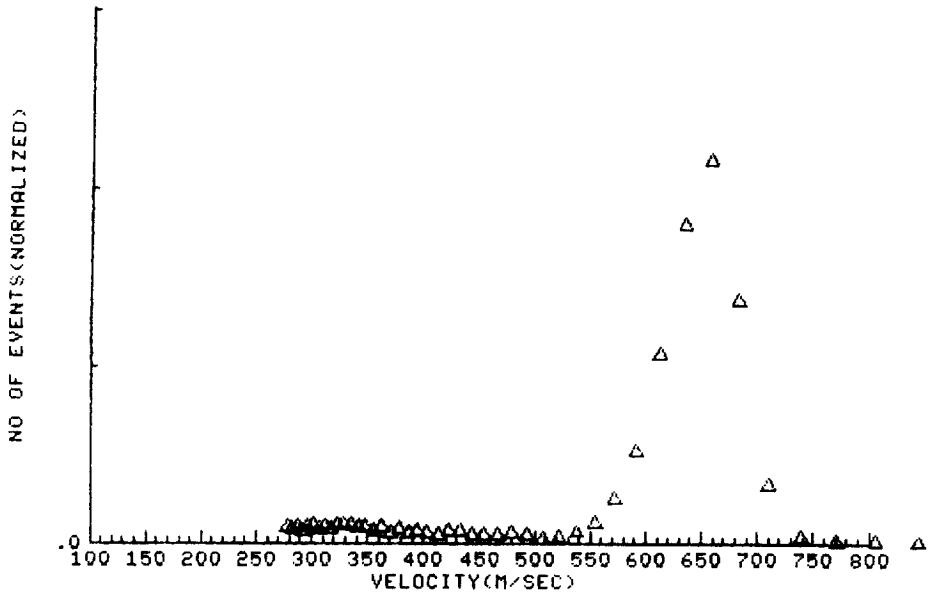
NO OF EVENTS(NORMALIZED)
.0
100 150 200 250 300 350 400 450 500 550 600 650 700 750 800
VELOCITY(M/SEC)

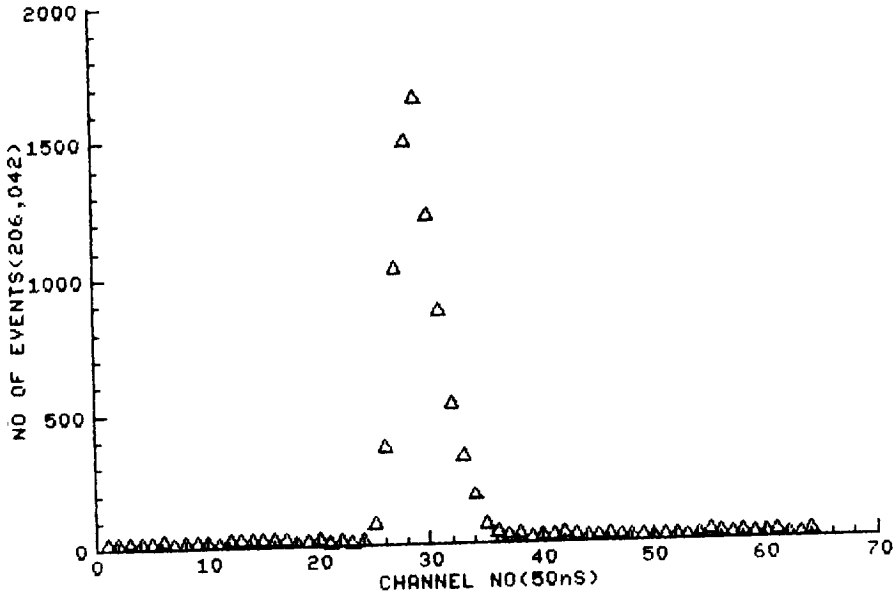
NO OF EVENTS(206,042)
2000
1500
1000
500
0
0
10
20
30
40
50
60
70
CHANNEL NO(50nS)

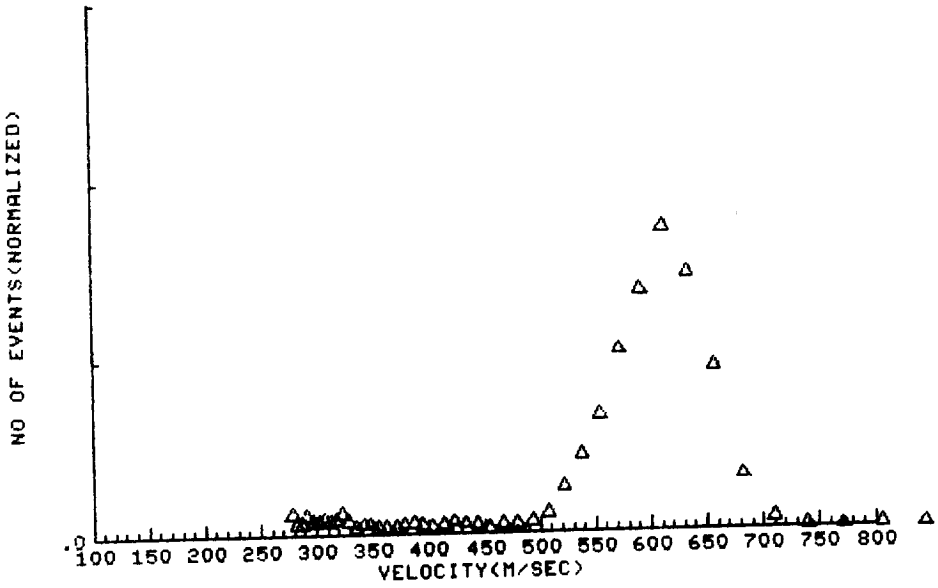
NO OF EVENTS(NORMALIZED)
.0
100 150 200 250 300 350 400 450 500 550 600 650 700 750 800
VELOCITY(M/SEC)

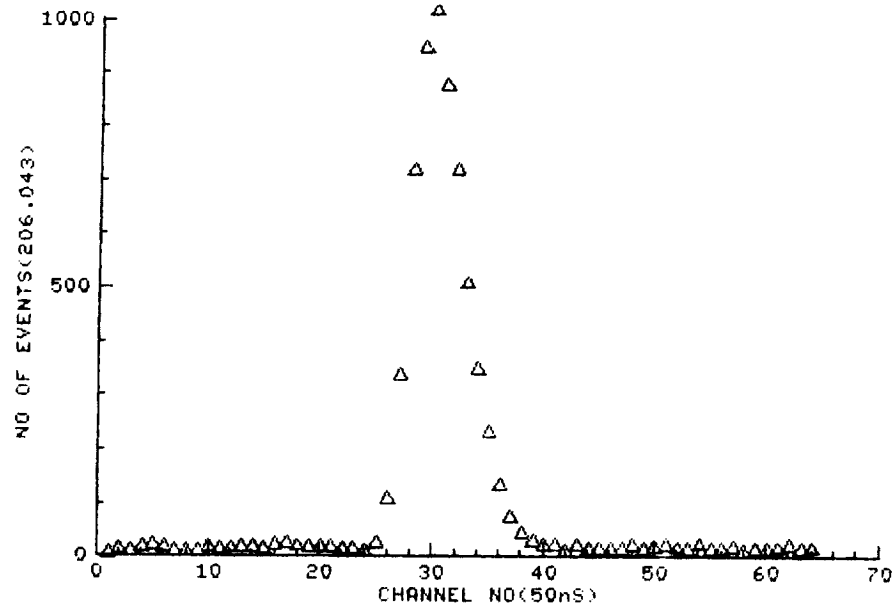
1000
500
0
NO OF EVENTS(206.043)
0
10
20
30
40
50
60
70
CHANNEL NO(50nS)

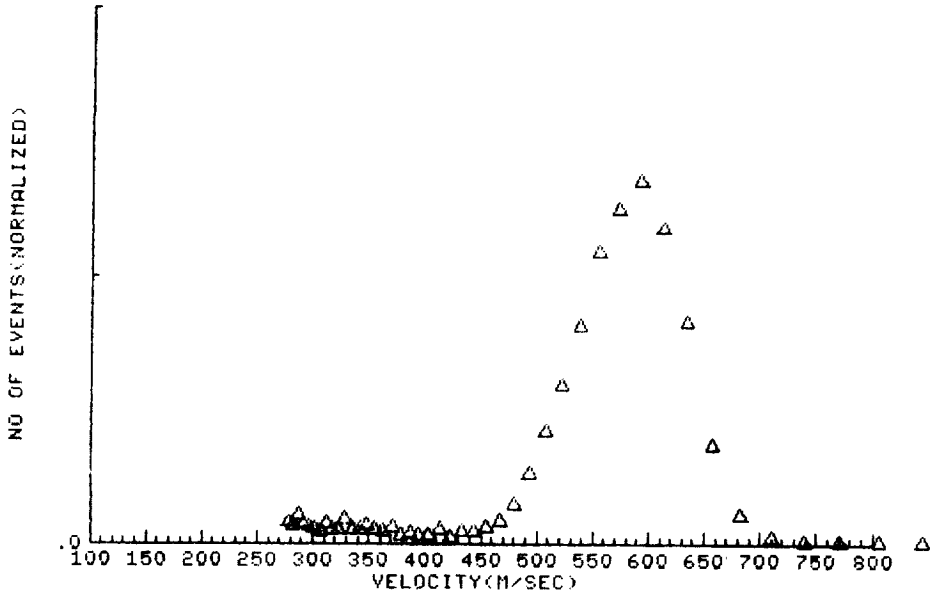
NO OF EVENTS(NORMALIZED)
.0
100 150 200 250 300 350 400 450 500 550 600 650 700 750 800
VELOCITY(M/SEC)

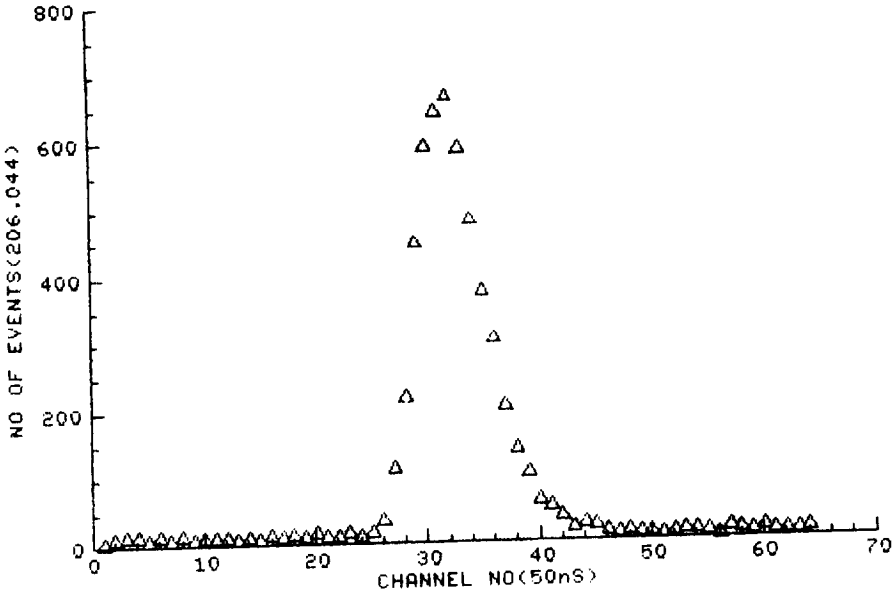
800
600
400
200
0
NO OF EVENTS(206.044)
0
10
20
30
40
50
60
70
CHANNEL NO(50nS)

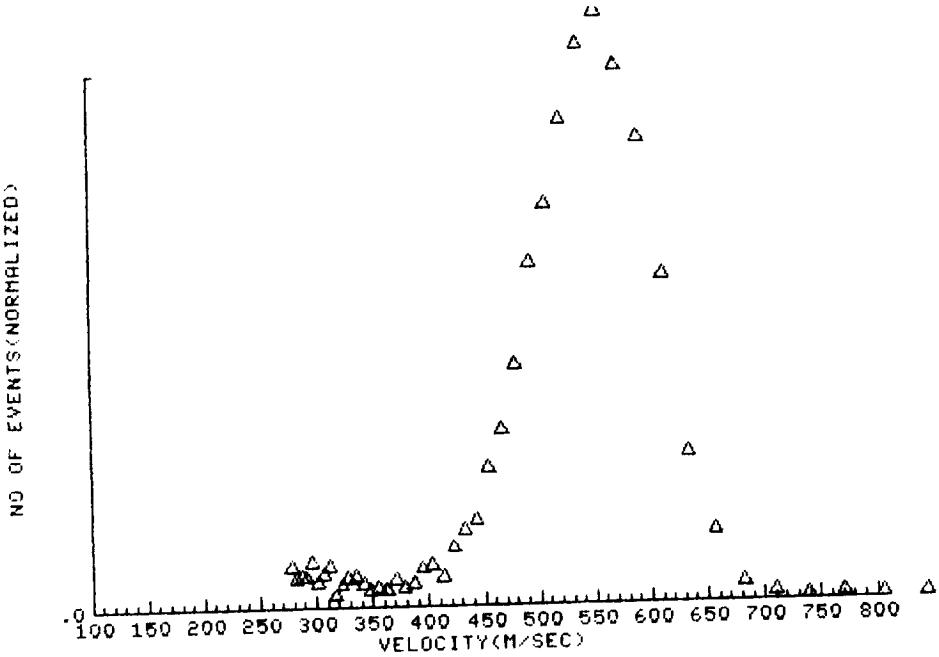
NO OF EVENTS(NORMALIZED)
0
100 150 200 250 300 350 400 450 500 550 600 650 700 750 800
VELOCITY(M/SEC)

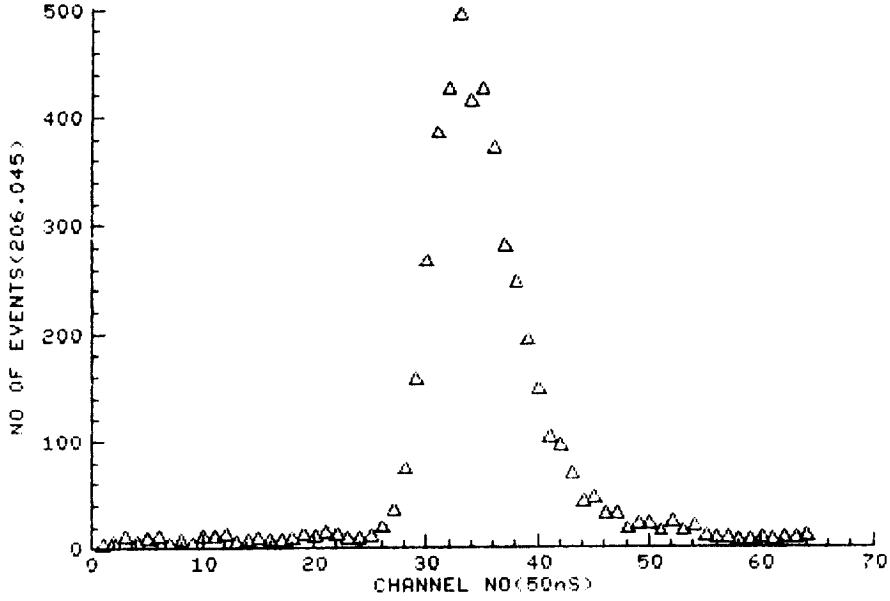
NO OF EVENTS(206.045)
500
400
300
200
100
0
0
10
20
30
40
50
60
70
CHANNEL NO(50nS)

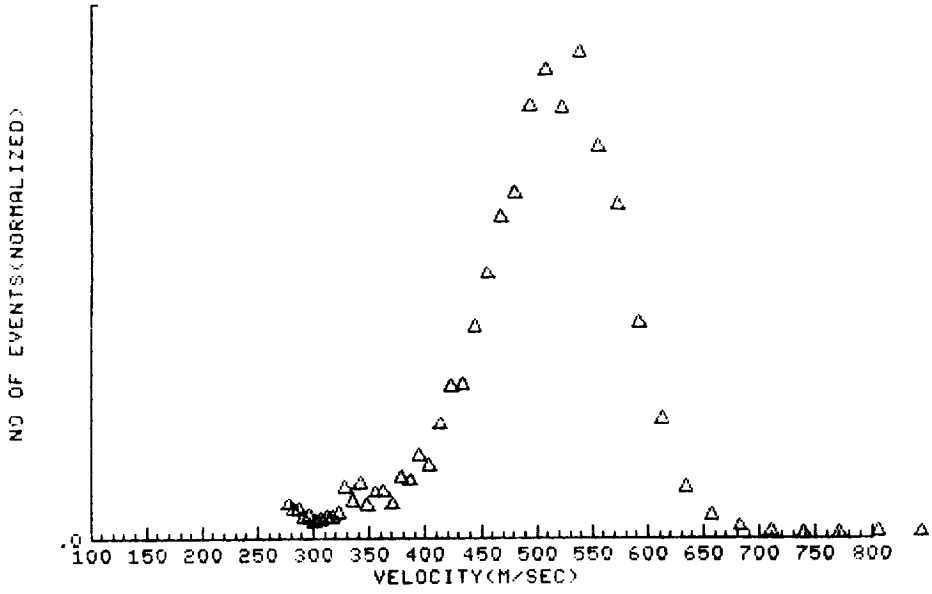
NO OF EVENTS(NORMALIZED)
.0
100 150 200 250 300 350 400 450 500 550 600 650 700 750 800
VELOCITY(M/SEC)

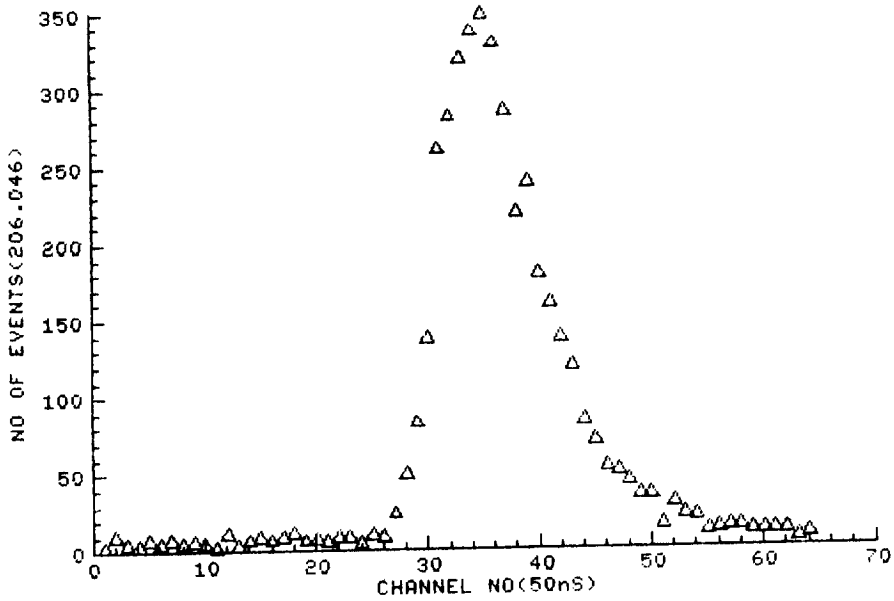
NO OF EVENTS(206.046)
350
300
250
200
150
100
50
0
0
10
20
30
40
50
60
70
CHANNEL NO(50nS)

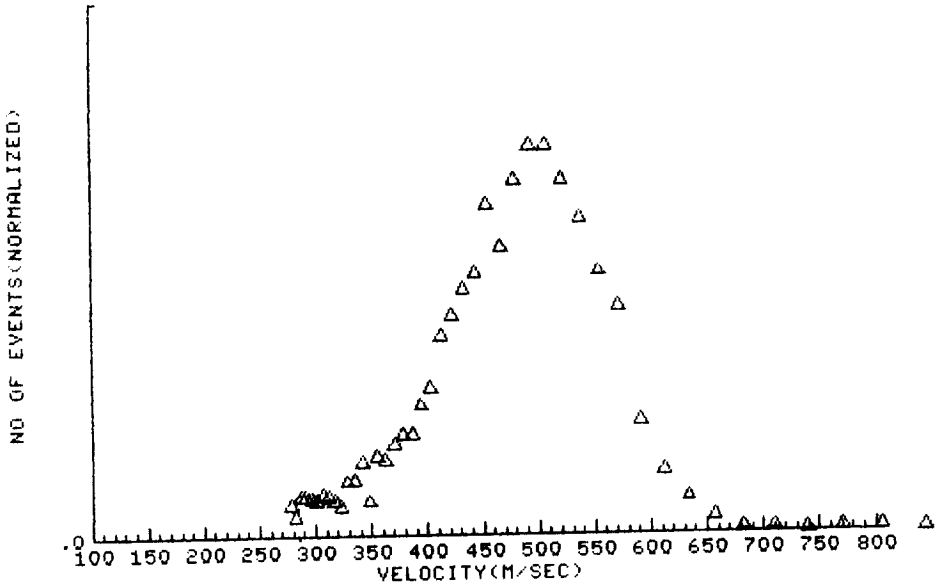
NO OF EVENTS(NORMALIZED)
.0
100 150 200 250 300 350 400 450 500 550 600 650 700 750 800
VELOCITY(M/SEC)

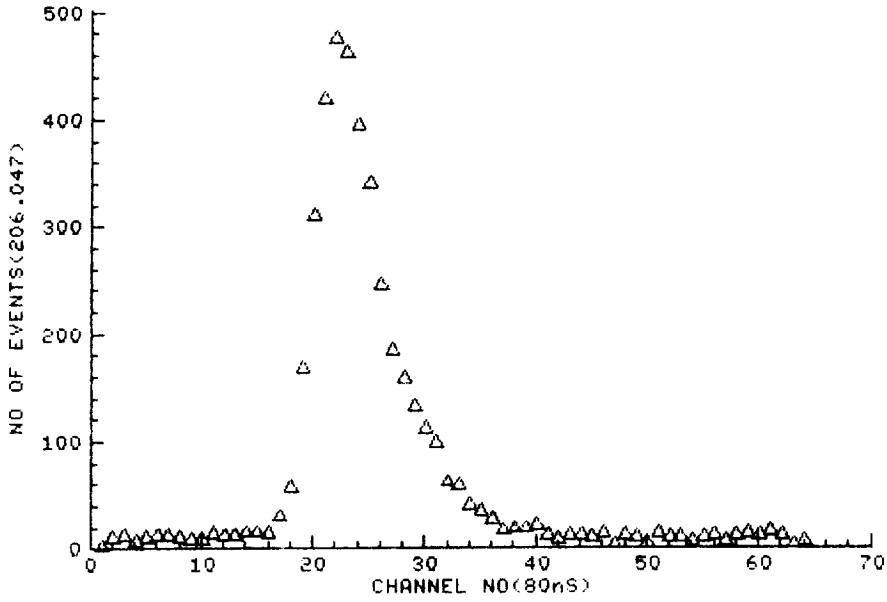
NO OF EVENTS(206.047)
500
400
300
200
100
0
0
10
20
30
40
50
60
70
CHANNEL NO(80nS)

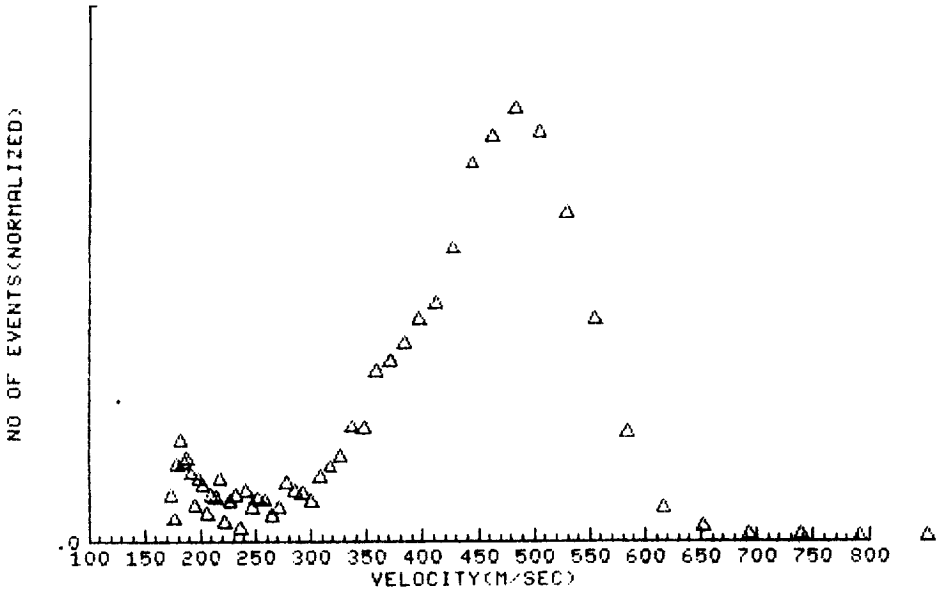
NO OF EVENTS(NORMALIZED)
.0
100 150 200 250 300 350 400 450 500 550 600 650 700 750 800
VELOCITY(M/SEC)

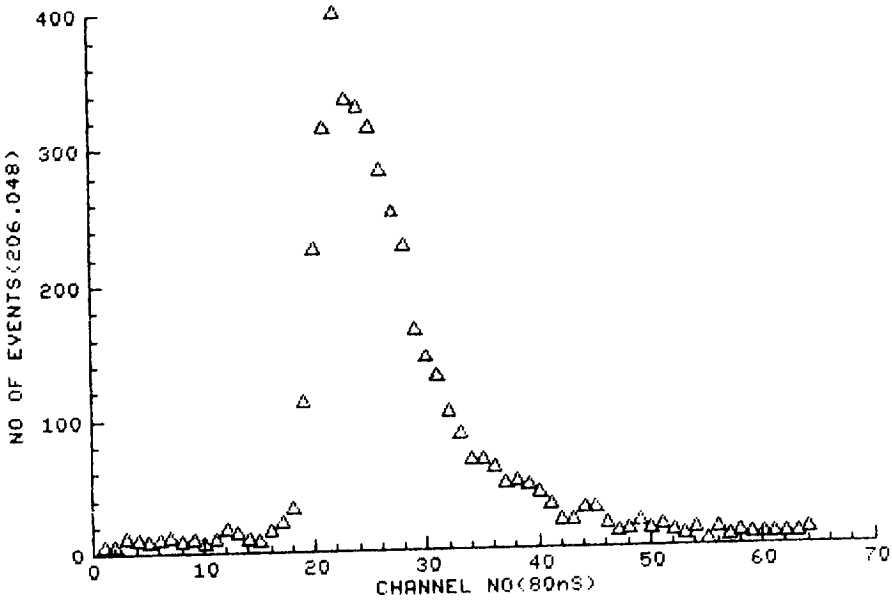
NO OF EVENTS(206.048)
400
300
200
100
0
0
10
20
30
40
50
60
70
CHANNEL NO(80nS)

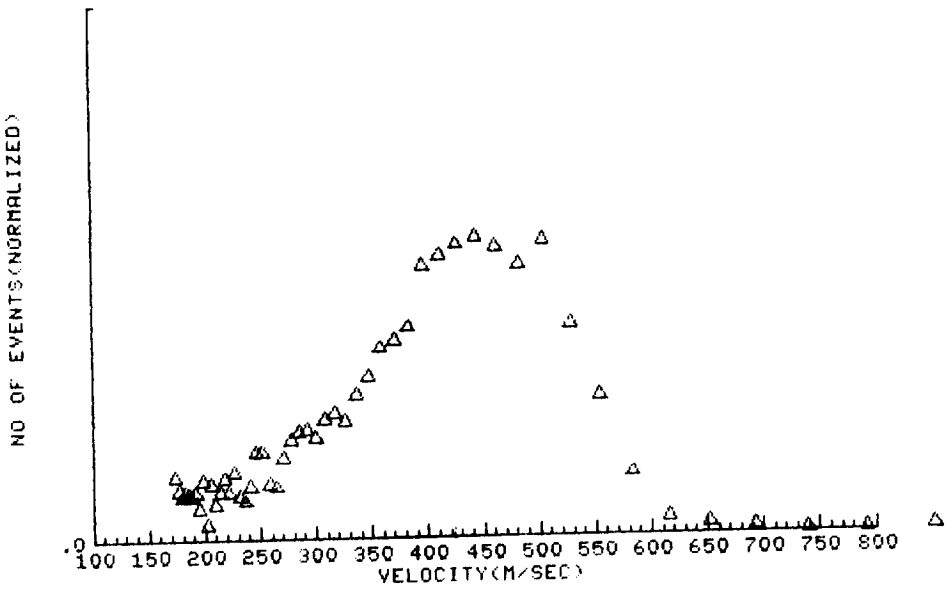
NO OF EVENTS(NORMALIZED)
.0
100 150 200 250 300 350 400 450 500 550 600 650 700 750 800
VELOCITY(M/SEC)

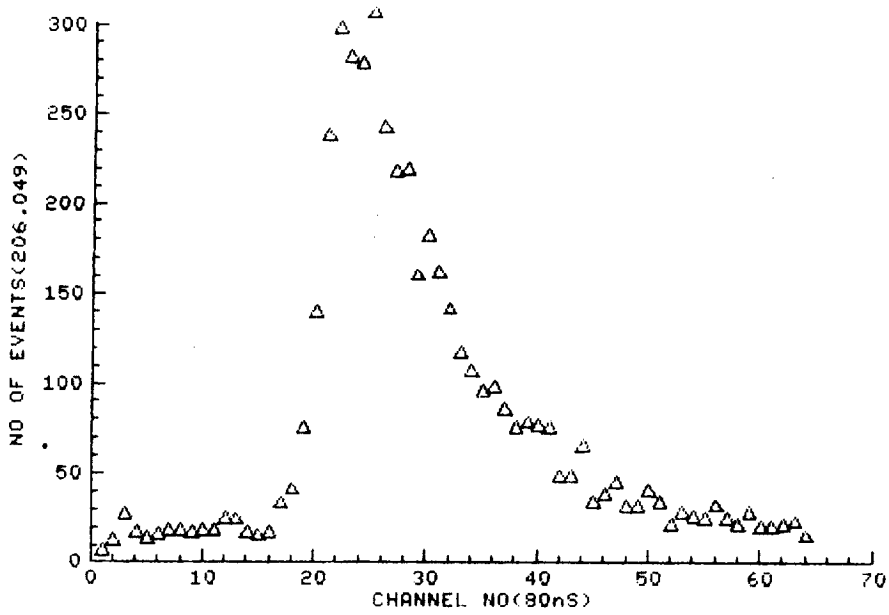
NO OF EVENTS(206.049)
300
250
200
150
100
50
0
0
10
20
30
40
50
60
70
CHANNEL NO(80nS)

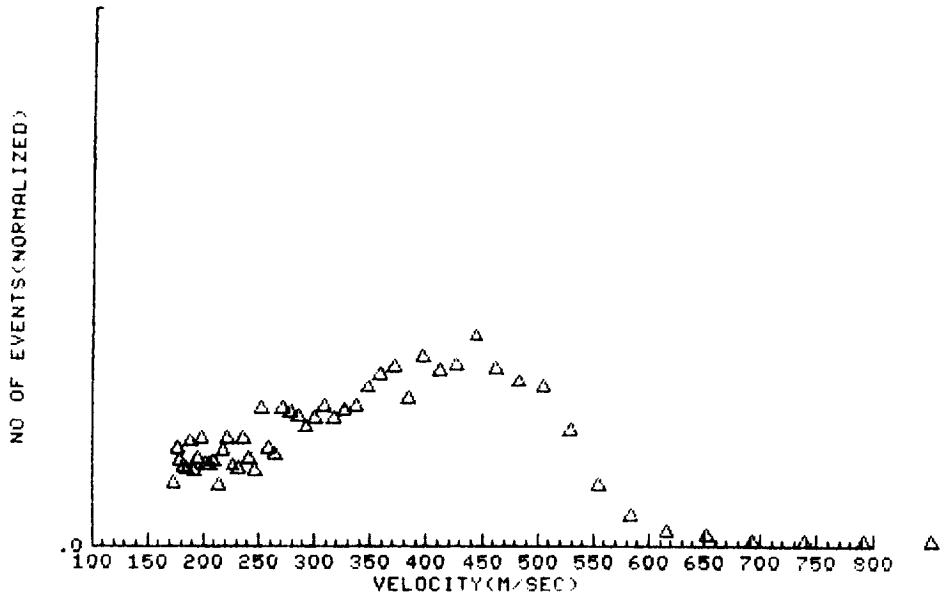
NO OF EVENTS(NORMALIZED)
.0
100 150 200 250 300 350 400 450 500 550 600 650 700 750 800
VELOCITY(M/SEC)

NASA
National Aeronautics and Space Administration

Report Documentation Page

1. Report No.	2. Government Accession No.	3. Recipient's Catalog No.
NASA TM-104101		

4. Title and Subtitle

LASER TRANSIT ANEMOMETER AND PITOT PROBE COMPARATIVE MEASUREMENTS IN A SHARP CONE BOUNDARY LAYER AT MACH 4

5. Report Date

July 1991

6. Performing Organization Code

7. Author(s)

W. W. Hunter, Jr.
S. L. Ocheltree
C. E Russ, Jr.

8. Performing Organization Report No.

10. Work Unit No.

505-59-54

9. Performing Organization Name and Address

NASA Langley Research Center
Hampton, VA 23665-5225

11. Contract or Grant No.

13. Type of Report and Period Covered

Technical Memorandum

12. Sponsoring Agency Name and Address

National Aeronautics and Space Administration
Washington, DC 20546-0001

14. Sponsoring Agency Code

15. Supplementary Notes

16. Abstract

Laser transit anemometer (LTA) measurements of a 7-degree sharp cone boundary layer were conducted in the Air Force/AEDC Supersonic Tunnel A Mach 4 flow field. These measurements are compared with pitot probe measurements and tricone theory provided by the AEDC staff. Measurements were made both in laminar and turbulent boundary layers of the model. Comparison of LTA measurements with theory showed agreement to better than 1% for the laminar boundary layer cases. This level of agreement was obtained after small position corrections, 0.01 to 0.6 millimeters, were applied to the experimental data sets. Pitot probe data when compared with theory also showed small positioning errors. The pitot data value was also limited due to probe interference with the flow near the model. The LTA turbulent boundary layer data indicated a power law dependence of 6.3 to 6.9. The LTA data was analyzed in the time (Tau) domain in which it was obtained and in the velocity domain. No significant differences were noted between Tau and velocity domain results except in one turbulent boundary layer case.

17. Key Words (Suggested by Author(s))	18. Distribution Statement
Laser velocimeter Laser transit anemometer	Unclassified - Unlimited Subject Category 35

19. Security Classif. (of this report)	20. Security Classif. (of this page)	21. No. of pages	22. Price
Unclassified	Unclassified	93	A05